PULSED LASER-EXCITED FLUORESCENCE

BY

STEPHAN JOHN WEEKS

A DISSERTATION PRESENTED TO THE GRADUATE COUNCIL OF
THE UNIVERSITY OF FLORIDA
IN PARTIAL FULFILLMENT OF THE REQUIREMENTS FOR THE
DEGREE OF DOCTOR OF PHILOSOPHY

UNIVERSITY OF FLORIDA

1977

This work is dedicated to the ones

whose love means so much to me.

ACKNOWLEDGMENTS

I would sincerely like to express my true appreciation to my friends and colleagues, who through their communication of knowledge and friendship have made this period of my life rewarding and memorable. I particularly want to express my thanks to Dr. James D. Winefordner and Dr. Hiroki Haraguchi for their help and example.

I also wish to thank my family and friends for providing continual encouragement and understanding.

TABLE OF CONTENTS

		Page
ACKNOWLEDGMENTS		iii
LIST OF TABLES		vi
LIST OF FIGURES		vii
ABSTRACT		x
CHAPTER		
I.	INTRODUCTION	1
II.	THEORETICAL CONSIDERATIONS	11
	Types of Fluorescence Transitions	12
	Atomic Fluorescence Radiance Expressions	17
III.	EXPERIMENTAL	46
	Excitation Source	46
	Detection System	61
	Experimental Conditions and Procedure	66
IV.	PULSED LASER-EXCITED ATOMIC FLUORESCENCE	70
	Optimization of System	70
	Analytical Figures of Merit	81
V	PULSED LASER-EXCITED MOLECULAR FLUORESCENCE	101
	Flame Background	101
	Selective Excitation of Molecular Species in Flames	103
	Laser-Excited Molecular Fluorescence of CaOH and SrOH	126

CHAPTER Page

VI. CONCLUSIONS AND DIRECTIONS FOR FURTHER RESEARCH . . . 149

REFERENCES 156

BIOGRAPHICAL SKETCH 163

LIST OF TABLES

Table		Page
1	Experimental Components of Laser-Excited Atomic Fluorescence Flame Spectrometric System	49
2	Molectron Model UV 400 N_2 Laser Specifications	51
3	Dye Laser Specifications	56
4	List of Laser Dyes	60
5	Optimization of Optical Arrangement in Laser-Excited Atomic Fluorescence Spectrometry	73
6A	Detection Limits by Laser-Excited Atomic Fluorescence Flame Spectrometry	83
6B	Detection Limits by Laser-Excited Atomic Fluorescence Flame Spectrometry	84
7	Comparison of Detection Limits in Flame Spectrometry and Inductively Coupled Plasma (ICP)	85
8	Investigation of Spectral Interferences Between Manganese and Gallium	97
9	Spectral Transitions of BaCl Green System $C^2\Pi$-$X^2\Sigma$	111
10	Relative Intensity of Peak Fluorescence for BaCl Transitions for the Observed Fluorescence Excitation Spectra	115
11	Approximate Energy Transitions of $A^2\Pi$-$X^2\Sigma$ (i) and $B^2\Sigma$-$X^2\Sigma$ (ii)	146

LIST OF FIGURES

Figure		Page
1	Types of atomic fluorescence transitions	14
2	Schematic diagrams of cell assumed for luminescence radiance expressions	18
3	Growth curves in atomic fluorescence	22
4	Two- and three-level atomic systems	30
5	Schematic diagram of laser-excited atomic fluorescence flame spectrometry system	48
6	Peak, average, and rms power of N_2 laser vs repetition rate	53
7	Optical schematic diagram of dye laser cavity	54
8A	Wavelength tuning curves for dyes	58
8B	Wavelength tuning curves for dyes	59
9	Optical arrangement around the burner for the examination of optimization of the optical system	72
10	Excitation and fluorescence profiles of sodium D lines	76
11	Dependence of atomic fluorescence signal of Na and Tl on slit width in the ari-acetylene flame	77
12	SNR vs Slit width of Na and Tl in the air-acetylene flame	79
13	Analytical calibration curves for elements having only strong resonance transitions above 355 nm in an air-acetylene flame	88
14	Analytical calibration curves for elements having both strong resonance and nonresonance transitions excited above 355 nm in an air-acetylene flame	90

Figure		Page
15	Analytical calibration curves for elements having transitions excited above 355 nm in a nitrous oxide-acetylene flame	92
16	Analytical calibration curves for elements having transitions excited below 355 nm in an air-acetylene flame	94
17	Excitation fluorescence spectrum for: (A) a 1 ppm Mn solution; and (B) 1 ppm Mn + 4 ppm Ga solution	98
18	Excitation spectrum of CN in a nitrous oxide-acetylene flame	102
19	Emission spectrum of barium in the air-acetylene flame	108
20	Energy level diagram of BaCl showing observed transitions	110
21	Fluorescence excitation spectra of BaCl in an air-acetylene flame	114
22	Fluorescence excitation spectra of BaOH and BaCl in an air-acetylene flame	118
23	Fluorescence excitation spectrum of BaOH in air-acetylene flame	120
24	Fluorescence excitation spectra of BaOH in an air-acetylene flame	123
25	Fluorescence excitation spectrum of BaO in an air-acetylene flame	125
26	Fluorescence excitation spectra of BaOH and BaO in an air-acetylene flame	128
27	Fluorescence excitation spectra of BaOH and BaO in an air-acetylene flame	130
28	Emission spectrum of CaOH in an air-acetylene flame	133
29	Fluorescence emission spectra of CaOH in an air-acetylene flame	136
30	Fluorescence excitation spectra of CaOH in an air-acetylene flame	139

Figure		Page
31	Fluorescence excitation spectra of CaOH in an air-acetylene flame	141
32	Near-resonance fluorescence excitation spectra of CaOH in an air-acetylene flame	143
33	Preliminary energy level diagram for $A^2\Pi$-$X^2\Sigma$ (i) and $B^2\Sigma$-$X^2\Sigma$ (ii) systems for CaOH, showing the sequences	145
34	Fluorescence emission spectrum of SrOH in an air-acetylene flame	148

Abstract of Dissertation Presented to the Graduate Council of the University of Florida in Partial Fulfillment of the Requirements for the Degree of Doctor of Philosophy

PULSED LASER-EXCITED FLUORESCENCE

By

Stephan John Weeks

December 1977

Chairman: James D. Winefordner
Major Department: Chemistry

Laser-excited atomic fluorescence flame spectrometry with a pulsed nitrogen laser pumped tunable dye laser has been investigated especially in terms of improvement of the detection limits. The detection limits for Ag, Ba, Bi, Ca, Cd, Co, Cr, Cu, Fe, Ga, In, Li, Mg, Mn, Na, Ni, Pb, Sr, and Tl in an air-acetylene flame and for Al, Ba, Mo, Ti, and V in a nitrous oxide-acetylene flame are evaluated in the cases of both resonance and nonresonance atomic fluorescence lines. The detection limits obtained in the present study have been improved by about 10 to 200 times over those obtained previously by a similar laser-excited atomic fluorescence flame spectrometry system. Detection limits for many elements and lines examined using the frequency doubled dye laser output are reported for the first time. Now, most elements examined can be detected at the $ng\text{-}ml^{-1}$ (ppb) level or less with ranges of analytical curve linearity of over five orders of magnitude. The improvement of the detection limits was achieved mainly by expanding the diameter of the laser beam to illuminate a larger analyte volume in the flame and by using a low dispersive

spectrometric system. The optical arrangement employed reduced the scatter signal and improved the signal-to-noise ratio (SNR) even at the resonance fluorescence wavelengths compared to the previously used system. Although a low dispersive spectrometric system was employed, the spectral resolution of the system was determined by the bandwidth of the laser (ca 0.03 nm). Conditions for optimizing analytical results are discussed, and laser-excited atomic fluorescence flame spectrometry is shown to be superior or equivalent to atomic absorption flame spectrometry, atomic emission flame spectrometry, atomic emission induction coupled plasma spectrometry, and conventional source atomic fluorescence flame spectrometry.

In addition, the utility of this laser fluorescence system in molecular flame fluorescence studies was examined. Molecular fluorescence spectra of BaO, BaOH, and BaCl in an air-acetylene flame have been investigated and compared to the flame emission spectra of the same species. Molecular fluorescences of BaO and BaOH in the flame were observed for the first time. Furthermore, BaO, BaOH, and BaCl, which have overlapping emission spectra in the wavelength region from 480 to 535 nm, can be selectively excited and observed by laser-excited molecular fluorescence spectroscopy. Also, pulsed laser-excited molecular fluorescence of CaOH and SrOH in an air-acetylene flame have been investigated. The spectra were examined in the wavelength region from ca. 500 nm to 700 nm. A preliminary energy level diagram is proposed for CaOH. Results are also given for SrOH.

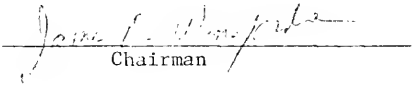

Chairman

CHAPTER I
INTRODUCTION

Atomic fluorescence spectroscopy has the potential of becoming the most widely used method for trace elemental analysis. The technique is based on the production of atoms, via any device which converts the sample into atoms, such as a flame or furnace; the photon excitation of the atoms via a suitable primary radiation source, such as a xenon arc lamp, electrodeless discharge lamp or laser; the absorption of the exciting radiation by atoms existing in the ground state energy level or a highly populated energy level producing atoms in a higher excited energy level which undergo radiational de-excitation over a period of time on the order of nanoseconds after excitation; and the subsequent detection and measurement of the induced radiation. The figures of merit achievable with the atomic fluorescence spectroscopic method, the simplicity of the experimental arrangement, and the applicability to both single and multielement trace analysis continue to stimulate development of this technique.

Winefordner (1) has recently written a brief review concerning the history, principles, instrumentation, methodologies and applications of atomic fluorescence spectrometry. Despite the fact that the physical principles upon which atomic fluorescence is based were known in the 1800's (2-6), the characteristics of atomic fluorescence were observed and described in the early 1900's (7-9); and that atomic absorption underwent rapid development in the 1950's and 1960's (10), it was not

until the early 1960's after Alkemade (11) reviewed the methods by which atoms undergo excitation in flames and described the use of atomic fluorescence flame spectrometry for measuring quantum efficiencies, that Winefordner and co-worker (12-14) pointed out and demonstrated the first analytical use of atomic fluorescence spectroscopy. Since this time, extensive research has been done, both theoretical and practical, in order to optimize the experimental conditions and arrangement for chemical analysis by both flame and nonflame methods. This is evidenced by the large number of references cited in recent reviews and books (1, 15-23). Because of the linear dependence of the fluorescence signal on the concentration of the isolated analyte atom and on the spectral irradiance of the excitation sources for nonlaser sources, most research in analytical atomic fluorescence spectroscopy has been directed towards the optimization and development of high efficiency atomizers (24-31) and high radiance excitation sources (32, 33). The impetus behind this research has been to improve the limits of detection and other figures of merit (e.g., linear dynamic range) for the atomic fluorescence method.

After the first laser was demonstrated (34) in 1960, spectroscopists immediately realized the usefulness of lasers. However, it was not until lasers became tunable that they became useful as an analytical tool for spectroscopy. The greatest advances in tunable lasers for analytical spectroscopy came after the demonstration of the organic dye laser (35, 36). Several reviews and books describe the developments and properties of tunable lasers (37-42). The lasers considered to be of most interest to analytical chemists for studies in atomic spectroscopy are the ion-laser pumped continuous wave (cw) dye laser; the flashlamp pumped dye laser; and the nitrogen (N_2) laser (or Nd^{+3}:YAG laser) pumped tunable

dye laser. Of these lasers the N_2 laser pumped dye laser possesses the widest tuning range (from ca 220-950 nm) and the most ease of changing dyes rapidly during operation. The "tuning" of wavelength in the N_2 laser pumped dye laser is accomplished by changing the lasing media (i.e., the dye) and the angle of the grating, which acts as one of the laser cavity mirrors. Because of the high spectral irradiances, narrow spectral bandwidth, wide range of wavelength tunability, coherent properties of the output beam, and short temporal duration of the pulses, the N_2 laser pumped tunable dye laser seems to be nearly an ideal source for atomic fluorescence spectroscopy.

In 1971, Fraser and Winefordner (43) reported the first application of a tunable dye laser used as a primary radiation source in atomic fluorescence spectroscopy. A N_2 laser pumped dye laser was used to excite nine different elements in air-hydrogen and nitrous oxide-acetylene flames. The detection limits obtained ranged from an improvement by a factor of ten to within fifty times that of the best reported literature values for conventional source atomic fluorescence. Besides low detection limits, they reported long linear dynamic ranges and freedom from flame background noise and also demonstrated that the spectral resolution was determined only by the spectral bandwidth of the laser output. The dye laser source used had a peak power greater than 10 kW, a pulse repetition rate of 1-25 Hz, a spectral bandwidth of 0.1-1 nm, and a temporal pulse width of about 2-8 ns. A 1P28 photomultiplier tube and a boxcar integrator (gated amplifier) with a 10 ns gate width were used for signal detection and processing.

In the same year, Denton and Malmstadt (44) also demonstrated the use of tunable organic dye lasers as excitation sources for atomic flame

fluorescence spectroscopy. They reported atomic flame fluorescence of barium excited by the output of a dye laser pumped by the second harmonic of a Q-switched ruby laser. They found conventional total consumption burners to be totally unusable due to high light scattering levels. An ultrasonic nebulizer was found to reduce the scatter level and allow linear calibration curves to be obtained. They also noted that considerable care had to be used to prevent radiation scattered from the environment (i.e., not the observed analyte volume in the flame) from striking the detector.

In 1972, Fraser and Winefordner (45) obtained limits of detection ranging from better to within tenfold of the best literature values by any other atomic flame spectrometric method. They also noted several additional advantages pulsed laser excitation has over conventional continuously operated line or continuum sources including the following: only one source is needed; freedom from analyte emission; and the simplicity of using nonresonance fluorescence to eliminate noise due to scatter of exciting radiation. Nonresonance fluorescence measurements yielded about a ten-fold improvement in the detection limits over resonance fluorescence. They observed several types of fluorescence including: resonance fluorescence; excited resonance fluorescence; Stokes direct line fluorescence; anti-Stokes direct line fluorescence; and excited anti-Stokes direct line fluorescence. They utilized the same N_2 laser pumped tunable dye laser atomic fluorescence flame spectrometric system as described above, except that the dynode chain for the photomultiplier tube base was modified for high current pulsed operation and the output of the boxcar integrator was fed into an additional analog integrator in order to minimize pulse-to-pulse variations. Noise sources were briefly dis-

cussed and interference due to CN formed in the nitrous oxide-acetylene flame was noted.

Since these initial studies, tunable organic dye lasers have been increasingly used as excitation sources for atomic fluorescence spectroscopy with both flame atomizers and nonflame atomizers. In these studies, pulsed (nitrogen, ruby, or Nd^{+3}:YAG laser pumped and flashlamp pumped) or continuous wave (cw) dye lasers have been employed as excitation sources for atoms. These studies point out additional advantages and uses of laser-excited atomic fluorescence spectroscopy, as well as some of the limitation.

Omenetto et al. (46, 47) examined the atomic fluorescence of some transition elements and atomic and ionic fluorescence of some rare earth elements in the nitrous oxide-acetylene flame with a N_2 laser pumped tunable dye laser. Very good results were obtained and the use of non-resonance fluorescence measurements were stressed.

Because lasers are highly coherent sources of radiation, the already high spectral irradiance output can easily be focused to even larger power densities. Omenetto et al. (48, 49) and Piepmeier (50, 51) were the first to visualize the influence of saturation of atomic levels due to the intense laser excitation, and derive the theories necessary to investigate saturation conditions. Kuhl et al. (52) discussed the influence of saturation on the atomic fluorescence measurements obtained using a flashlamp pumped tunable dye laser. Complete saturation occurs in a two-level system when the ratio of the populations in the upper energy to that of the lower energy level becomes equal to the ratio of the statistical weights for the two levels. Ordinarily, the fluorescence radiance, when excited by conventional low intensity light sources,

is linear with source intensity. However, this relationship will hold only up to the point which the source intensity becomes large enough to alter the thermal atomic equilibrium distribution which exists in the atomizer (i.e., flame or other plasma). Saturation or near saturation conditions offer a number of advantages including: greatly enhanced signals, less dependence on source intensity and its fluctuations, and less dependence on quantum efficiency.

In 1973, Kuhl and Spitschan (53) were the first to utilize frequency doubled dye laser output to obtain fluorescence signals from Mg, Ni, and Pb at wavelengths below ca 350 nm. Because the fundamental output of dye lasers currently lies above ca 350 nm, nonlinear frequency doubling crystals must be used in order to investigate the many strong atomic transitions which lie below this wavelength. A flashlamp pumped dye laser was used in the above studies to excite atoms formed on a flame atomizer. To date, no frequency doubled detection limits have been reported using a N_2 laser pumped dye laser atomic fluorescence system.

De Olivares (54) has investigated several practical and fundamental aspects of laser-excited atomic fluorescence spectroscopy (AFS) using a N_2 laser pumped dye laser.

Green et al. (55) and Smith et al. (56) have recently used cw dye lasers to excite atoms in flames. The cw dye laser should be an optimal excitation source because of the higher average output power, the greater ease of modulation, and the increased ease of signal processing when compared to the pulsed dye lasers. Good detection limits were reported for sodium and barium and some nonresonance excited state transitions were observed. However, the available wavelength range of cw dye lasers is presently limited to the longer visible wavelength region, primarily

above 520 nm, making cs dye lasers of limited analytical use. Pulsed N_2 laser pumped tunable dye lasers, on the other hand, offer the greatest advantages to date, primarily because a wavelength range from ca 220 to 950 nm can be quickly and easily obtained.

Other recent studies in flames have used flashlamp pumped dye lasers to excite Na atoms. Again, the advantages of laser-excited nonresonance fluorescence were pointed out (57) and saturation was investigated (58).

In 1971, Kuhl and Marowsky (59) observed fluorescence in a sodium vapor (nonflame) cell with a flashlamp pumped dye laser. Later, Fairbank et al. (60) were able to detect 100 atoms-cm^{-3} in a sodium vapor cell with a cw dye laser. In other works (61, 62) where a sodium vapor cell was employed, flashlamp pumped dye lasers were used to obtain additional theoretical analysis. Sodium also has been investigated in a quartz tube and furnace using a cw dye laser (63).

In 1974, Neumann and Kriese (64) reported the detection of subpicogram amounts of Pb by nonflame atomic fluorescence spectrometry with a frequency doubled flashlamp pumped dye laser. More recently, Bolshov et al (65) reported subpicogram amounts of Pb and Fe by graphite tube atomic fluorescence analysis using the grequency doubled radiation of a dye laser pumped by the second harmonic radiation of a Nd^{+3}:YAG laser. The absolute detection limits obtained in this study are at present the lowest achieved by any atomic spectroscopic method. In the case of Pb, saturation was reached. In another study (66) picogram detection of Cs in a graphite furnace was reported using a N_2 laser pumped dye laser to excite the atoms. Nonresonance fluorescence was utilized.

Several works (67-69, 54) have examined both theoretical and fundamental characteristics of saturation of the energy levels of atoms. Steady state expressions were given for two and three level atomic systems.

Steady state expressions were given for two and three level atomic systems.

The research and theoretical studies performed to date have indicated the many advantages of laser-excited atomic fluorescence spectroscopy and the great potential of this method for both fundamental research and practical analysis. So far, laser-excited atomic fluorescence spectroscopy with a N_2 laser pumped dye laser has produced detection limits comparable to those obtained by flame emission spectrometry and atomic absorption flame spectrometry (45-47). Detection limits in laser-excited atomic fluorescence spectrometry have been comparable with those obtained in atomic fluorescence flame spectrometry using conventional narrow line light sources, such as hollow cathode lamps, electrodeless discharge lamps, and xenon arc continuum sources (70, 71). Unfortunately, previous results obtained with laser excitation have not been as good as expected based upon the high intensity output (72). Although many factors influencing the results have been noted, the experimental arrangement and conditions in laser-excited atomic flurescence spectrometry need to be more fully and carefully investigated; a pulsed source with high spectral irradiance combined with gated detection should be a nearly ideal system for improvement of detection limits and signal-to-noise ratios (SNR) of atomic fluorescence, as has been predicted (71, 73, 74).

During the investigation of atomic fluorescence detection limits, strong spectral interferences were noted in the 380 nm wavelength region due to the formation of CN in the nitrous oxide-acetylene flame. Although a N_2 laser pumped dye laser atomic fluorescence spectrometric system using gated detection has negligible interference from flame background or sample emission because of the low duty factor (ratio of

detector on time to the total time of analysis), ca 10^{-7}, the atomic fluorescence signal-to-noise ratio can be greatly affected by flame background fluorescence and sample matrix effects. Knowledge of interferences from flame background fluorescence and matrix effects is extremely important for the practicing analytical chemist because often it is possible to choose the lines used for analysis and the flame conditions and composition to eliminate or minimize the interference without having to use further sample pretreatment methods.

The observation of strong molecular fluorescence in flames indicated the possibility of using the pulsed dye laser spectrometric system to conduct a number of studies. These studies included determination of the fluorescence background due to the flame gases and its dependence on flame conditions, composition, fuel-to-oxidant ratio, and quenchers, and a discussion on the possibility of removing spectral interferences in atomic fluorescence spectrometry based upon the results; the possibility of utilizing molecular fluorescence for the analysis of nonmetallic elements, such as P, S, O, C, N, and the halogens, which are difficult to determine by atomic fluorescence because their atomic resonance lines are in the far or vacuum UV; fundamental studies such as the identification of molecular species via selective excitation, determination of energy levels and molecular parameters, study of reaction kinetics and determination of quantum efficiencies; reduction of fluorescence background in Raman spectrometry; and combustion diagnostics including the profiling of species concentration and flame or plasma temperature. In this thesis, the flame background fluorescence of CN in the nitrous oxide-acetylene flame will be reported, and the molecular fluorescence of alkaline earth compounds in the perspective of utilizing the pulsed

N_2 laser pumped tunable dye laser fluorescence spectrometric system for the identification of molecular species via selective excitation and for the determination of energy levels of molecular species formed in flames or plasmas will be investigated.

The primary purpose of this research is to improve the detection limits and obtainable signal-to-noise ratio (SNR) through the investigation of factors influencing the atomic fluorescence signal and the system noise in a N_2 laser pumped tunable dye laser atomic fluorescence spectrometric system. Equally important is the need to point out additional figures of merit for the method such as long linear dynamic range of the analytical calibration curve and lack of spectral interferences which are of tremendous importance to the practicing analytical chemist. A comparison with other trace elemental analysis methods is also necessary for the analyst and is made here. Another equally important purpose is the need to consider this as only an initial study and therefore state where additional improvements could be made in the system. A pulsed laser radiation source with high spectral irradiance, narrow spectral bandwidth, and wide wavelength tuning range combined with gated detection should prove to be an ideal system for elemental analysis.

CHAPTER II
THEORETICAL CONSIDERATIONS

The usefulness of atomic fluorescence spectroscopy lies in the fact that it is a method of chemical analysis that is both qualitative and quantitative and that it has distinct advantages over atomic emission and atomic absorption spectroscopy and other methods of atomic analysis. These advantages must be put in perspective by a comparison of the figures of merit for each technique. Excellent discussions of quantitation in analysis describing figures of merit can be found in literature (23, 75, 76). Analytical figures of merit refer only to a definite complete analytical procedure, which is specified in every detail with respect to the analytical task, the apparatus, the external conditions, the experimental conditions, the experimental procedure, the measurement process, the means of calibration and the evaluation of data (23). The figures of merit of an analytical method include: limit of detection; linear dynamic range of the analytical calibration curve; sensitivity; selectivity; specificity; accuracy; and precision.

The limiting detectable measure, x_L, is given by

$$x_L = \bar{x}_{bl} + ks_{bl}$$

where $\bar{x}_{bl}$ is the average value of the blank measure calculated from a sufficiently large number of blank analyses (at least 16); k is a protection factor, generally accepted to be 3 (23,77); and s_{bl} is the standard deviation of the blank measures.

The linear dynamic range of the analytical calibration curve is given by the ratio of the upper limit of concentration, at which the signal deviates from linearity by 5%, to the concentration at the detection limit, c_L, where $c_L = \frac{x_L - \bar{x}_{bl}}{S} = \frac{ks_{bl}}{S}$.

The sensitivity of the measurement procedure is defined as the slope S of the analytical calibration curve when the concentration, c, is plotted versus the signal intensity, x. The sensitivity is not redundant with the detection limit.

Many articles and books give detailed discussions of the analytical figures of merit, atomic fluorescence radiance expressions, the types of atomic fluorescence, the shape of the analytical curves, nebulization, atomization, and other theoretical and practical considerations as well as comparisons of the various methods for analysis (1, 11, 12, 15-23, 31, 48-52, 54, 67-79).

Types of Fluorescence Transitions

Since the discovery of atomic fluorescence as an analytical tool, various types of atomic fluorescence transitions have been utilized for analytical studies. Due to the rapid development of atomic fluorescence and with the advent of tunable dye laser sources, which have made it possible to observe many new fluorescence transitions, Omenetto and Winefordner (78) have proposed a consistent nomenclature to identify atomic fluorescence transitions, in order to avoid possible confusion in the literature. Basically, there are five types of atomic fluorescence transitions, which are reported, together with their possible variation, in Figure 1.

Figure 1. Types of atomic fluorescence transitions (the spacings between atomic levels is not indicative of any specific atom). a, resonance fluorescence (either process); b, excited state resonance fluorescence; c, Stokes direct line fluorescence; d, excited state Stokes direct line fluorescence; e, anti-Stokes direct line fluorescence; f, excited state anti-Stokes direct line fluorescence; g, Stokes stepwise line fluorescence; h, excited state Stokes stepwise line fluorescence; i, anti-Stokes stepwise line fluorescence; j, excited state anti-Stokes stepwise line fluorescence; k, thermally assisted Stokes or anti-Stokes stepwise line fluorescence (depending upon whether the absorbed radiation has shorter or longer wavelengths, respectively, than the fluorescent radiation); l, excited state thermally assisted Stokes or anti-Stokes stepwise line fluorescence (depending upon whether the absorbed radiation has shorter or longer wavelengths, respectively, than the fluorescence radiation); m, sensitized fluorescence (D = donor; D* = excited donor; A = acceptor; A* = excited acceptor; $h\nu_F$ = fluorescence radiation); n, two photon excitation fluorescence (multiphoton processes involving more than two identical photons are even less probably than the two photon processes). Taken from Reference 78.

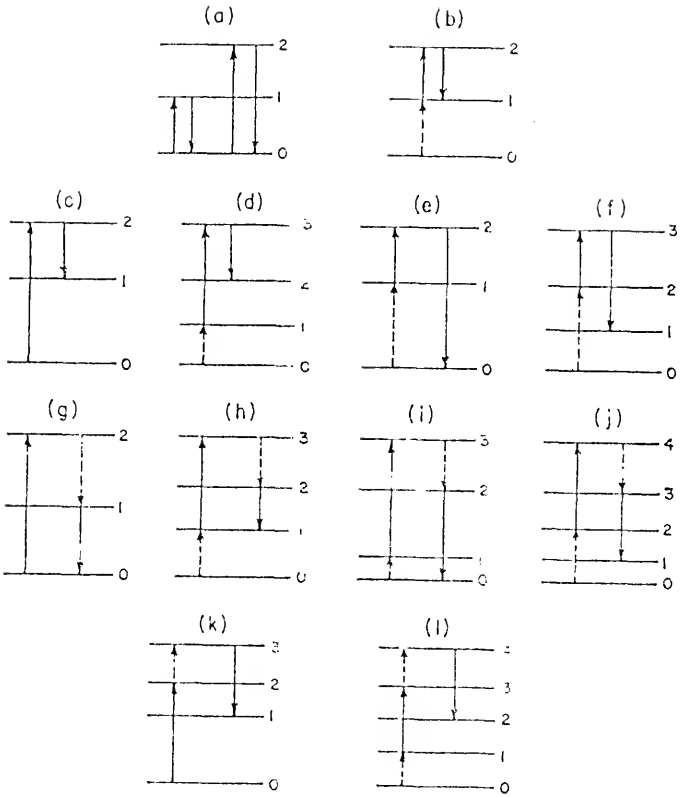
(a)
2
1
0
(b)
2
1
0
(c)
2
1
0
(d)
3
2
1
0
(e)
2
1
0
(f)
3
2
1
0
(g)
2
1
0
(h)
3
2
1
0
(i)
3
2
1
0
(j)
4
3
2
1
0
(k)
3
2
1
0
(l)
4
3
2
1
0
(m)
D + hν_E ⟶ D*
D* + A ⟶ A* + D
A* ⟶ A + hν_E
(n)
1
HYPOTHETICAL LEVEL
0

Resonance fluorescence results when the same lower and upper energy levels of the atom are involved in the excitation and de-excitation processes. A radiationally excited atom reemits (fluoresces) a quantum of radiation of the same energy as was absorbed. The transition probabilities for resonance transitions involving the ground electronic state are typically much greater than for nonresonance transitions. Because resonance fluorescence signal intensities are generally significantly greater than the intensities observed with other types of transitions, resonance fluorescence has been shown to be most useful for routine chemical analysis (80).

Direct line fluorescence results when the same upper level is involved in the radiational excitation and de-excitation processes; however, the photon energy emitted (fluoresced) is different from that which was absorbed. Direct line fluorescence is most useful analytically when scatter of source radiation (e.g., from particles within the analyte flame volume) is the predominant source of noise in the spectroscopic system. Direct line fluorescence has also proved to be useful for temperature measurement and species and temperature profiling of flame atomizers (81-87).

Stepwise line fluorescence results when different upper levels are involved in the radiational excitation and de-excitation processes. Again, the photon energy reemitted (fluoresced) is different from that which was absorbed. Stepwise line fluorescence has analytical usefulness when the excitation source scatter is the predominant noise source and there is no possibility or the transition probabilities are not favorable for the direct line fluorescence. Stepwise line fluorescence can be used to study quenching mechanisms in flames (87).

The remaining two types of atomic fluorescence have only theoretical interest at present in analytical flame spectrometry. Sensitized fluorescence results when one species (called the donor) is excited by an external light source, collides with an atom of the same or another species (called the acceptor), transfers energy to the acceptor, after which either may de-excite radiationally. The final type of atomic fluorescence is multiphoton fluorescence. This type of fluorescence results when two or more photons excite an atomic species to an upper energy level after which radiative de-excitation occurs. The excitation may involve either virtual or real energy levels.

If the photon energy of fluorescence is less than the photon energy of absorption, the process is called Stokes (type) fluorescence. If the reverse is true, the process is called anti-Stokes (type) fluorescence. If the radiational absorption and fluorescence processes involve only excited states, then the word excited is introduced in front of the fluorescence process. If after radiational excitation, radiationless processes (e.g., collisions) populate either a higher or lower level from which fluorescence occurs, then the phrase thermally assisted is inserted prior to the name of the fluorescence process (1).

The identification of excitation and de-excitation processes involved in fluorescence measurements is important for several reasons. First, it helps determine the relative contributions of various radiational excitation energies as well as that of thermal collisions in populating the upper level from which fluorescence occurs. It also permits correct use of nomenclature and reporting of fluorescence processes.

Evaluation of quantum efficiency and flame temperatures requires a clear knowledge of the overall process. Finally and probably most

importantly from an analytical point of view, it allows one to take advantage of the difference existing between the excitation and fluorescence wavelengths in order to eliminate scattered light, which may cause the limiting noise in resonance fluorescence measurements. Because lasers are a single radiation source having an output which has a narrow spectral bandwidth with high spectral irradiance and are tunable, lasers represent an ideal source because no filters (or other frequency selective devices) are necessary to isolate the excitation (absorption) wavelength. Also, the excited level population is greatly enhanced, thereby favoring efficient mixing between adjacent levels resulting in strong fluorescence.

Atomic Fluorescence Radiance Expressions

Atomic fluorescence can be considered to be divided into three processes: conversion of sample into atoms; absorption of radiation by atoms; and fluorescence emission of radiation from excited atoms. Figure 2 shows a schematic diagram of the cell assumed for atomic fluorescence measurements with the common right angle case (i.e., fluorescence is observed perpendicular to the exciting radiation). The signal expression is the expression that relates the measured signal to the analyte concentration. The radiance expressions for atomic fluorescence spectroscopy are given below for various cases of continuum or line excitation sources; high or low optical atomic densities; and high or low source spectral irradiances. The expressions hold under the conditions of homogeneous distributions of atoms in the analyte volume; uniform temperature, T, throughout the analyte volume; thermodynamic equilibrium of species; negligible effect of source radiation upon the energy dis-

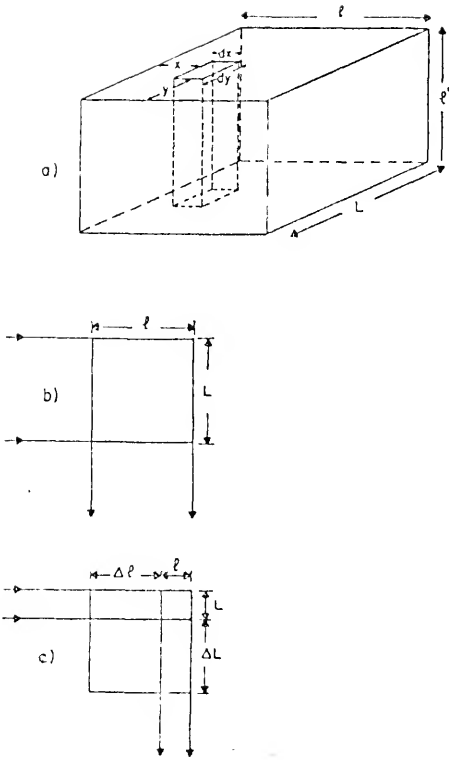

Figure 2: Schematic diagrams of cell assumed for luminescence radiance expressions: (a) three-dimensional diagram of cell to show dimensions of unit cell; (b) top view of cell, right angle configuration - complete illumination of cell, complete measurement of right angle fluorescence; (c) top view of cell, right angle configuration - incomplete illumination of cell, incomplete measurement of fluorescence. Taken from reference 19.

tribution, velocity distribution or temperature of species in the analyte volume; spatial uniformity and constancy of radiation density of the source throughout analyte volume; and negligibility of polarization and coherence effects and prefilter and postfilter effects.

Low Source Spectral Irradiance

Continuum source, low optical density case

$$B_F = C_1 \left(\frac{\ell}{4\pi}\right) E_{C_{\lambda_{ij}}} n_i K_o f_{ij} \delta\lambda_D Y_{P_{kl}} \quad (1)$$

The fluorescence radiance is linearly proportional to concentration, source spectral irradiance, absorption path length and quantum efficiency. Self-absorption is negligible in this case. This is the normal condition under which atomic fluorescence measurements are made.

Continuum source, high optical density case with atomic fluorescence terminating in ground or near ground states

$$B_F = \frac{C_2}{C_1} \left(\frac{1}{4\pi}\right) E_{C_{\lambda_{ij}}} a \delta\lambda_D \left(\frac{L}{\ell}\right)^{1/2} Y_{P_{kl}} \quad (2)$$

Equation (2) assumes reabsorption of some fraction of emitted radiation, (i.e., self-absorption). The fluorescence radiance is not a function of atomic concentration.

Continuum source, high optical density case with atomic fluorescence terminating in excited states

$$B_F = \left(\frac{\ell}{4\pi}\right)^{1/2} E_{C_{\lambda_{ij}}} \left(\frac{K_o n_i f_{ij} \sqrt{\pi}}{\ln 2}\right)^{1/2} \delta\lambda_D Y_{P_{kl}} \quad (3)$$

Reabsorption of fluoresced radiation is assumed to be minimal. Fluorescence radiance is proportional to $(n_i \ell)^{1/2}$, i.e., the fluorescence signal is proportional to the square root of the concentration. Therefore, with a continuum source, many nonresonance fluorescence analysis schemes are still analytically useful at high analyte concentrations but with reduced sensitivity.

Line source, low optical density case

$$B_F = \left(\frac{\ell}{4\pi}\right) E_L \, n_i K_o f_{ij} \delta_{ij} Y_{P_{kl}} \qquad (4)$$

In the case of a line source, the source half-width is assumed much smaller than the absorption line width. This case is similar to that of equation (1) and is again a normal condition for analysis in atomic fluorescence spectrometry.

Line source, high optical density case with atomic fluorescence terminating in ground or near ground states

$$B_F = \left(\frac{1}{4\pi}\right) E_L \left(\frac{4aL}{\sqrt{\pi} K_o n_i f_{kl} \ell^2}\right)^{1/2} Y_{P_{kl}} \qquad (5)$$

In equation (5) it is assumed that reabsorption of fluorescence radiation occurs. The fluorescence radiance decreases with increasing analyte concentration.

Line source, high optical density case with atomic fluorescence terminating in excited states

$$B_F = \left(\frac{1}{4\pi}\right) E_L \, Y_{P_{kl}} \qquad (6)$$

Fluorescence radiance is not dependent on concentration of analyte.

Equations (1) through (6) are shown graphically in Figure 3. These curves relate the fluorescence radiance, B_F, to the concentration of species in level i, n_i. These curves are called growth curves.

When absoprtion from excited states takes place, the population of that level, n_i, is found under conditions of thermodynamic equilibrium by using the Boltzmann equation,

$$n_i = n_o \left(\frac{g_i}{g_o}\right) \exp\left(\frac{-E_i}{kT}\right)$$

where the subscript o refers to the ground state.

Figure 3: Growth curves in atomic fluorescence. (A) Resonance fluorescence: curve A - continuum source; curve B - line source. (B) Nonresonance fluorescence: curve A - continuum source; curve B - line source. Taken from reference 88.

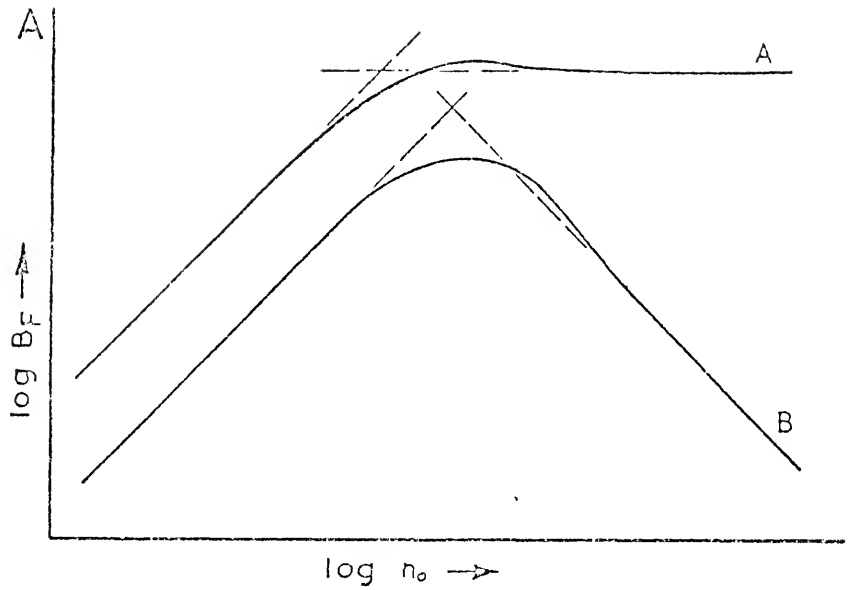
A
A
log B_F
B
log n_o

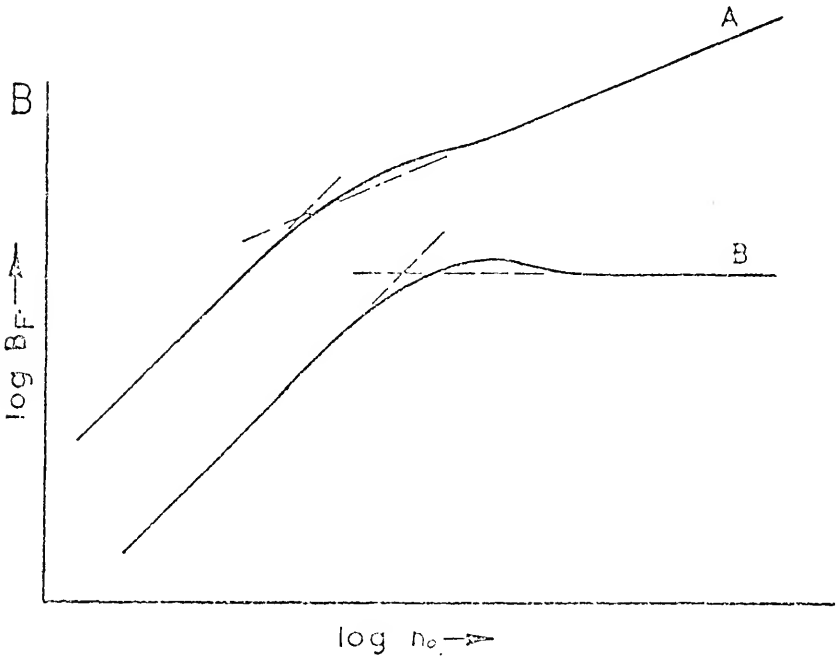
B
A
B
log B_F
log n_o

The terms and symbols used in the above equations are as follows:

$B_F = A_{i \to j} \; B_{F_{k \to l}}$ = fluorescence radiance,

where the absorption transition occurs from level i to level j and the fluorescence transition occurs from level k to level l, (i,j,k,l designate energy levels of the Grotrian energy level diagram), W m^{-2} sr^{-1};

4π = number of steradians in a sphere (fluorescence is isotropic), sr;

$C_1 = \sqrt{\pi}/2\sqrt{\ln 2}$, no units;

$C_2 = \sqrt{\pi}\sqrt{\ln 2}$, no units;

ℓ = absorption path length, m:

$E_{C_{\lambda_{ij}}}$ = continuum source spectral irradiance of exciting radiation at the absorption wavelength λ_{ij}, W $m^{-2}m^{-1}$;

E_L = line source irradiance of exciting radiation at the absorption wavelength λ_{ij}, W m^{-2};

n_i = concentration of species in level i, m^{-3};

$Y_{P_{kl}} = \frac{h\nu_{kl}}{h\nu_{ij}} Y_{kl}$ = fluorescence power (quantum) efficiency, W fluoresced/W adsorbed;

$K_o = k_o/n_i f_{ij}$ = modified absorption coefficient, m^2;

k_o = absorption coefficient for pure Doppler (Gaussian) broadening, m^{-1};

$$k_o = K_o n_i f_{ij} = \frac{2\sqrt{\ln 2}\; \chi\; \lambda_{ij}^2 F_s}{\sqrt{\pi} c\; \delta\lambda_D} n_i f_{ij}, \; m^{-1};$$

$$\chi = \frac{e^2}{4mc\varepsilon_o} = 2.65 \times 10^{-6} \; m^2 s^{-1};$$

F_s = source factor to account for saturation of energy levels, no units;

e = electron charge, 1.602×10^{-19} C;

c = speed of light, m s^{-1};

m = electron mass, 0.9107×10^{-30} kg;

$\delta\lambda_D$ = Doppler half-width, m;

f_{ij} = absorption oscillator strength for transition from energy level i to energy level j, no units;

a = damping constant, $\sqrt{\ln 2}\ \delta\lambda_C/\delta\lambda_D$, no units;

$\delta\lambda_C$ = Lorentzian (collisional) half-width, m;

L = fluorescence path length, m;

ℓ' = height of fluorescence volume;

δ_{ij} = Voight profile factor to account for finite line width of source compared to absorption line, no units;

ε_0 = permittivity of vacuum, 8.854×10^{-12} $C^2 N^{-1} m^{-2}$.

If the sample cell is not completely illuminated, the fluorescence radiance, B_F, emitted towards the detector is reduced by reabsorption of radiation in the area $\Delta L x \ell' x \ell$. This is the postfilter effect. If the fluorescence radiation is not completely measured, then the incident irradiance from the source may be reduced in the area $\Delta\ell x L x \ell'$ and therefore also reducing the fluorescence radiance, B_F. This is known as the prefilter effect. Both prefilter and postfilter effects are only significant for high concentrations of analyte.

The amount of fluorescence signal reaching the detector is determined by the optical conductance, G ($m^2 sr$), of the spectrometric system. The radiant flux, Φ, impinging on the detector is given by:

$$\Phi_F = B_F G\tau$$

where τ = transmission factor of optical system (dimensionless).

The concentration of analyte in the lower atomic level, n_o, atoms m^{-3}, must be related to the concentration of the analyte in solution. When the solution is nebulized, and introduced into the flame as an aerosol, it can be shown that (19):

$$n_o = \frac{N_A F \varepsilon \beta C g_o}{Q_t e_f Z_t}$$

where:

N_A = Avogadro's number, 6×10^{23} mol^{-1};

F = solution transport rate, $m^3 s^{-1}$;

ε = nebulization and solute vaporization efficiency, no units;

β = atomization efficiency, no units;

C = concentration of analyte in solution, mol m^{-3};

g_o = statistical weight of state o, no units;

Q_t = flow rate of unburnt gases into the flame, $m^3 s^{-1}$;

e_f = expansion factor for flame gases, no units;

$Z_t = \sum_i g_i \exp\left(\frac{-E_i}{kT}\right)$ = normalized electronic partition function, no units;

k = Boltzmann constant, 8.31×10^{-5} eV K^{-1};

T = flame temperature, K;

E_i = energy of level i, eV.

The final relationship necessary to relate the solution concentration to the final signal relates the fluorescence radiant flux to the detector output. This is given by $S = \Phi_F \gamma R_T$, where S = signal, V; γ = photodetector sensitivity, A W^{-1}; and R_T = electronic system transfer function V A^{-1}.

High Source Spectral Irradiance Considerations

The advent of lasers in spectroscopic analysis made it necessary to consider the possibility of saturating a particular transition. As the source spectral irradiance becomes increasingly large, the rate of induced emission becomes much more important among the deactivation processes, and the absorption of source radiation becomes nonlinear and and approaches zero. The use of lasers as excitation sources has the important consequence that the conventional photon transport equation (Beer's law) is strictly valid in the limit of zero incident light flux and is therefore an accurate approximation only for low intensity sources. The high radiation density of a laser focussed into an atomic vapor is able to redistribute the populations of the levels involved in the absorption process. When this effect occurs, saturation of the optical transition is said to be approached or in the limit to occur, and the fluorescence signal will no longer be proportional to the

source irradiance and will reach a limiting value depending only upon the properties of the atomic system (67).

A more general fluorescence radiance expression which holds for low or high intensity continuum sources and at low optical densities is given by:

$$A_{i\to j}{}^{B}F_{k\to l} = \left(\frac{\ell}{4\pi}\right) Y_{P_{kl}} E_{\nu_{ij}} \int_0^{\infty} k_\nu d\nu$$

$$= \left(\frac{\ell}{4\pi}\right) Y_{P_{kl}} E_{\nu_{ij}} \left(\frac{h\nu_{ij}}{c}\right) B_{ij}\, n_i \left(1 - \frac{g_i n_j}{g_j n_i}\right)$$

$$= \left(\frac{\ell}{4\pi}\right) A_{kl} h\nu_{kl} n_k$$

where:

$E_{\nu_{ij}}$ = spectral irradiance of continuum source at frequency ν_{ij}, W m^{-2} Hz^{-1};

$\int_0^{\infty} k_\nu d\nu$ = integrated absorption coefficient over absorption line, m^{-1} Hz;

$B_{ij} = \left(\frac{g_j}{g_i}\right)\left(\frac{c^3}{8\pi h\nu_{ij}^3}\right)$ $A_{ij} = \left(\frac{e^2}{4\varepsilon_0 m h\nu_{ij}}\right) f_{ij}$ = Einstein coefficient of induced absorption, i.e., absorption transitions per spectral energy density per absorbing species, m^3 J^{-1} s^{-1} Hz;

A_{kl} = Einstein coefficient of spontaneous emission, s^{-1};

h = Planck's constant, 6.626 x 10^{-34} J s;

ν_{ij} = frequency of transition occurring from energy level i to energy level j, Hz;

$h\nu_{ij}$ = energy of exciting photon, J.

Using the steady state rate equation approach, where the rate of excitation equals the de-excitation rate and the assumption made previously for Equations (1) - (6), (except for low source intensity), fluorescence radiance expressions can be derived for: continuum source excitation under both high and low spectral irradiances; low optical densities; and atoms which can be approximated by a two-level system or a three-level system (see Figure 4). The general expressions are as follows (69):

Two-level atom, low source spectral irradiance

$$B_F = \left(\frac{\ell}{4\pi}\right) A_{21} h\nu_{12} \frac{E_{\nu_{12}}}{E^*_{\nu_{12}}} \left(\frac{g_2}{g_1}\right) n_T \qquad (7)$$

Two-level atom, high source spectral irradiance

$$B_F = \left(\frac{\ell}{4\pi}\right) A_{21} h\nu_{12} \left(\frac{g_2}{g_1 + g_2}\right) n_T \qquad (8)$$

where:

$$E^*_{\nu_{12}} = E^S_{\nu_{12}} \left(\frac{g_2 + g_1}{g_1}\right) = \frac{cA_{21}}{Y_{21} B_{21}} = \text{modified saturation spectral irradiance, W m}^{-2}\text{ Hz;}$$

Figure 4: a. Two-level atomic system with radiational, A, and radiationless, k, rate constants.
b. Three-level case I (e.g., Na) atomic system with radiational, A, and radiationless, k, rate constants k_{13}, k_{12}, $A_{32} \approx 0$). Left hand diagram is for 1→3 excitation. Right hand diagram is for 1→2 excitation.
c. Three-level case II (e.g., Tl) atomic system with radiational, A, and radiationless, k, rate constants (k_{13}, k_{23}, $A_{21} \approx 0$). Left hand diagram is for 1→3 excitation. Right hand diagram is for 2→3 excitation.
Taken from reference 69.

a.

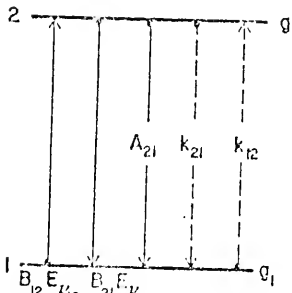
2
g
A_{21} k_{21} k_{12}
1
g_1
$\frac{B_{12}E_{\nu_{12}}}{c}$ $\frac{B_{21}E_{\nu_{12}}}{c}$

b.

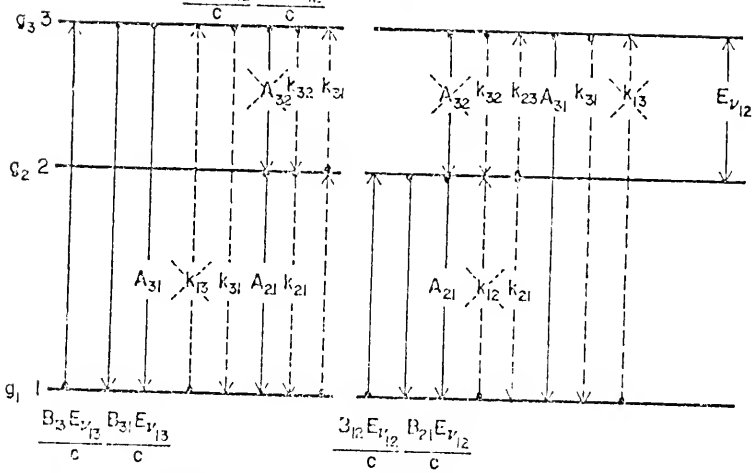
g_3 3
A_{32} k_{32} k_{31}
g_2 2
A_{31} k_{13} k_{31} A_{21} k_{21}
g_1 1
$\frac{B_3E_{\nu_{12}}}{c}$ $\frac{B_{31}E_{\nu_{13}}}{c}$
A_{32} k_{32} k_{23} A_{31} k_{31} k_{13}
$E_{\nu_{12}}$
A_{21} k_{12} k_{21}
$\frac{B_{12}E_{\nu_{12}}}{c}$ $\frac{B_{21}E_{\nu_{12}}}{c}$

c.

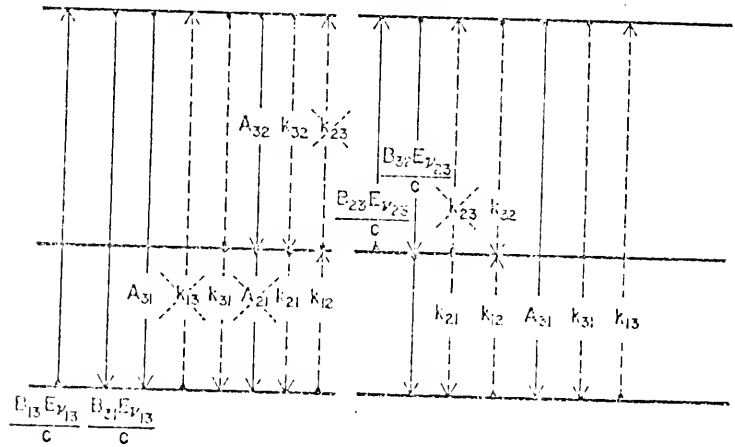
A_{32} k_{32} k_{23}
A_{31} k_{13} k_{31} A_{21} k_{21} k_{12}
$\frac{B_{13}E_{\nu_{13}}}{c}$ $\frac{B_{31}E_{\nu_{13}}}{c}$
$\frac{B_{32}E_{\nu_{23}}}{c}$
$\frac{B_{23}E_{\nu_{23}}}{c}$
k_{23} k_{22}
k_{21} k_{12} A_{31} k_{31} k_{13}

$E^{s}_{\nu_{12}}$ = saturation spectral irradiance (i.e. source spectral irradiance where the fluorescence signal is 50% of the maximum possible value), W m^{-2} Hz:

n_T = total atom population, m^{-3}.

Three-level system

There are two major types of three-level atomic systems: (I) systems where the levels 2 and 3 are close together and radiative transitions between levels 2 and 3 are not allowed e.g., Na; and (II) systems where 1 and 2 are close together and radiative transitions between levels 1 and 2 are not allowed, e.g., Tl. Specific expressions are given by Boutilier et al. (69). More general expressions are as follows:

Case I for 1→3, 3→1 or 1→2, 2→1 [excitation (absorption) transition, from level i to level j (i→j), fluorescence transition from level k to level 1 (k→1)]

low source spectral irradiance ($E_{\nu_{ij}} << E^{*}_{\nu_{ij}}$)

$$B_{F_{(lo)}} = \left(\frac{\ell}{4\pi}\right) A_{kl} h\nu_{lk} \left(\frac{g_j}{g_i}\right) \left(\frac{E_{\nu_{ij}}}{E^{*}_{\nu_{ij}}}\right) n_T \qquad (9)$$

high source spectral irradiance ($E_{\nu_{ij}} >> E^{*}_{\nu_{ij}}$)

$$B_{F_{(hi)}} = \left(\frac{\ell}{4\pi}\right) A_{kl} h\nu_{lk} n_T \left[\frac{1}{1 + \frac{g_i}{g_j} + \frac{k_{km'}}{A_{m'1} + k_{m'1} + k_{m'k}}}\right] \qquad (10)$$

Case I for 1→3, 3 --→2, 2→1 or 1→2, 2 --→3, 3→1

(dashed arrow, --→, denotes radiationless process)

$$B_{F_{(lo)}} = \left(\frac{\ell}{4\pi}\right) A_{kl}\, h\nu_{lk} \left(\frac{g_j}{g_i}\right)\left(\frac{E_{\nu_{ij}}}{E^*_{\nu_{ij}}}\right) n_T \left[\frac{k_{jk}}{A_{kl} + k_{kl} + k_{kj}}\right] \qquad (11)$$

$$B_{F_{(hi)}} = \left(\frac{\ell}{4\pi}\right) A_{kl}\, h\nu_{lk}\, n_T \left[\frac{1}{1 + (1+\frac{g_i}{g_j})\ \frac{A_{kl} + k_{kj} + k_{kl}}{k_{jk}}}\right] \qquad (12)$$

Case II for 1→3, 3→1 or 1→3, 3→2 or 1→2, 2→1 or 2→3, 3→1

$$B_{F_{(lo)}} = \left(\frac{\ell}{4\pi}\right) A_{kl} h\nu_{lk} \left(\frac{g_j}{g_i}\right)\left(\frac{E_{\nu_{ij}}}{E^*_{\nu_{ij}}}\right) n_T \left[\frac{1}{1 + (\frac{g_{m'}}{g_i})\ \exp\ (-E_{12}/kT)}\right] (13)$$

$$B_{F_{(hi)}} = \left(\frac{\ell}{4\pi}\right) A_{kl}\, h\nu_{lk}\, n_T \left[\frac{1}{1 + \frac{g_i}{g_j} + \frac{g_{m'}}{g_j}\exp\ (-E_{12}/kT) + \frac{A_{jm'}+k_{jm'}}{k_{m'i}}}\right] (14)$$

where $E^*_{\nu_{ij}} = \dfrac{cA_{ji}}{Y_{ji} B_{ji}}$;

k_{ij} = radiationless rate constant from level i to level j; and

prime (e.g. m') indicates the energy level not involved in the absorption process.

From the above fluorescence radiance expressions, it is important to point out and stress the characteristic features of laser-excited fluorescence which result in great advantages for analytical atomic spectroscopy (1, 43-69, 88-90).

(1) Attainment of the maximum possible value of the fluorescence signal for a given n_T is reached under saturation conditions, i.e. $E_\nu > E_\nu^s$. If the atomic system closely approximates a two-level system, then the absolute value n_T can be determined if B_F is measured under steady state conditions, i.e., the radiative lifetime of the excited state must be much less than the temporal pulse width of the exciting source. For a three-level system, nonradiational de-excitation rate constants must be known. It should be noted that for high spectral irradiances, $E_\nu > E_\nu^s$, the fluorescence radiance is determined only by well-known atomic parameters and radiationless rate constants; therefore, increasing the source spectral irradiance above E_ν^s will only increase the fluorescence signal by at most a factor of two, while the signal-to-noise ratio obtained under these conditions may deteriorate due to increased noise from larger scatter or molecular fluorescence signals.

The possibility of simultaneous multiple line detection for more complicated (multi-level) atomic systems should not be overlooked as a means to obtain the largest possible fluorescence signal. In this case, fluorescence from more than one atomic transition is allowed to impinge upon the detector.

(2) Increased linear dynamic range of the analytical calibration curve is obtained under saturation or near saturation conditions. The linearity of B_F with n_T (analytical calibration curve) is greater as

E_ν increases because as E_ν increases n_T must increase for $k_\nu \ell$ to exceed 0.05 (high optical density). If the source irradiance is such that the atomic system is saturated at any value of the population density, then the absorption coefficient goes to zero, and no self-absorption occurs, thus making the calibration curve obtained under idealized illumination conditions linear over all concentration ranges. This holds for a continuum as well as for a line source of excitation (67). However, unavoidable tradeoffs in practical situations do not allow the observation of such extended linearity. For example, when the laser beam is focussed at the center of the atomizer, postfilter (self-reversal) effects in the observation path toward the detector certainly have to be included to account for the observed shape of the analytical calibration curve. On the other hand, if the beam is defocussed to illuminate a larger volume of atoms, then the irradiance can decrease to the point where saturation is no longer approached, and therefore, the shape of the curve will resemble that obtained with conventional sources of excitation. Linear dynamic ranges of 5 orders of magnitude are common for laser excited fluorescence. Kuhl et al. (89) compared relative fluorescence curves of growth obtained when lead vapor from a carbon rod atomizer was excited with a hollow cathode lamp, an electrodeless discharge lamp and a dye laser. The linear dynamic range, defined as the ratio of upper to lower concentration limits, found here was 1.25×10^5, 3.33×10^3, and 1×10^3 for dye laser, electrodeless discharge lamp and hollow cathode excitation, respectively. The lower concentration limit corresponds to the detection limit while the upper limit was defined as the lead concentration resulting in a signal whose deviation from linearity did not exceed 5%.

(3) Independence of fluorescence radiance upon the source irradiance and stability occurs under saturation conditions. Under the high source spectral irradiance cases described above, E_ν no longer appears in the equations. As the source irradiance is increased above E_ν^s, the absorption (excitation) process becomes less and less efficient; therefore, source flucuations will produce progressively smaller variations in the excited state atom population. This means that upper level of the fluorescence transition will have a relatively stable population, which will in turn produce a relatively stable fluorescence signal.

(4) Independence of fluorescence radiance on fluorescence quantum efficiency is achieved under saturation conditions. The equations describing the high source spectral irradiance cases do not have a quantum efficiency, Y, dependence. The dependence of fluorescence radiance on quantum efficiency is often quoted as a fundamental and major limitation of the fluorescence process. Therefore, the importance of this consequence is obvious. Also, it means that atomizers with high atomization efficiencies can be used even if strongly quenching species are present in the atomic vapor, (i.e., fluorescence radiance is now independent of flame chemistry whereas at low spectral irradiance, the flame gas composition greatly influences Y). When a high spectral irradiance excitation source is used for fluorescent measurements, the rates of population and depopulation of the excited state become predominantly radiationally induced. When such stimulated processes dominate, any other activation (chemical or thermal) or deactivation (quenching, spontaneous radiation) pathways do not

strongly affect the equilibrium population of the excited state. Consequently, the magnitude of the detected (spontaneous) fluorescence becomes nearly constant (1, 54, 67).

Although not considered in the above fluorescence radiance equations (7)-(14), two other advantages of using high spectral irradiance (laser) sources should be mentioned.

(5) Elimination of prefilter and inner-filter (self-absorption) effects occurs under saturation conditions. The spectral irradiance of the laser output experiences minimal attenuation as it passes through the prefilter region. Also because the absorption coefficient approaches zero as saturation is reached, reabsorption of the fluorescence radiation becomes negligible. The postfilter effect is unaffected by source irradiance.

(6) Elimination of scatter noise limitation is possible by using a nonresonance fluorescence analysis scheme. Generally, resonance fluorescence transitions have higher transition probabilities than nonresonance transitions. However, the higher spectral irradiances of laser sources make nonresonance transitions not only easily detectable, but sometimes the preferred analysis scheme. Also, because lasers emit a single narrow spectral bandwidth line, no frequency selective device is necessary for the exciting radiation.

All of the above advantages (1) - (6) are due to the high spectral irradiances of lasers and are distinct advantages which lasers have over conventional sources (e.g. electrodeless discharge lamps (EDLs), hollow cathode lamps (HCLs), and xenon arc lamps).

(7) Monochromaticity is a distinct advantage of laser sources. The fact that their output is a single monochromatic line, and not a

series of lines or bands due to emission of lines from atomic or molecular vapor and filler gases as is the case with EDLs and HCLs, or a continuum such as that of xenon arc lamps, means that there is no off-wavelength background other than source induced emission in a well baffled (to eliminate stray radiation) detection system.

(8) Narrow spectral bandwidth of the laser output is a tremendous advantage as can be demonstrated by the lack of spectral interferences occurring in laser-excited atomic fluorescence. Laser sources are unique in that they can have spectral bandwidths varying from 20 nm to less than 0.0006 nm. Typically, lasers have bandwidths of ca. 0.01 nm and, therefore, must be considered to be a pseudocontinuum radiation source because their bandwidths are greater than the atomic linewidth in a flame (typically 0.001 nm to 0.005 nm). However, most lasers have available frequency narrowing etalons to reduce the spectral bandwidth at the cost of a reduction in average output power. If the laser output is frequency narrowed so that it becomes a "line" source, the exact expressions for B_F given above in equations (7) - (14) are more complex, but are generally similar. B_F is still linearly related to n_T, but now the source irradiance absorbed is determined by the width and profile of the exciting line and the velocity distribution of the absorbers and the broadening mechanism for the absorbers. Line source excitation has been discussed in literature (62, 67, 91). It should also be noted that the linewidth of the laser output beam is a function of wavelength and beam waist. The linewidth decreases at lower wavelengths. The narrow spectral bandwidth along with a pulsed output allow for the use of a low dispersive or nondispersive spectrometric system in order to gain larger optical collection efficiencies of the fluorescence detection system.

(9) The coherent output of the dye laser with its high degree of beam collimation and directionality, plus the small beam diameter make the laser beam easy to work with from an experimental point of view (e.g. ease of focussing, beam expanding, beam direction, etc.). These factors also make the use of a multipass cell more attractive and viable even for local plasma diagnostics. The small beam diameter of the laser output is considered to be essential in those laser spectroscopic studies where saturation of energy level is required or where spatial diagnostics (e.g., profiling temperature, T, or concentration, n_T) in flames or plasmas are to be probed. A small beam diameter, however, is not necessarily required in (analytical) atomic fluorescence flame spectrometry. In fact, using spectral irradiances greater than the saturation spectral irradiance, E_ν^s, will at most double the atomic fluorescence signal, while the scatter signal will continue to increase linearly with source power, E_ν, i.e., laser power is being wasted and SNR decreased (71, 73). However, assuming the atomic vapor is excited to near saturation conditions with the expanded beam as well as with the beam not expanded, the fluorescence signals will increase in direct proportion to the ratio of the illuminated volumes. Therefore, laser beam expansion with sufficiently high powered lasers is analytically useful because the source irradiance can be optimized (saturation spectral irradiances for each transition should be calculated or experimentally determined in order to determine the best compromise source irradiance to use) (54, 71, 74). Illumination of a larger flame volume excites more analyte (larger volume) and makes the optical alignment of the system less critical. Also, near saturation conditions maintain the benefits

achieved with saturation (67), namely: (i) large signal levels; (ii) large linear dynamic range; (iii) less dependence on source flucuations; and (iv) less dependence on quantum yield.

When pulsed sources are used, the temporal behavior of fluorescence must be considered (54, 67, 73, 74, 88, 92, 93). Practically, a gated detection system is used, so that the detection system is active only during the period of time when the fluorescence signal (radiant flux) is present at the detector. The nitrogen laser pumped tunable dye laser used in this study has a 2-6 ns temporal pulse width. Typical fluorescence lifetimes of atoms in flames are on the order of 1 ns. When the duration of the excitation radiation pulse is comparable to or shorter than the fluorescence lifetime of the upper state of the transition being observed, the steady state assumption does not strictly hold. Also, if laser excitation (i.e., high spectral irradiance) is used and the atomic system approaches saturation under continuum excitation conditions, then an effective lifetime term called the response time, t_L, must replace the spontaneous lifetime, $\tau_L \equiv A_{ij}^{-1}$, in equations describing the temporal behavior of the fluorescence. Short pulses mainly affect the growth of fluorescence radiance (i.e., the rate of population of the upper level). General radiance expressions describing the temporal behavior under high and low spectral irradiance are discussed in literature. The attainment of steady state conditions is governed by the ratio t/t_L where t = any instantaneous time after initiation of the source and $t_L = \tau_L E_\nu^S/(E_{\nu_o}+E_{\nu_o}^S)$, and therefore also by the spectral irradiance of the source. If the spectral irradiance is much less than the saturation irradiance, then t_L is simply the fluorescence lifetime. However, if $E_\nu >> E_\nu^S$, then steady state conditions

are generally achieved and the previous equation holds. In order to compare signal intensities with other systems, the signal, S_F, present at the output of the detector must be multiplied by an effective duty factor, d_{eff}. The exact fluorescence intensity expression under pulsed source-gated detected conditions is complicated because the shapes of the source intensity growth and decay and the detector response during gate opening and closing vary greatly with instrument and time, especially on the very fast time scale required for atomic fluorescence. The effective duty factor for pulsed (p) laser excitation and a gated (g) detection system is given by (74):

$$d_{eff}^{p/g} = \frac{f\{t_g - t_L[1 - \exp(-t_g/t_L)]\}}{1 - \exp(-1/ft_L)}$$

where f is the repetition rate, and t_g is the gate width.

Detection systems for pulsed laser-excited fluorescence generally use a photomultiplier tube to convert the radiant fluorescence flux into an electrical signal. The signal is then processed with either a sampling oscilloscope or a boxcar (gated) integrator. It has been stressed (45, 88, 94-97) that photomultipliers suitable for pulsed operation must possess certain specific requirements such as short transit time of the electron cloud, small transit time spread, short rise time and minimal parasitic capacitance. The photomultiplier tube must also be able to sustain high peak anode currents. For such high currents, the dynode chain must be modified. The laser output can also be monitored with a photodiode. Both the signals

can be fed into a boxcar integrator and the signals can be ratioed. The boxcar integrator essentially performs a sample and hold operation. The sampling time is determined by an appropriate reference pulse which has a definite time difference with respect to the signal. When pulse measurements are performed, the timing and width of the sampling window (gate) are adjusted so as to coincide with the occurrence of the fluorescence signal pulse (67).

For any measurement system, there are nine major noises to consider. These are detector shot noise (e.g., photomultiplier dark current); background shot and flicker noise (e.g., flame background from OH emission): scatter shot and flicker noise (e.g., Rayleigh and Mie particle scatter from flame gases); source induced fluorescence background shot and flicker noise (e.g., CN fluorescence in a nitrous oxide-acetylene flame); and analyte luminescence shot and flicker noise. All other noises such as 60 Hz pickup or radio frequency interference (RFI) noise or noises that arise in the electronic signal processing are system noises not inherent in the signal flux detection [i.e., they occur after the radiant flux strikes the photocathode and, therefore, do not result from signal generated in the sample cell or the photocathode (transducer) surface]. Shot noise is due to the fundamentally discontinuous (quantized) nature of radiation (photons) and electrical current (electrons). Photons arrive at the photocathode randomly even though the overall radiant flux is constant. The same is true for thermionic emission from the photocathode. Signal shot noise has a square root dependence to the signal level. Flicker noises describe the relative flucuations in the signal level and are, therefore, proportional to the signal level. Boutilier et al. (74) have compared

signal-to-noise ratios for pulsed and cw sources in atomic and molecular luminescence spectrometry. Bower and Ingle (98) give a procedure for determining the noise which limits the precision with which a measurement can be made in flame atomic absorption spectrometry. Obviously, the source of the limiting noise is where refinements of the system and/or research should be directed.

(10) The gain for pulsed operation compared to cw operation as proposed by Omenetto et al. (67, 71-73) is an advantage for the N_2 laser pumped dye laser fluorescence system. Assuming that the total noise in a fluorescence setup is due to atomizer-source-detector shot noise, the gain, G, in signal-to-noise ratio due to source pulsing (po) and detector gating as compared to continuous wave operation (cw) of both source and detector can be expressed as follows:

$$G(po/cw) = \{(E_\lambda^P)_{av}/(E_\lambda^c)_{av}\}\{ft_p\}^{-1/2}$$

$$= \{(E_\lambda^P)_{peak}/(E_\lambda^c)_{av}\}\{ft_p\}^{1/2} \qquad (15)$$

in the case of background shot noise limited systems; and

$$G(po/cw) = \{(E_\lambda^P)_{av}/(E_\lambda^c)_{av}\}^{1/2}$$

$$= \{(E_\lambda^P)_{peak}/(E_\lambda^c)_{av}\}^{1/2}\{ft_p\}^{1/2} \qquad (16)$$

in the case of source-related or source-induced shot noise limited systems. Here, $(E_\lambda^c)_{av}$ stands for the average spectral irradiance

$(W\ m^{-2}\ nm^{-1})$ of an excitation source operated in the cw mode and $(E_\lambda^P)_{peak}$ and $(E_\lambda^P)_{av}$ represent the peak and average spectral irradiance of the pulsed source, which is characterized by a pulse duration t_p (s) and a repetition rate f, Hz. The product ft_p is the duty cycle. If the source stability is poor causing flicker noise which is source-related (scatter) or source-induced (molecular fluorescence of flame gas species) signal, then there will be no gain or a reduction of the gain with the pulsed excitation source. For narrow line sources, E_λ is replaced by E_L, the line irradiance, i.e., $E_L = \int_0^\infty E_\lambda d_\lambda$.

As can be seen in Equation (15), the advantages of gated detection appear to be exploited by the high peak power and low duty factor of a N_2 laser pumped tunable dye laser fluorescence instrumental system. The highest average power, $(E_\lambda^P)_{av}$, consistent with the lowest duty factor, ft_p, appears to be the most desirable operating conditions. For resonance fluorescence, the Rayleigh scatter shot noise limit should be approached. For nonresonance fluorescence cases where higher spectral irradiances are tolerable, the lowest detectable signal will be limited by dark current noise, amplifier noise, molecular fluorescence background noise or simply the ability to collect efficiently the fluorescence radiation. However, because not all elements have strong nonresonance fluorescence lines, a system should be designed to optimize as best possible, both resonance fluorescence and nonresonance fluorescence signals in order that the the system be generally analytically useful.

As can be seen in Equation (16), when the system is source-carried shot noise limited, the characteristic advantage of pulsed excitation-gated detection is lost; this case will be encountered in

many resonance fluorescence measurements, as pointed out by some workers (43, 45). Therefore, efforts to reduce the scatter must be made. By laser beam expansion and proper baffling, aperturing and trapping of the optical light path, source-related scatter can be greatly reduced.

(11) Minimization of the emission background noise results from the extremely low duty cycle of the N_2 laser pumped dye laser source ($\sim 10^{-7}$). A narrow gate width ($t_g \simeq 10$ ns) of the boxcar integrator can then be utilized so that the detection system only "views" the flame emission background for an extremely small period of time. The ratio of detector on time to the total analysis time is the duty factor, ft_g.

(12) High optical conductance (i.e., high optical throughput or luminosity, $L = G\tau$) results from the combination of low duty cycle with gated detection (i.e., low duty factor) and the narrow spectral bandwidth of the laser. The former minimizes the emission background, while the latter helps to minimize scatter over the spectral bandpass of the detection system (i.e., negligible scatter exists at wavelengths different from the excitation wavelength). Therefore, low dispersive spectrometric detection systems (e.g., interference filters) can be used. The larger collection efficiency of fluorescence gives high fluorescence signal levels. The spectral resolution of these systems is still excellent because it is determined solely by the spectral bandwidth of the dye laser output.

(13) The wide wavelength tuning range of the N_2 laser pumped dye laser (ca. 217 - 950 nm), particularly its extension into the UV where most of the strong atomic fluorescence lines exist, is of obvious

benefit for atomic excitation. Moreover, this is accomplished through the use of only one source.

(14) Relative ease of wavelength selection and dye changing of the N_2 laser pumped dye laser compared to most other dye laser systems aids greatly in the operation of the system. Most dye laser systems use a flowing dye system which contains ca 4 l of expensive dye solution. However, the N_2 laser pumped dye laser system can operate with only 2 ml of dye solution in a cuvette. Cuvettes on a carousel can be rotated into the laser cavity. Selection of wavelength, then, involves rotating the proper dye solution into place and changing the angle of the grating, which acts as the wavelength selective device and the back laser cavity mirror.

(15) Fluorescence itself must be considered as an advantage to the spectroscopic system. The reasons are inherent to the fluorescence process. First of all, at low concentrations, a low signal level must be detected which is easier than detecting a small change in a large signal level. Second, fluorescence is emitted in 4π steradians. This not only makes optical alignment simpler, but also allows the use of two detectors so that optical conditions for the detection of resonance and nonresonance fluorescence could be optimized separately. Multi-element analysis is also possible using only one source and a slew-scan type system similar to that used by Johnson et al. (99).

From the theoretical and practical advantages described above, the N_2 laser pumped dye laser fluorescence spectroscopic system with gated detection should provide greatly improved analytical figures of merit

CHAPTER III
EXPERIMENTAL

Any fluorescence instrumental system consists of an excitation radiation source, a sample cell, associated optics and a means of detecting the fluoresced radiation. The basic components of the atomic fluorescence flame spectrometric system used in this study are a nitrogen laser pumped tunable dye laser excitation source; a beam expander for increasing the diameter of the dye laser output beam; a pneumatic nebulization sampling system; a flame atom reservoir; a monochromator for wavelength selective radiant flux isolation; a photomultiplier detector and transducer which converts the radiant flux impinging upon the photocathode into a signal current; a boxcar (gated) integrator for signal processing of transient repetitive signals; and a strip chart recorder. A schematic diagram of the present laser-excited atomic fluorescence flame spectrometric system is shown in Figure 5. The experimental components used in the system are described in Table 1, along with their model numbers and manufacturers.

Excitation Source

The nitrogen laser pumped tunable dye laser has many characteristics which make it an apparently ideal excitation source for atomic fluorescence spectroscopy. Many of these characteristics have been indicated in the previous two chapters. Much research continues to be done in the field of dye laser development alone, such as: dye research to extend the wavelength tuning range and lifetime of the dyes and to improve the output power of the dye laser; N_2 laser research

Figure 5: Schematic diagram of laser-excited atomic fluorescence flame spectrometry system

A: N_2 laser, B: dye laser, C: dye laser control unit, D: vacuum pump, E: N_2 laser power supply, F: trigger source, G: beam expander, H: Panel, I: diaphragm, J: burner/nebulizer, K: light trap, L: light trap, M: diaphragm, N: light baffle and lens, O: monochromator, P: photomultiplier detector, Q: recorder, R: boxcar integrator, S: photomultiplier power supply.

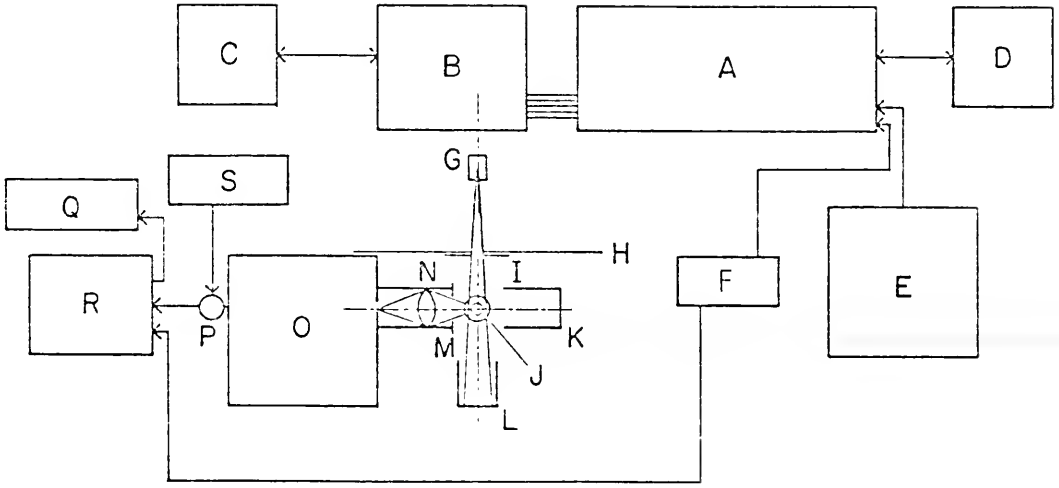
C
B
A
D
G
S
Q
H
N
I
R
P
O
F
E
M
K
J
L

Table 1. Experimental Components of Laser-Excited Atomic Fluorescence Flame Spectrometric System

Component	Model No.	Company Address
Nitrogen laser/power supply	UV-400	Molectron Corp., Sunnyvale, CA 94086
Trigger source	TG-100	
Dye laser	DL 200	
Dye laser control unit	DL-040A and DL-050	
Vacuum pump	Type 1030	Alcatel Vacuum Products, Hanover, MA 02399
Beam Expander	---	Laboratory constructed
Nebulizer and premix burner assembly	303-0110 290-0107	Perkin Elmer, Norwalk, CT 06852
Nebulizer and premix burner assembly	20851-01 42240	Instrumentation Laboraotry Inc., Wilmington, MA 01887
Capillary burner head	---	Laboratory constructed
Monochromator	EU-700	Heath Co., Benton Harbor, MI (now McPherson Inst., Acton, MA 01720)
Photomultiplier	R212UH R818	Hammamatsu TV Co., Middlesex, NJ 08846
Power supply	412B	John Fluke Manuf. Co., Seattle, WA 98133
Boxcar integrator	160 or 162/164	Princeton Applied Research, Princeton, NJ 08540
Recorder	Servo/riter II	Texas Instrument Co., Houston, TX 77006

to optimize its peak power, pulse width, pulse energy, triggering and switching circuit with respect to being used as a pump source for a dye laser and to minimize its radio frequency output so that its operation does not interfere with the operation of sensitive detection instrumentation and also to improve its reliability and stability; and dye laser cavity optics and amplifier configuration in order to obtain the most efficient use of the N_2 laser pump source and to provide continually improved characteristics demanded by spectroscopists. However, because the N_2 laser and the dye laser are commercially available such details will not be discussed. The ease of operation and the dye laser output beam characteristics are of primary interest to the analytical spectroscopist, and these will be described.

The pulsed N_2 laser unit consists of a laser head, power supply, triggering unit, and vacuum pump. The laser head houses the laser discharge channel and high voltage circuit, thyratron (fast switch) pulser circuit, and pressure and N_2 gas control valves. The laser channel is typically operated at 50 torr with the flow of N_2 gas through the channel determined by the pulse repetition rate used. The specifications for the four basic components are given in Table 2. Figure 6 shows the typical peak, rms, and the average power of the Model UV-400 N_2 laser as a function of repetition rate.

The dye laser is based on the Hänsch design (100). Figure 7 shows a schematic of the optical design as viewed from above. The dye laser is transversely pumped by the output of the N_2 laser, which is focussed onto the dye cell with a cylindrical quartz lens. Some of the fluorescent radiation produced in the dye cell travels along the laser cavity, which is formed by the grating (acting as the back

Table 2. Molectron Model UV 400 N_2 Laser Specifications

PULSED N_2 LASER	
Peak Power Output	400 kW @ 20 Hz; 100 kW @ 100 Hz
RMS Power:	190 W @ 50 Hz
Average Power:	130 mW @ 50 Hz
Wavelength:	337.1 nm
Pulse Width:	10 nsec
Repetition Rate:	1 - 100 pps
Beam Dimensions:	6 mm vert.; 25 mm horiz.
Beam Divergence: (Half-Angle)	<1 mrad vert. <7 mrad horiz.
Stability:	±5% power variation @ 100 Hz
Time Delay From Trigger	500 - 1000 nsec
Time Delay Jitter:	<4 ns @ 60 pps
System Leakage:	<1 Torr/s
Gas Supply:	Molectron recommends the use of standard high purity gas (99.9%) or the use of a LN dewar with a built-in gas converter.
PPS-TUV PULSED POWER SUPPLY SYSTEM	
Input Requirements	117 V(ac) nominal, 20 A, 60 Hz
Charging Voltage:	0 to + 30 kV(dc)
Max. Avg. Output Current:	40 mA(dc) @ 100 pps
VACUUM PUMP	
Electrical Service	208/440 V(ac), 3 phase, 60 Hz, 5.2/2.6 Amp
TG100 TRIGGER GENERATOR	
Output Voltage:	-250 V peak
Output Energy:	0.3 mJ
Internal Rate Generator	Variable from 1 - 100 pps
Pulse Rise Time:	0.5 μsec max.
Repetition Rate:	Single pulse to 100 pps
Manual Operation:	Single pulse with local or remote triggering

Table 2. (Continued)

TG100 TRIGGER GENERATOR (con't)	
External Signal Operation:	External pulses +5 to +30 V peak, with maximum 1 μsec risetime into a 50 Ω load
Controls	MODE switch (including power OFF positions), COARSE and FINE pulse rate controls, MANUAL operation pushbutton switch
External Sync Output:	Output pulse of 4 V peak @ 400 μsec is available at the SYNC OUT connector. Sync pulse occurs at same time as output pulse and may be used to trigger an oscilloscope, etc.

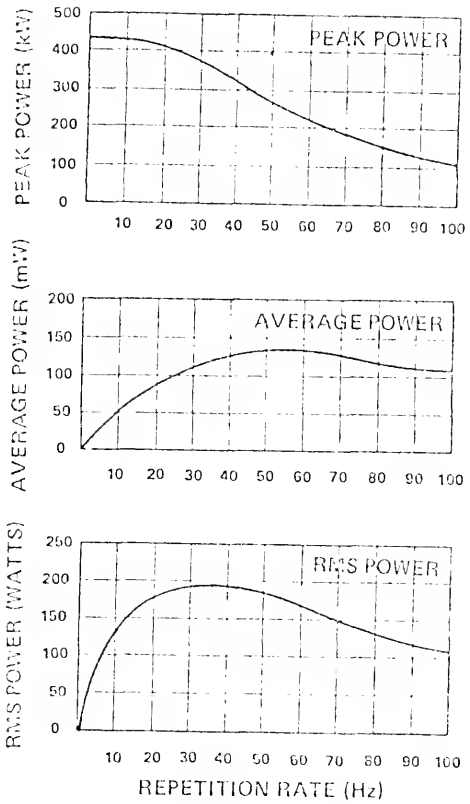

Figure 6: Peak, average, and rms power of N_2 laser vs repetition rate

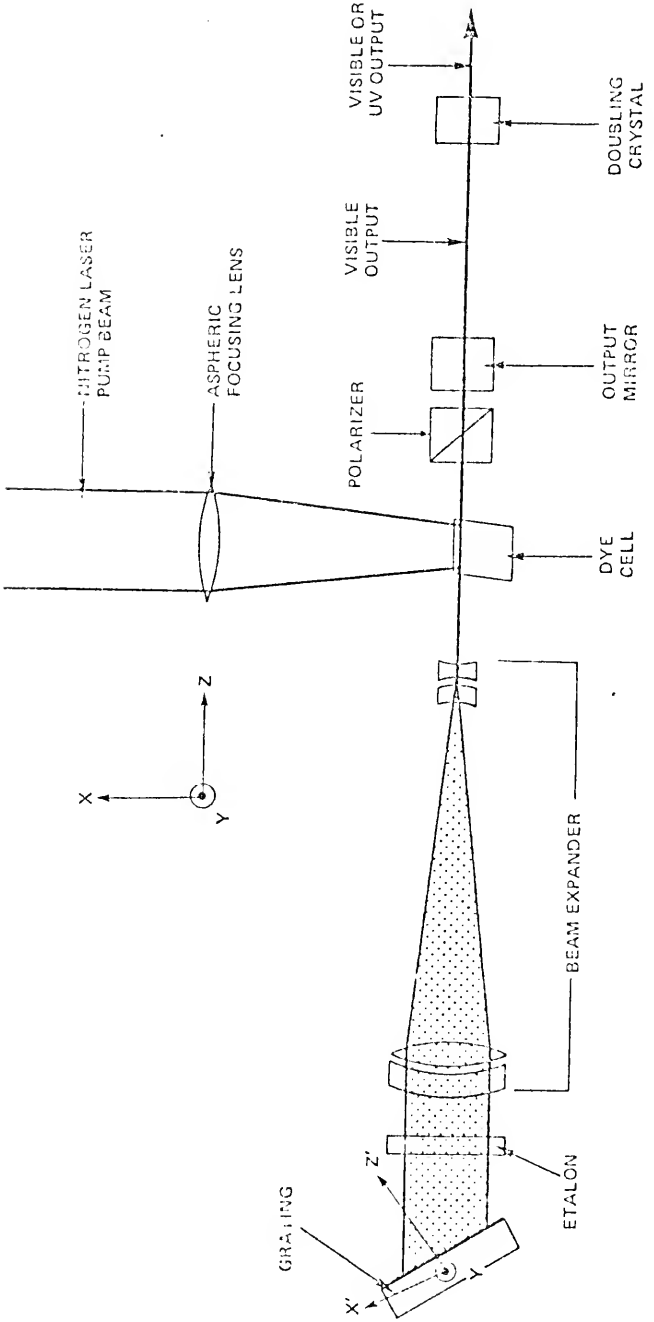

Figure 7: Optical schematic diagram of dye laser cavity

mirror) and the front output mirror. The grating acts as the frequency selective (tuning) device and returns a particular wavelength within the fluorescent emission band of the dye to the dye cell for amplification in the laser cavity. Because the single pass gains are so high with this configuration, only a 4% reflectivity of the front output mirror is required to sustain lasing action. Table 3 lists the specifications for the three available cavity configurations. The DL100 is the basic dye laser consisting of the grating, dye cell, and output mirror. The DL200 adds the beam expander. The beam expanding telescope collects a larger solid angle of radiation from the dye cell; expands the beam so that a larger surface area of the grating is illuminated; and reduces the beam divergence on the grating. This has the effect of increasing the output power, narrowing the bandwidth of the output beam and reducing cavity losses. The DL300/DL400 inserts a Fabry-Perot etalon between the beam expander and grating. This provides an even narrower laser output bandwidth and also improves the frequency stability of the laser cavity; however, it also reduces the output power. Such narrow bandwidths are extremely useful for high resolution spectroscopy because source broadening effects (54) can be essentially eliminated. The mode structure of the laser output beam for this Hänsch-type dye laser has recently been reported (101).

Of particular importance to analytical spectroscopy is the capability to frequency double the fundamental output of the dye laser. The most sensitive lines of many elements lie in the ultraviolet region of the spectrum. However, because the efficiency of frequency doubling is typically 5 - 10%, the dye laser output power

Table 3. Dye Laser Specifications

	DL100	DL200	DL300/DL400	Units
Fundamental tuning range	360-950	360-950	360-950	nm
Frequency doubled range	217-360	217-360	217-360	nm
Bandwidth	10	.4	.3	cm^{-1}
Resolution at 600 nm	.3	.01	.001	nm
Wavelength accuracy-absolute	.3	.1	.1	nm
Wavelength reproducibility	.01	.01	.001	nm
Wavelength stability	.01	.01	.0005	nm/°C
Output power at 460 nm	40	75	8	kw
580 nm	30	55	7	kw
Output pulse energy at 460 nm	225	450	50	μj
580 nm	170	340	40	μj
Amplitude stability	Better than N_2 pump (typically ±5%)		1-2xN_2 pump (typically ±10%)	
Beam divergence at 600 nm	2	2	2	mrad
Beam diameter	.3	.3	.3	nm
Beam polarization	100:1 horizontal or vertical with optional polarizer; otherwise nominally unpolarized			
Background fluorescence	<0.01%	<0.01%	<0.01%	

is considerably reduced. Frequency doubling is accomplished by changing the output mirror to one that can focus the fundamental dye laser beam into one of a series of KDP or KPB nonlinear crystals. The crystal used is determined by output wavelength desired. The crystals are mounted on a rotation device, so that they can be angle phase matched (necessary for frequency doubling to occur). Filters or a prism can be used to eliminate the fundamental beam from the frequency doubled output. Because the nonlinear crystals only double the horizontally-polarized component of the fundamental dye laser beam, a linear polarizer can be inserted into the dye laser cavity in order to maximize the horizontal component and therefore, increase the doubling efficiency. Because the extracavity power is almost equal to the intracavity power, efficient frequency doubling is accomplished through the use of a nonlinear crystal external to the laser cavity, which is far more convenient and less critical.

A scan control unit controls the sine-bar grating drive and a synchronized etalon-tilting mechanism. It also houses the dye cell interchange control. Six dyes can be in cuvettes on a carousel. The dye chosen for the desired wavelength is rotated into the dye laser cavity. Each cuvette contains a magnetic stirrer which is set in motion when the dye cell is being irradiated by the N_2 laser output, so that the dye does not degrade or photodecompose quickly.

The N_2 laser pumped dye laser has the widest continuous tuning range of any laser. In Figure 8, typical dye tuning curves are given. The organic dyes used are listed in Table 4 where the concentrations of the dyes, solvents, and their peak lasing wavelength and wavelength range are also given.

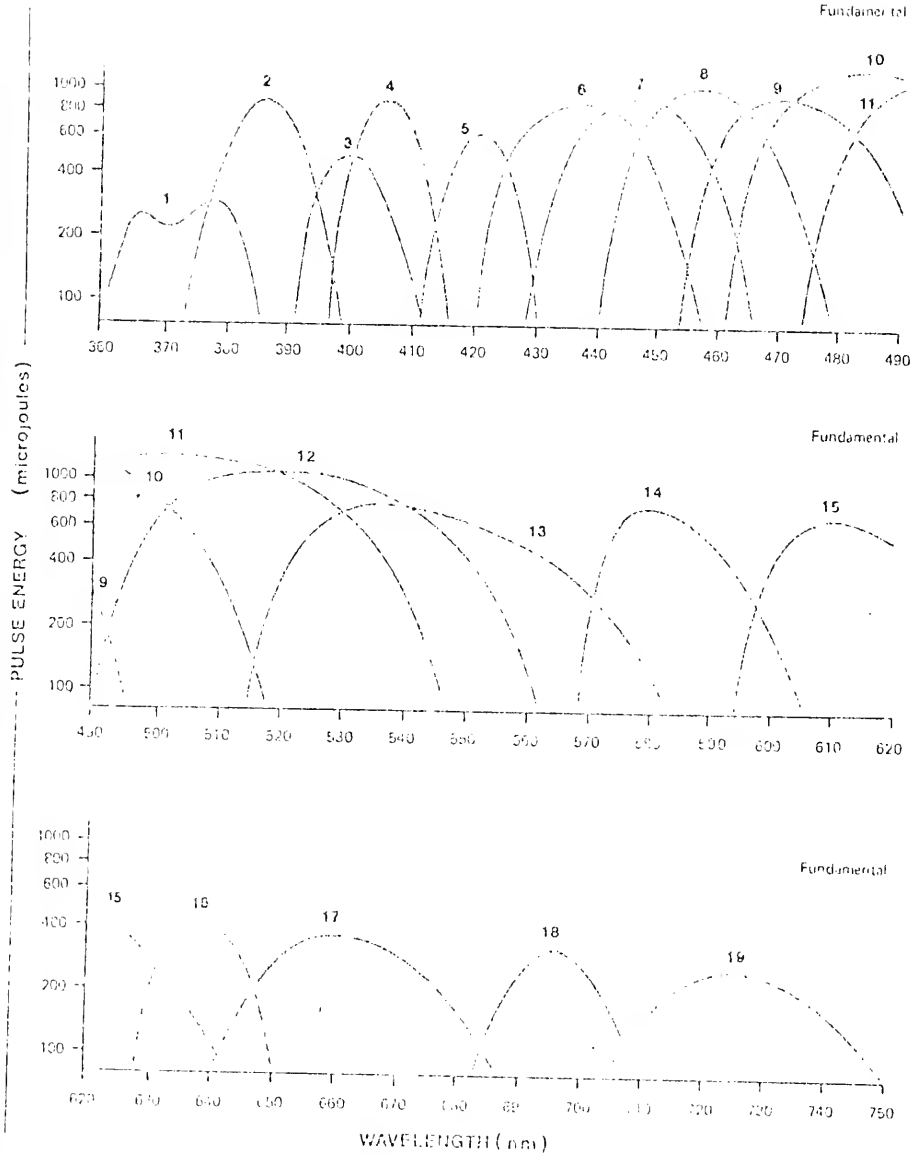

Figure 8A: Wavelength tuning curves for dyes. See Table 4 for dye description.

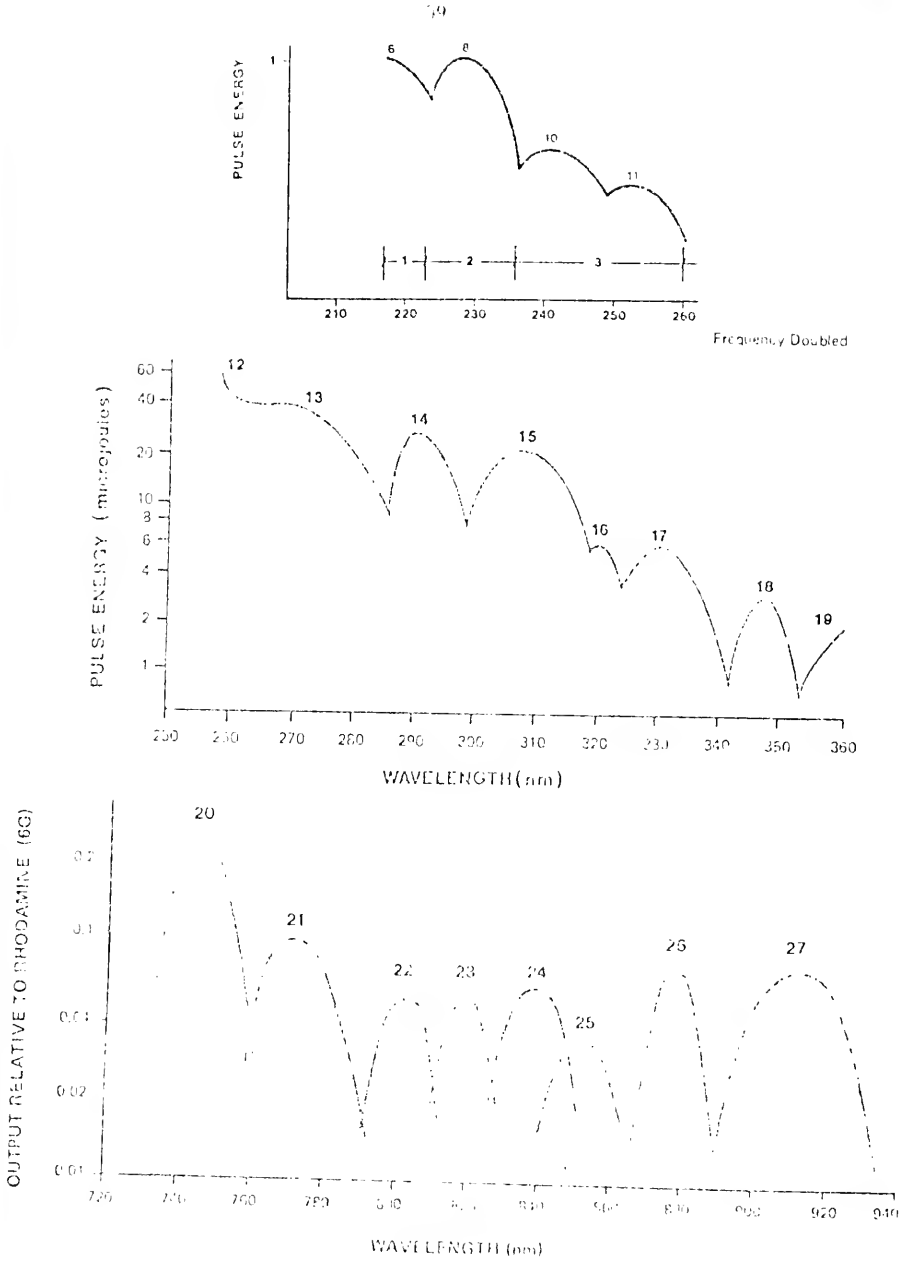

Figure 8B: Wavelength tuning curves for dyes. See Table 4 for dye description

Table 4. List of Laser Dyes[a]

No.	Dye	Concentration (mol/l)	Solvent	Wavelength Peak (nm)	Wavelength Range (nm) (10% points)
1	PPD	5×10^{-3}	toluene/ethanol 50/50	366, 378	360-386
2	BBQ	2.5×10^{-3}	toluene/ethanol 50/50	386	373-399
3	PBBO	5×10^{-4}	toluene/ethanol 70/30	400	391-411
4	DPS	Saturated $<1.2\times10^{-3}$	p-dioxaoe	406	396-416
5	Bis-MSB	1.2×10^{-3}	p-dioxane	421	411-430
6	C120	5×10^{-3}	ethanol	437	420-457
7	C2	10^{-2}	ethanol	446	428-465
8	7D4MC	10^{-2}	ethanol	457	440-478
9	C102	10^{-2}	ethanol	470	453-495
10	7D4TMC	10^{-2}	p-dioxane	483	460-517
11	C500	10^{-2}	ethanol	500	473-547
12	C485	10^{-2}	ethanol	520	490-562
13	C495	10^{-2}	ethanol	536	515-583
14	R6G	5×10^{-3}	ethanol	579	568-605
15	RB	5×10^{-3}	ethanol	609	594-643
16	RB + CVP	2.5×10^{-3} 6×10^{-4}	ethanol	639	628-651
17	R6G + CVP	2.5×10^{-3} 3.3×10^{-3}	ethanol	660	641-487
18	RB + NBAP	3.8×10^{-3} 8×10^{-4}	ethanol	696	683-710
19	RB + OX1P	5×10^{-3} 5×10^{-3}	ethanol	725	705-750
20	OX1P	2×10^{-2}	DMSO	744	730-762
21	DOTC	1.2×10^{-3}	DMSO	770	758-794
22	21 + 24	10:1	DMSO	802	790-815
23	21 + 24	1:1	DMSO	820	812-830
24	HITC	1.2×10^{-3}	DMSO	838	824-852
25	DTTC	1.2×10^{-3}	DMSO	852	840-865
26	IR144	2.5×10^{-3}	DMSO	877	865-890
27	IR125	2.5×10^{-3}	DMSO	916	890-936

[a] From "Molectron Dye List" by Molectron Corp., Sunnyvale, CA 94086.

The characteristics of the N_2 pumped tunable dye laser excitation source are summarized below:

(i) high peak power;

(ii) narrow spectral bandwidth;

(iii) wide wavelength tuning range;

(iv) low duty cycle;

(v) small diameter, nearly collimated, coherent output beam;

(vi) single monochromatic source; and

(vii) ease of wavelength selection.

The advantages derived from these characteristics were discussed in Chapter II.

Detection System

The wavelength selective device used in these studies was a 0.35 m Czerny-Turner grating monochromator with a f-number (i.e., relative aperture) of 6.8. Fluorescence systems, in general, allow the use of low cost, low dispersion monochromators as compared to emission or Raman systems which generally require higher dispersion. Nondispersive fluorescence systems, which allow a greater solid angle for collection of fluorescence radiation, are also attractive possibilities.

The photomultiplier tube (PMT) used for most studies was a R212UH, (which is a high sensitivity variant of the 1P28, more commonly used in UV-Visible spectrometers). As mentioned earlier, photomultiplier tubes used for the detection of fast transient signals must meet specific requirements. They must have a rapid rise time, short transit time, small transit time spread, minimal parasitic capacitance, and be able to sustain peak anodic currents on the order of amperes (80). To provide the best transient response and largest

signal levels, the highest possible high voltage not causing PMT electrical breakdown or excessive dark current should be applied. At high signal levels, care should be taken to ensure that the PMT is still responding linearly to the signal, that PMT fatigue does not occur and that space charge buildup around the last few dynodes is minimal. Modification of the conventional PMT detector base circuit is necessary for high gain, clean transient response, linearity, and prevention of space charge buildup at high currents (88, 96). Impedance matching to avoid pulse distortion, reflections, and reduce ringing is necessary. The use of neutral density filters prior to the monochromator entrance slit was used to extend linearity at high signal levels. At high signal levels the PMT will saturate and respond nonlinearly. Particular care in the above considerations would have to be taken if a nondispersive optical system were used with a high background atomizer.

Coupling the signal from the anode of the photomultiplier to the signal processing device (e.g., gated integrator) is crucial to maintain pulse shape and amplitude and avoid reflections and additional noise pickup (e.g., RFI pickup). Cables should be kept as short as possible, a good ground plane should be maintained, and impedances should be matched.

To take full advantage of the increased gain provided by a high intensity, low duty cycle pulsed excitation source, it is necessary to use a gated detector synchronized with the excitation source. The gated detector used in these studies was a boxcar integrator. The gated integrator is a device that is used to measure and improve the signal-to-noise ratio of repetitive pulsed signals. Any electrical

signal pulse whose intensity is to be measured, but which is too fast to be recorded directly on a strip chart recorder, can be effectively measured and averaged with a gated integrator. The gated integrator is basically an RC integrator with a switch (gate) at the input. When the switch is closed, an input pulse can charge the capacitor. If the switch is opened immediately following the pulse and if the leakage current is small, the capacitor will remain charged. If the RC time constant is much longer than the signal pulse width, t_p, a true time integration of the pulse intensity will occur. However, the capacitor voltage will be reduced from the signal voltage level by the factor t_p/RC. When processing repetitive pulses, the capacitor charge will increase with each pulse as long as the output voltage is less than the signal voltage. Therefore, the integral of many pulses appears on the capacitor, and an averaged value is obtained and displayed at the output of the gated integrator. Because some leakage does occur, the average is weighted towards more recent pulses. Not only does the averaging process improve the SNR by approximately the square root of the number of pulses averaged, but it also ignores all noise signals which occur outside of the gate. Therefore, the main advantage of using gated detection is that the detection system is only active when the pulsed fluorescence signal (i.e., the signal of interest) is present at the detector and that all other noise signals are not processed. Only the noise signals present during the short period the gate is open will be processed. Gated detection also helps eliminate large transients (e.g., RFI) that often plague pulsed systems. A trigger signal is necessary to synchronize the boxcar integrator to the laser output pulse (and therefore the fluorescence

signal). This can be accomplished by either using the "sync pulse" from the laser trigger unit or by beam splitting off a small fraction of the laser output onto a high speed photodiode and using the photodiode signal pulse to trigger the boxcar integrator.

The PAR Model 160 and Model 162/164 boxcar integrators use these sampling and averaging techniques to extract synchronous waveforms from noise. They synchronously sample the input signal with a variable gate width, and a variable gate delay, which can be fixed at any point on or slowly scanned across the input signal. That signal which is passed by the gate is averaged by variable time constant integrators, the output of which is the average of some number of repetitions of the input signal over the gate width interval. Because the average of noise over a large number of repetitions is zero, an improvement in signal to noise occurs. If the gate is fixed, the output rises asymptotically toward the amplitude of the input signal. The boxcar integrators used here are sophistocated instruments whose operation is complex; many inter-related and often subtle factors must be considered for achieving optimum performance for the detection of fast transient signals. In particular, the time constants used must be suitable for analytical work, and the settings should yield the highest possible signal-to-noise improvement ratio and precision with respect to the chosen time constants.

Pulsed lasers used as excitation sources present many problems which can be solved by a gated integrator. The troublesome characteristics of pulsed lasers are: pulses are very short (2 - 8 ns); pulse-to-pulse reproducibility is poor (flucuations as large as 10% are common); long term drift can be severe; electrical pickup can be comparable to

or larger than the desired signal voltage; jitter in the time between triggering and laser pulse can be significant; and repetition rates are low (1-100 Hz). Some of these problems are solved directly by using a gated integrator. Others may be solved by the use of combinations of integrators or signal processing followed by integration. As mentioned previously a single gated integrator rejects any signals or electrical noise occurring outside the gate. Also, an integrator with a small leakage current is not bothered by low repetition rates. Further SNR improvements can result from using two integrators. A small fraction of the incident laser excitation beam may be split off using a small quartz flat. This fraction of the laser beam is allowed to impinge upon a photodiode, and the signal from the photodiode is fed into one integrator (reference channel). The fluorescence signal processed by the other integrator may then be ratioed to the reference channel. This provides a correction for both pulse-to-pulse laser intensity fluctuations and long term drift as long as the fluorescence signal remains on the linear portion of the saturation irradiance curve (i.e., the log-log plot of fluorescence intensity vs source spectral irradiance). Few integrators can respond accurately to the 3 - 10 ns fluorescence signal pulse produced from the N_2 laser pumped dye laser excitation pulse. The minimum gate width of the boxcar integrators used in this study was 10 ns. Although the ideal gate width would exactly match the fluorescence signal pulse, the wider 10 - 15 ns gate width was found to be necessary to compensate for jitter and drift in the time between the trigger pulse and the signal pulse. Another way to avoid jitter problems and improve the SNR can be realized by signal processing followed by gated integration.

The signal processing consists of preintegration, amplification, and pulse stretching. Stretching the pulse out to 1 - 5 μs will allow the integrator to perform more effectively and will also reduce the effective noise bandwidth and increase the charging duty factor. Pulse stretching is generally followed by pulse shaping, during which high frequencies are attenuated.

Experimental Conditions and Procedure

The nitrogen laser (Model UV-400, Molectron Corp.) was operated under the following conditions: applied high voltage 26 - 28 kV; pressure of nitrogen in laser channel 50 torr; and repetition rate 20 Hz. The N_2 laser had a 10 ns pulse width and ca 400 kW peak output power at 337.1 nm. The dye laser, which was pumped by the N_2 laser, had 6 dye cells mounted in a carousel which rotates the desired dye cell into the optical path of the laser cavity. Each cell contained ca 2 ml of dye solution, which is magnetically stirred during operation. The output of the dye laser had ca 3 - 8 ns pulse width and ca 1 - 80 kW peak power depending upon the dye and wavelength. The beam diameter of the dye laser output was ca 0.3 mm. A beam expander/ spatial filter was placed in the optical path of the dye laser beam. The beam expander was mounted on a support with fine x, y, z adjustments. The pinhole (spatial filter) could be used to minimize the fluorescence background of the dye laser output and also produced a more spatially homogeneous excitation beam of radiation. The beam diameter at the flame position was expanded to about 5 mm. A panel fitted with an adjustable diaphragm was placed between the beam expanded and burner. As will be seen and discussed in Table 5, this panel with diaphragm played an important role in minimizing the fluorescence background and the stray or scattered light of the laser beam.

A standard capillary burner head 10 mm in diameter (about 50 capillaries of 1 mm i.d. for the air/C_2H_2 flame and of 0.84 mm i.d. for the N_2O/C_2H_5 flame, arranged into an area 10 mm in diameter) was used with an inert gas sheath which provides flame "separation" (84). The burner head was mounted on either a Perkin-Elmer chamber/nebulizer assembly or an Instrumentation Laboratory chamber/nebulizer assembly. The entire burner system was placed on an adjustable mount which allows x, y, z, θ positioning of the burner system. Flame gases were passed through calibrated rotameters after two-stage regulation at the cylinders. Before the flow meter, the acetylene gas was passed through a trap of charcoal (for elimination of acetone vapor) and a phosphine (PH_3) trap (for elimination of phosphine included in commercial acetylene gas as an impurity)(102-104). Air was passed through a trap of Drierite (for removal of water vapor, The W.A. Hammon Drierite Co., Xenia, OH 45385). The flow rates of the flame gases passed through rotameters were calibrated with a linear mass flowmeter (Model ALK 50k, Hastings-Teledyne, Hampton, VA).

The fluorescence was imaged on the monochromator entrance slit through a lens (76 mm focal length, 50 mm diameter), which was mounted inside a light baffle. The light baffle (60 mm i.d.) had an adjustable diaphragm (30 mm i.d. maximum) mounted on the front and also allowed for positioning of the lens. The diaphragm was set to optimize the fluorescence signal with respect to the scatter. The monochromator was a 0.35 m focal length Czerny-Turner grating spectrometer (2.0 nm/mm reciprocal linear dispersion, 1180 lines/mm grating blazed at 250 nm).

The detection system consisted of a photomultiplier tube, a boxcar integrator, and a chart recorder. The electronic circuit for the

photomultiplier base was the same as the one previously used by Fraser and Winefordner (45). The photomultipliers were operated at 1000 V for the R212 UH and 1200 V for the R818. The boxcar integrators (PAR Model 160 or Model 162/164) were operated with 50Ω input, an aperture time ca 15 ns, and for the Model 160 an observed time constant between 0.5 s and 5 s with 50 mV to 10 V imput sensitivity, and for Model 162/164 an observed time constant for the gated integrator (Model 164) of 3 s and the main frame (Model 162) time constant 0.1 ms to 1 s, with an input sensitivity of 100 mV.

The gas flow rates were ca 2.3 l-min^{-1} of acetylene and 12.3 l-min^{-1} air for the air-acetylene flame, and ca 6 l-min^{-1} of acetylene and 10.6 l min^{-1} of nitrous oxide for the nitrous oxide-acetylene flame. Most measurements were performed under slightly fuel-rich flame conditions. The atomic fluorescence signals were maximized by changing the flow rate of acetylene in both of the flames. Argon gas with ca 10 - 15 l-min^{-1} flow rate was used for flame separation in both of the flames. An 800 or 1000 μm slit width of the monochromator was used in most resonance fluorescence cases, unless scatter and background noises were found to be small, in which case 2000 μm slit widths were used. In most nonresonance fluorescence cases and most cases in the UV (<350 nm), 2000 μm slit widths were used.

After optimization of the experimental arrangement and conditions, analytical curves were measured for each at their atomic fluorescence lines in suitable flames. The rms noise levels were evaluated by measuring 1/5 of the observed peak-to-peak noise on the baseline (98) while aspirating deionized water (blank). The detection limits were then evaluated by extrapolating the analytical curves to a signal-to-noise ratio of 3 (77).

All the chemicals used were reagent grade. Stock solutions of each element (1000 $\mu g\text{-}ml^{-1}$) were prepared in accordance with the procedure given by Smith and Parsons (105). Deionized water was used as a blank solution in all the experiments.

CHAPTER IV
PULSED LASER-EXCITED ATOMIC FLUORESCENCE

Based upon the preceding considerations, a pulsed N_2 laser pumped tunable dye laser should provide nearly an ideal source for atomic fluorescence spectroscopy. The flame has proven to be the most common and convenient atomization source in atomic spectroscopy. Combining the above with a gated detection system to greatly improve the signal-to-noise ratio (SNR) should produce results which surpass any other analytically useful method for trace elemental analysis. The results previously obtained were only comparable to those obtained by other atomic methods. In this study, the experimental arrangement and conditions were investigated in order to optimize the analytical results. Analytical calibration curves were obtained for 23 elements and 37 transitions, many of which lie in the UV region of the spectra and, therefore, require frequency doubling of the dye laser output. Several analytical figures of merit are discussed for the method of pulsed laser-excited atomic fluorescence flame spectrometry.

Optimization of System

Reduction of Scatter Signal

As mentioned earlier, the characteristic advantage of the pulsed excitation-gated detection system is lost when the fluorescence signals are limited by source-carried (scatter fluorescence background) shot noise. This circumstance can be avoided by using nonresonance atomic fluorescence lines. However, because many elements such as

Ba, Ca, Cd, Li, Mg, Na, and Sr (mostly alkali and alkaline earth elements) have only one strong resonance fluorescence line, source-carried shot noise can deteriorate their detection limits. In order to overcome this situation for resonance fluorescence lines, an effort to reduce the scatter noise and optimize the optical system was made in the present experiment.

The experimental system used for the optimization study is shown in Figure 9, and the results are summarized in Table 5. In these studies, strontium was chosen as a typical element which only has available a resonance atomic fluorescence line. As can be seen from Table 5, the use of a focussing lens between the dye laser and the flame does not improve the SNR because of the low signal levels and the large scatter signal levels. The low signal level in case (i) is due to the excitation and observation of smaller flame volume. The use of a panel with a diaphragm mounted on it and a light trap (cases (ii)-(iv) in Table 5) reduced the scatter signal level to almost half of that in case (i); this indicated that the scatter signal observed in these cases was due to the scattered light reflected by the surroundings, not due to the unvaporized particles in the flame. It should be stressed here that the addition of only the beam expander (case (v)) without a spatial filter enhanced the atomic fluorescence signal, but also increased similarly the scatter signal. The large scatter signal, which varied with wavelength, was clearly a result of radiation scattered by the surroundings. However, the panel and the light trap which were set at the positions shown in Figure 9 reduced the scattered signal level as well as the noise level. Therefore, the best SNR was obtained in case (xii), where the beam expander, the panel, and the light trap

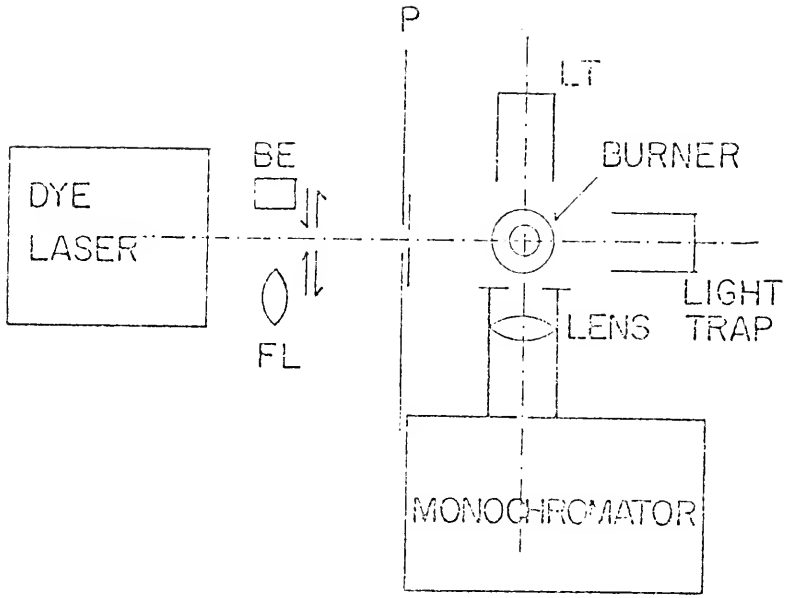

Figure 9: Optical arrangment around the burner for the examination of optimization of the optical system (see Figure 1 and Table 30)

FL: focusing lens for laser beam (focal length 17.8 cm),
BE: beam expander, P: panel with diaphragm, LT: light trap.

Table 5. Optimization of Optical Arrangement in Laser-Excited Atomic Fluorescence Spectrometry[a]

Code	Optical Arrangement[b]	Signal[c] S	Noise[c] N	Scatter[c] Sc	S/N	S/Sc
(i)	FL	12	1	76	12	0.16
(ii)	FL, P	12	1	45	12	0.27
(iii)	FL, LT	12	1	35	12	0.34
(iv)	FL, LT, P	12	0.8	38	15	0.32
(v)	BE	48	3	145	16	0.33
(vi)	---	21	0.8	48	26	0.44
(vii)	LT	22	0.8	32	27	0.7
(viii)	P	23	0.8	45	29	0.6
(ix)	P, LT	25	0.8	42	31	0.6
(x)	BE, LT	41	0.7	27	59	1.5
(xi)	BE, P	41.5	0.4	6.5	104	6.4
(xii)	BE, P, LT	42	0.3	3.5	140	12

[a] A solution of 0.1 ppm Sr was used. Experimental conditions and instruments were described in the previous chapter.

[b] See Figure 9. In the optical arrangement, each device or a combination of the devices was set around the burner (flame), as can be seen in Figure 9.

[c] Relative units.

were simultaneously used. According to this optical arrangement, the SNR was improved by more than a factor 10, and the fluorescence signal-to scatter signal ratio by about a factor 75, compared to those obtained by the use of only a lens (case (i)), as can be seen in Table 5. As a result of these studies, the optical arrangment of case (xii) was employed in all of the following experiments. It should be noted that a rigorous comparison was not attempted, because arrangement (xii) proved to be significantly superior. Considerations such as reflection losses at lens surfaces, the laser beam shape, variation in laser intensity with time, collection efficiency, etc., needed to compare the arrangements on an absolute basis were not taken into account.

The scatter signals for many analyses using arrangement (xii) were found to be very small and due mainly to scatter from the environment (not the flame). Due mainly to the lower output and the lower reflectivity of surrounding materials in the frequency double range, scatter was found to be negligible for lines in the 220-330 nm range.

Slit Width vs SNR

For most spectral measurements using conventional dispersive spectrometers, relatively narrow spectrometer slit widths must be used to distinguish the analyte signal from the signals of other elements and background components; this leads to collecting less signal with the monochromator-detection system (i.e., lower optical conductance). The spectral narrowness of the source allowed larger slit widths to be used with only a solid angle consideration for collection of scattered light at resonance wavelengths (i.e., additional radiation from a spectral continuum or inert gas lines does not exist and the fluorescence background of the laser beam is orders of

magnitude smaller and can be minimized and spatially filtered if necessary). The fact that the laser is a single tunable source with only one narrow spectral line emitted is a primary advantage for atomic analysis. Recently, interferometric and multiplex instruments which permitted the use of a wide slit width (Jacquinot advantage) have been investigated in order to overcome the disadvantage of conventional dispersive spectrometers mentioned above. However, these situations are not valid when the analyte signal can be spectrally differentiated from any background by other means (106, 107).

In laser-excited atomic fluorescence spectrometry, signal selectivity depends upon the spectral bandwidth of the laser output, not upon the spectral bandwidth of the monochromator. An example of signal selectivity is shown in Figure 10 (a) in terms of the excitation of sodium D lines (doublet separated by 0.6 nm). The spectral bandwidth of each line is ca 0.03 nm despite the use of an 800 μm monochromator slit width, i.e., spectral resolution is better than 0.03 nm, which is determined only by the spectral bandwidth of the laser output (a spectral profile of sodium atomic fluorescence observed by wavelength scanning the monochromator spectromether is shown in Figure 10 (b), where an 800 μm slit width was used). Because the emission signal of sodium is essentially negligible due to the low duty factor (3×10^{-7} here) of the pulsed source-gated detection system, wide monochromator slit widths can be used in the present instrumental system. The spectral purity of the source is seen in Figure 11 more clearly, where the fluorescence signal vs slit width is shown in terms of sodium (resonance atomic fluorescence; excited at 589.0 nm and observed at 589.0 nm) and thallium (both of resonance and nonresonance atomic

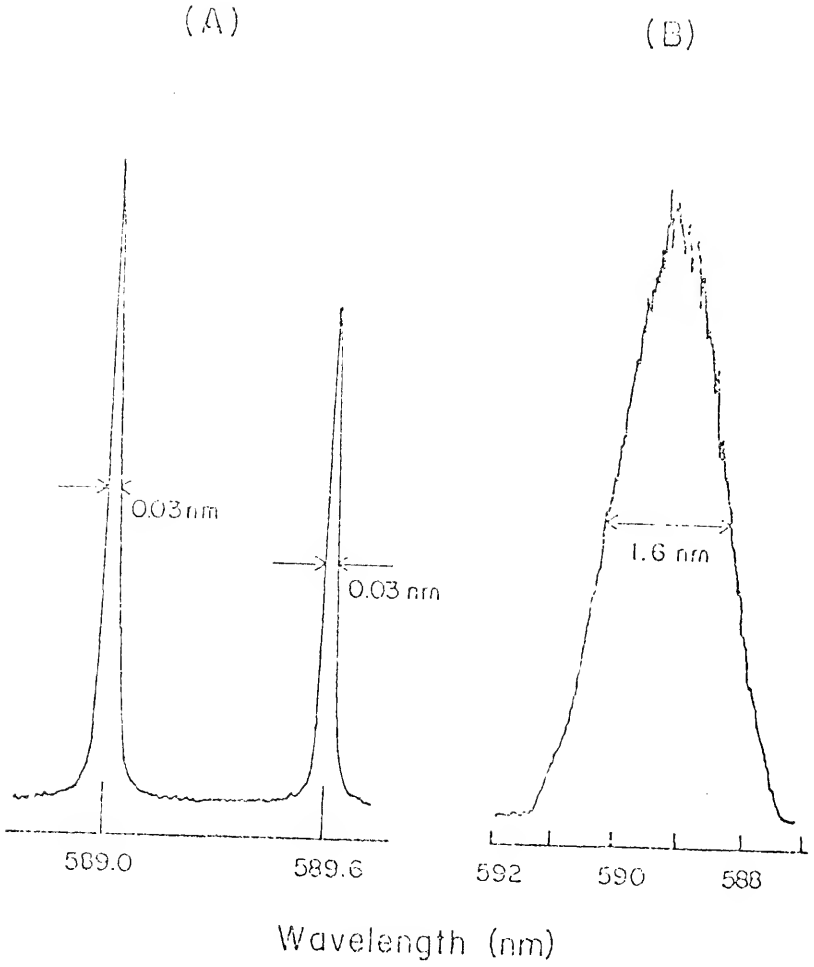

Figure 10: Excitation and fluorescence profiles of sodium D lines (at 589.0 and 589.6 nm) in the air-acetylene flame

(A) Profile observed by scanning the laser
(B) Profile observed by scanning monochromator
Slit width was 800 μm in both cases

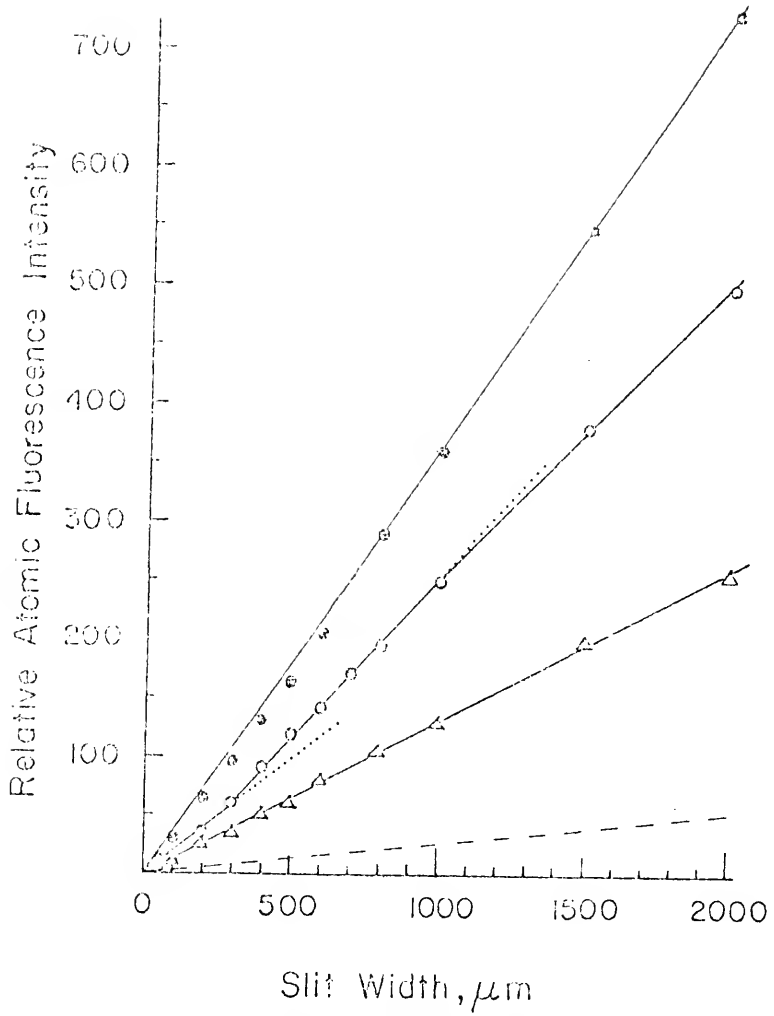

Figure 11: Dependence of atomic fluorescence signal of Na and Tl on slit width observed in the air-acetylene flame

-◇- : resonance fluorescence of sodium. Excited at 589.0 nm, observed at 589.0 nm (---: Scatter level)

● : resonance fluorescence of thallium
Excited at 377.6 nm, observed at 377.6 nm

△ : nonresonance fluorescence of thallium
Excited at 377.6 nm, observed at 535.0 nm

fluorescence; excited at 377.6 nm and observed at 377.6 nm and 535.0 nm; respectively). As can be seen in Figure 11, all fluorescence signals increase almost linearly with increase of slit width. In the case of sodium, the curve has three different slopes in the ranges of 0-300 μm, 300-1000 μm, and >1000 μm. This can be interpreted as follows. Spectral overlap between the lines at 589.0 nm and 589.6 nm takes place with the slit width wider than 400 μm, i.e., both of the sodium D lines are observed by the spectrometer with the wide slit width (simultaneous multiple line observation). This gives the larger signals (i.e., a larger slope in Figure 11) observed by spectrometer in the slit width range 300-1000 μm. The simultaneous multiple line observation suggests another advantage of laser-excited atomic fluorescence spectrometry, when multiplet lines of each element are within the slit width used (e.g., Mn), in that greater signal levels are easily obtainable. In Figure 11, the slope of the curve for sodium becomes smaller for slit widths exceeding 1000 μm slit width because of saturation of the photomultiplier (anodic current); saturation was evaluated by using the neutral density filters to reduce the signal to the photomultiplier detector. For analyses at high concentration, the monochromator slit width could also be reduced to minimize saturation of the photomultiplier.

In Figure 12, the curves of SNR vs slit width are shown in the cases of sodium and thallium, which were observed under the same experimental conditions as those in Figure 11. For both the Na and Tl resonance cases, the SNR's reach plateaus at slit widths between 800 μm and 1000 μm. Therefore, the system becomes source-carried noise limited above a slit width of 1000 μm in the present experimental

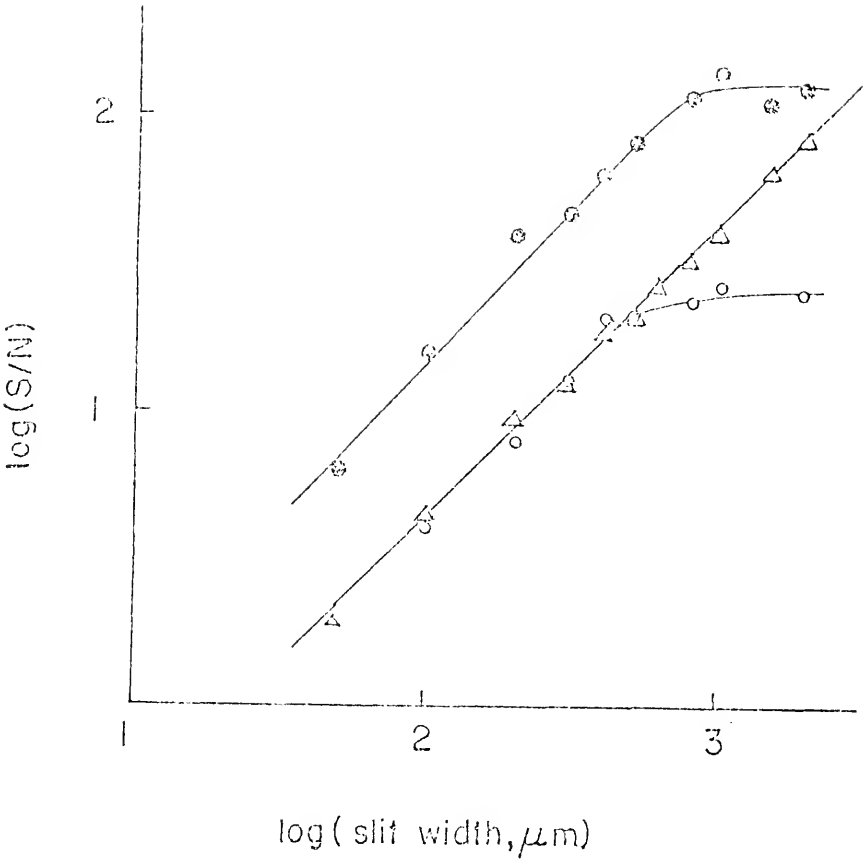

Figure 12: SNR vs Slit width of Na and Tl in the air-acetylene flame

○ : resonance fluorescence of sodium
Excited at 589.0 nm, observed at 589.0 nm

● : resonance fluorescence of thallium
Excited at 377.6 nm, observed at 377.6 nm

△ : nonresonance fluorescence of thallium
Excited at 377.6 nm, observed at 535.0 nm

arrangement, and Equation (16) applies. Scatter signal levels are shown in Figure 11 for Na. Considerations which determine the optimum monochromator slit width in atomic fluorescence are (i) type of transition; (ii) source irradiance; (iii) optical configuration (i.e., efficiency of signal collection and degree to which system is baffled and apertured to eliminate environmental scatter); (iv) saturation of photomultiplier anode current; (v) flame background fluorescence; and (vi) spectral bandwidth of source radiation and spectrometer. In the present experimental arrangement, an 800 or 1000 μm slit width provides a generally useful setting, because the scatter noise limit is approached here as determined experimentally for Na and Tl by the SNR vs slit width plot (Figure 12).

However, in the nonresonance case, no leveling off of the slope in SNR vs slit width curve was observed. This indicates that the signal was not source-carried noise limited (Equation (15) approximately applies here). Therefore, for nonresonance fluorescence, a nondispersive system, using, for example, only interference filters and neutral density filters before the photomultiplier, should yield the optimal system (i.e., lowest limit of detection and largest linear dynamic range). It should also be noted that because fluorescence is emitted in 4π steradians, a system could be designed using two detectors and two optical arrangements to optimize both resonance and nonresonance signals with little added expense or inconvenience.

Flames

Flame conditions were adjusted to give the maximal signal. For most elements in either air/C_2H_2 or N_2O/C_2H_2 a slightly fuel-rich flame with its good reducing properties yielded the best results in

atomic fluorescence spectrometry. A more fuel-rich flame was used in some cases (e.g., Al, Bi, Cr). A fuel-lean flame yielded slightly better results for Ni, Ag, Cu. The flame height at which the atomic fluorescence measurements were taken was ca 20-30 mm above the burner head. The position of the exciting beam in the flame was not extremely critical due to the larger beam diameter. No significant difference in signal intensity or SNR was observed between the "separated" or "unseparated" flames (i.e., use of an inert sheath gas around the flame does not appear to be necessary).

Air-acetylene and nitrous oxide-acetylene flames were used here because of their relative freedom from matrix interferences, good atomization characteristics, and simple procedure for safe utilization.

Analytical Figures of Merit

Limits (Powers) of Detection

The usefulness of any analytical method is given by its figures of merit. The limits of detection are the most often quoted figure of merit because these values indicate the detection power of the technique. For proper choice of a method for any analysis, it is necessary to compare the limits of detection of all possible methods. Therefore, limits of detection will be mainly discussed in the following discussion.

The detection limits and analytical curves were obtained for 23 elements, including 37 transitions, and 7 different fluorescence processes. Ten elements were observed using the frequency doubled dye laser output, most of which represent the first time these transitions have been observed by laser-excited atomic fluorescence. The work also demonstrates the wide tuning range of the N_2 laser pumped dye laser

as a single line source for atomic spectrometry as elements from Cd at 228 nm to Li at 671 nm were observed.

The limits of detection have been improved by a factor of ca 10-200 times over those previously obtained with a N_2 laser pumped tunable dye laser system for all elements examined, except cobalt. The linearity of the analytical curves has also been extended to about five orders of magnitude for almost all elements examined. These results are presented in Table 6 together with all pertinent data and conditions necessary for discussing detection limits except for the system time constant which was 1 s for most cases. In all cases, at least five time constant intervals were allowed before signals were measured. The noise level was evaluated by taking 1/5 the peak-to-peak noise over at least a 50 s time period when only the blank was being aspirated (98). This approach was equivalent to calculating the standard deviation of 16 separate measurements for evaluating the noise, N. The limit of detection (LOD) was calculated on the basis of a signal-to-noise (SNR) equal to three [as recommended by IUPAC (77)]. However, it should be noted that, it is generally accepted that a SNR $\geq$ 10 should be used for practical determination.

In Tables 6 and 7, the results are compared with previous laser-excited fluorescence studies in flames, and with the best values for the limit of detection obtained by conventional source flame atomic fluorescence (AF), flame atomic emission (AE), flame atomic absorption (AA), and by atomic emission induction coupled plasma (ICP). It should be noted that all limits of detection except those determined in the persent work were based on a SNR = 2 value. In Table 7, it is clearly shown that laser-excited atomic fluorescence flame spectrometry

Table 6A. Detection Limits by Laser-Excited Atomic Fluorescence Flame Spectrometry (Experimental Conditions and Spectral Parameters)

Element	EX/FL* (nm)	FL[a] (cm^{-1})	Type of AF[b]	gf value[a]	Dye[c]	Flame Type[d]	Slit Width (mm)
Ag	328.1	0-30473	RF	0.53	(R6G+CVP)	A/A	2.0
Al	394.4	0-25348	RF	0.15	PBBO	N/A	---
	396.1	112-25348	E-RF	0.31	PBBO	N/A	1.0
	394.4/396.1	0-25348/112-25348	S-DLF	0.15/0.31	PBBO	N/A	2.0
Ba	553.7	0-18060	RF	0.90	C495	A/A	0.8
	553.7	0-18060	RF	0.90	C495	N/A	2.0
Bi	306.8	0-32588	RF	0.99	(RF)	A/A	1.0
Ca	422.7	0-23652	RF	0.20	Bis-MSB	A/A	0.8
Cd	228.8	0-43692	RF	0.92	(7D4MC)	A/A	2.0
Co[e]	357.5/347.4	816-28777/0-28777	AS-DLF	0.22/0.64	PBD	A/A	2.0
	230.9	0-43295	RF	0.54	(7D4MC)	A/A	2.0
Cr	359.3	0-27820	RF	1.4	PBD	A/A	1.0
Cu	324.7	0-30784	RF	0.64	(RB+CVP) or (R6G+CVP)	A/A	2.0
Fe	296.69/373.49	0-33695/6928-33695	S-DLF	0.51/4.2	(R6G)	A/A	2.0
Ga	403.3	0-24788	RF	0.24	DPS	A/A	0.8
	403.3/417.2	0-24788/826-24788	S-DLF	0.24/0.53	DPS	A/A	0.8
In	410.4	0-24373	RF	0.47	DPS	A/A	0.8
	410.4/451.1	0-24373/2213-24373	S-DLF	0.47/0.66	DPS	A/A	0.8
Li	670.8	0-14904	RF	0.80	R6G+CVP	A/A	2.0
Mg	285.2	0-35051	RF	1.1	(C495)	A/A	1.0
Mn	403.1	0-24803/0-24802	RF	0.33/0.33	DPS	A/A	0.8
	279.5	0-35770/0-35770	RF	0.97/0.97	(C495)	A/A	2.0
Mo	379.8	0-26321	RF	0.94	BBQ	N/A	0.8
	390.3	0-25614	RF	0.47	BBQ	N/A	1.0
Na	598.0	0-16973	RF	0.95	R6G	A/A	0.8
	589.6/589.0	0-16956/0-16973	TA-SLF	0.47/0.95	R6G	A/A	0.8
Ni	232.0	0-43090	RF	0.86	(7D4MC)	A/A	2.0
	361.9/352.4	880-28569/205-28569	E-AS-DLF	0.15/0.85	PBD	A/A	2.0
Pb	405.8	10650-35287	E-RF	2.3	DPS	A/A	0.8
	405.8/283.3	10650-35287/0-35287	AS-DLF	2.3/0.22	DPS	A/A	0.8
	283.3	0-35287	RF	0.22	(C495)	A/A	2.0
	283.3/405.8	0-35287/10650-35287	S-DLF	0.22/2.3	(C495)	A/A	2.0
Sr	460.7	0-21698	RF	0.27	7D4MC	A/A	0.8
Ti	399.9	387-25388	E-RF	1.5	PBBO	N/A	2.0
	365.4	387-27750	E-RF	2.0	PBD	N/A	2.0
Tl	377.6	0-26478	RF	0.22	BBQ	A/A	0.8
	377.6/535.0	0-26478/7793-26478	S-DLF	0.22/0.92	BBQ	A/A	0.8
V	411.2	2425-26738	E-RF	2.8	DPS	N/A	0.8
	370.4/411.2	2425-29418/2425-26738	E-S-SLF	2.8/2.5	PBD	N/A	2.0

*EX/FL = excitation wavelength/fluorescence wavelength (if different than excitation wavelength), and EL = energy level.

[a]Values taken from C.H. Corliss, W.R. Bozman, "Experimental Transition Probabilities for Spectral Lines of Seventy Elements," NBS Monograph 53 (1962).

[b]RF = resonance fluorescence; E-RF = excited resonance fluorescence; S-DLF = Stokes direct line fluorescence; AS-DLF = anti-Stokes direct line fluorescence; TA-SLF = thermally assisted stepwise line fluorescence; E-AS-DLF = excited anti-Stokes direct line fluorescence; and E-S-SLF = excited Stokes stepwise line fluorescence. (See Reference 19 for detailed discussion).

[c]See Table 4. Parantheses mean that the dye laser output is frequency doubled.

[d]A/A = air-acetylene flame and N/A = nitrous oxide-acetylene flame.

[e]Experimental difficulty was encountered in obtaining good laser output at the Co lines attempted.

Table 6B. Detection Limits by Laser-Excited Atomic Fluorescence Flame Spectrometry* (Analytical Figures of Merit)

Element	This Work			Previous Work			
	LOD[a] (ng/ml)	UL[a] (ng/ml)	LDR[a]	LOD[a] (ng/ml)	UL[a] (ng/ml)	LDR[a]	Reference[b]
Ag	4P0	6P4	2P4	---	---	---	---
Al	---	---	---	1P2	2P5	1P3	1
	2P0	6P5	3P5	3P2	1P5	1P4	1
	6P-1	3P5	5P5	5P0	2P5	1P5	1
Ba	1P2	1P7	1P5	8P0	>1P6	>1P5	2
	8P0	>1P6	>1P5	4P1	---	---	3
Bi	3P0	5P5	2P5	---	---	---	---
Ca	8P-2	6P3	8P4	5P0	5P4	1P4	1
Cd	8P0	3P3	3P3	---	---	---	---
Co[c]	1P3	>2P6	>1P3	2P2	2P5	1P3	1
	1P3	>2P6	>1P3	---	---	---	---
Cr	1P0	3P5	3P5	2P1	2P4	1P3	1
Cu	1P0	1P5	1P5	---	---	---	---
Fe	3P1	>1P6	>3P4	---	---	---	---
Ga	7P0	3P5	4P4	1P2	5P5	5P3	1
	9P-1	2P5	2P5	2P1	2P4	1P3	1
In	8P-1	4P5	5P5	1P1	5P4	3P4	1
	2P-1	3P5	2P6	2P0	5P4	3P4	1
Li	5P-1	>1P4	>2P4	---	---	---	---
Mg	2P-1	2P4	1P5	3P-1	---	---	4
Mn	1P0	8P4	8P4	1P1	2P4	2P3	1
	4P-1	1P5	3P5	---	---	---	---
Mo	1P1	>1P6	1P5	1P3	1P5	1P2	1
	1P1	>1P6	1P5	3P2	1P5	3P2	1
Na	<1P-1	5P4	5P5	1P-1	---	---	3
	1P0	6P4	6P4	---	---	---	---
Ni	1P1	1P5	1P4	---	---	---	---
	2P0	1P6	5P5	5P1	2P5	4P3	1
Pb	2P2	>1P6	>5P3	6P0	---	---	6
	3P1	>1P6	>3P4	---	---	---	---
	2P1	1P6	5P4	---	---	---	---
	1P1	>1P6	>1P5	3P1	---	---	4
Sr	3P-1	3P4	1P5	1P1	2P4	2P3	1
Ti	5P0	1P6	2P5	1P2	2P5	2P3	1
	2P0	4P5	2P5	---	---	---	---
Tl	4P0	3P5	7P4	1P3	5P4	5P1	1
	7P0	6P5	9P4	2P2	1P5	5P3	1
V	5P1	>1P6	>1P5	---	---	---	---
	3P1	>1P6	>3P4	5P2	---	---	5

*APB means A x 10^B.

[a] LOD = Limit of Detection, UL = Upper Limit of linearity, and LDR = linear dynamic range = UL/LOD.

[b] Values taken from: (1) Reference 45; (2) Reference 55; (3) Reference 56; (4) Reference 53; (5) Reference 47; and (6) Reference 54.

[c] Experimental difficulty was encountered in obtaining good laser output at the Co lines attempted.

Table 7. Comparison of Detection Limits in Flame Spectrometry and Inductively Coupled Plasma (ICP)

Element	Detection limit, ng ml^{-1}					
	AF[a] laser This Work	AF[b] conventional source	AE[b]	AA[b]	ICP pneumatic nebulization[c]	ICP ultrasonic nebulization[d]
Ag	4	0.1ß[e]	2	1	4†	---[f]
Al	0.6ß	100	3	30*	2	0.5**
Ba	8	---	1	20	0.1†ß	0.01
Bi	3ß	5ß	20,000	50	50†	---
Ca	0.08	20	0.1ß	1*	0.07†ß	0.0001
Cd	8	0.001ß	800	1	1.0	0.07*
Co[g]	1000	5ß	30	2ß	2ß	0.1*
Cr	1ß	5	2ß	2ß	0.9ß	0.08*
Cu	1	0.5	0.1ß	1*	0.2ß	0.04*
Fe	30	8	5	4	0.2ß	0.09
Ga	0.9ß	10	10*	50	14†	0.6
In	0.2ß	100	0.4ß	30	30†	---
Li	0.5	---	0.02ß	1	---	---
Mg	0.2ß	0.1ß	5*	0.1ß	0.7†	0.003
Mn	0.4ß	1	1	0.8	0.1ß	0.01*
Mo	12ß	500	100	30	4ß	0.2
Na	<0.1ß	---	0.1ß*	0.8	0.2†ß	0.02
Ni	2ß	3ß	20	5ß	4ß	0.2
Pb	13ß	10ß	100	10ß	10ß	1*
Sr	0.2	30	0.2	5	0.02†ß	0.003
Ti	2ß	4000	30	90*	3†ß	0.03
Tl	4ß	8ß	20	20	200†	---
V	30	70	7	20	1ß	0.06

[a] Limits of detection represent concentrations required to produce a line signal three times as great as the standard deviation of the background noise. All other values listed in the table represent concentrations required to produce a line signal twice as great as the standard deviation of the background noise, except where noted.

[b] Values taken from J.D. Winefordner, J.J. Fitzgerald, and N. Omenetto, Appl. Spectrosc., 29, 369 (1975) except for those designated *, which were taken from V.A. Fassel and R.N. Kniseley, Anal. Chem., 46, 1110A (1974).

[c] All values taken from K.W. Olson, W.J. Haas, Jr., and V.A. Fassel, Anal. Chem., 49, 632 (1977) except those with †, which are from V.A. Fassel and R.N. Kniseley, Anal. Chem., 46, 1110A (1974).

[d] All values taken from P.W.J.M. Boumans and F.J. deBoer, Spectrochim. Acta., 30B, 309 (1975) except those designated *, which were taken from K.W. Olson, W.J. Haas, Jr., and V.A. Fassel, Anal. Chem., 49, 632 (1977) and those designated **, which were taken from M.H. Abdallah, R. Diemiaszonek, J. Jarosz, J.M. Mermet, J. Robin, and C. Trassy, Anal. Chem. Acta, 84, 271 (1976). Limit of detection designated ** represent concentrations required to produce a line signal six times as great as the standard deviation of the background noise.

[e] ß designates best value with pneumatic nebulization. All values within a factor of 3 are considered to be equal.

[f] --- indicates no value reported.

[g] Experimental difficulties were encountered in obtaining good laser output at the Co lines.

is equivalent or superior to all the methods listed where pneumatic nebulizers are used. The use of an ultrasonic nebulizer should also provide ca 10 fold improvement in the detection limits (108). As noted earlier, optimization of the fluorescence emission optics should also improve nonresonance fluorescence detection limits.

The analytical calibration curves plotted in Figures 13-16 are divided according to whether the element (i) has transitions which are excited by the fundamental (>355 nm) or frequency doubled (>355 nm) dye laser output; (ii) has only strong resonance transitions or has both strong resonance and nonresonance transitions; and (iii) is best excited in an air-acetylene or nitrous oxide-acetylene flame.

The limits of detection for the nonresonance cases are typically one order of magnitude lower than for the resonance cases, as seen in Figure 14.

Linear Dynamic Range

A very important figure of merit to the practical analyst, which often is not reported and compared, is the linear dynamic range (109), i.e., the linearity range of the analytical calibration curve. A technique which offers a low limit of detection, but whose analytical curve is only linear over one or two orders of magnitude is analytically practical but is difficult to use, because often it means time consuming dilutions will have to be made until one is ensured to be within the linear range for that technique or one is destined to work within the nonlinear portion of the analytical curve requiring extensive standardization.

The linear dynamic range is determined by the lower and upper limits of concentration. The upper limit of concentration is determined

Figure 13: Analytical Calibration Curves for Elements having only strong resonance transitions above 355 nm in air-acetylene flame

	$\lambda_{ex}=\lambda_{fl}$ (nm)
: resonance fluorescence of Ba	554
: resonance fluorescence of Ca	422
: resonance fluorescence of Cr	359
: resonance fluorescence of Li	670
: resonance fluorescence of Mn	403
: resonance fluorescence of Na	589
: resonance fluorescence of Sr	460

(: indicates the limit of detection.)

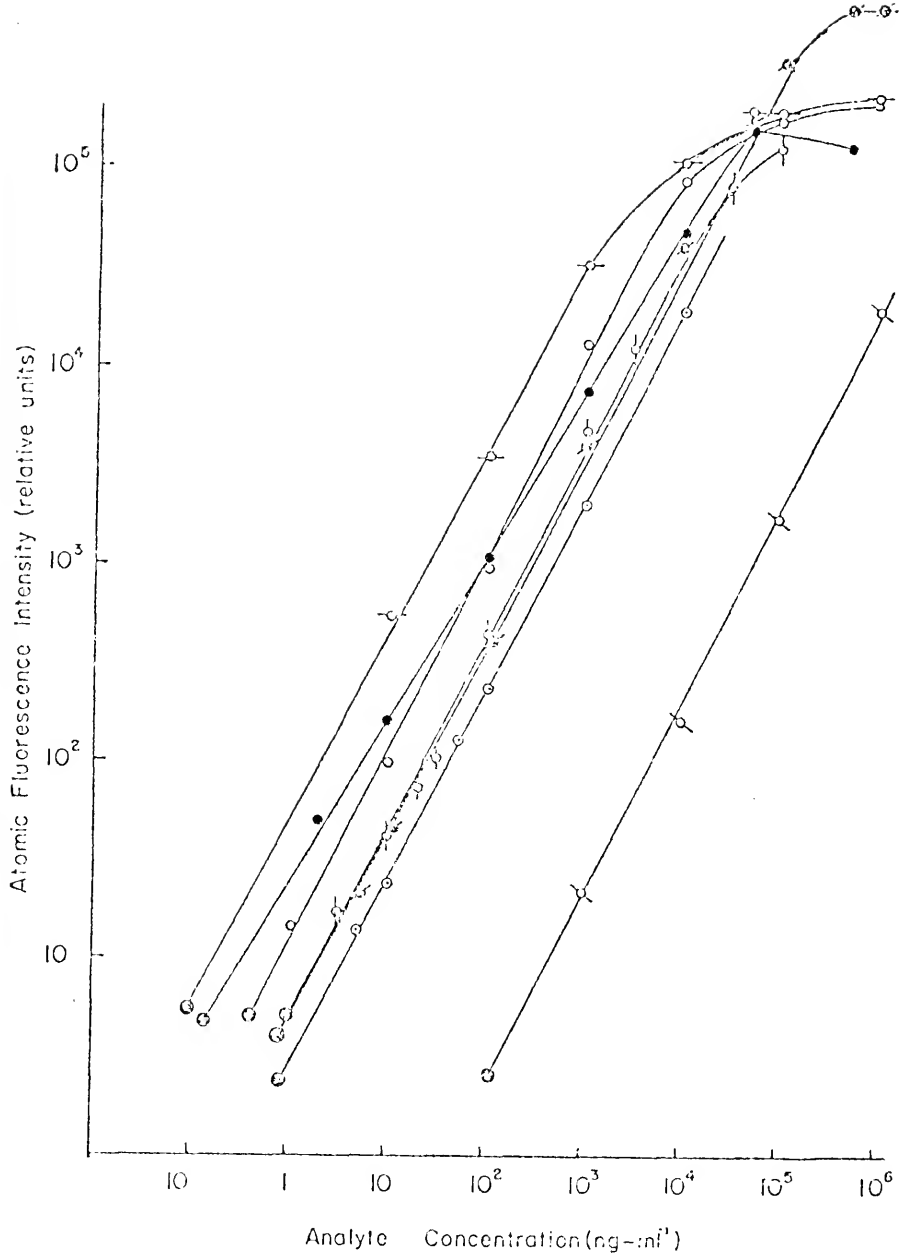
Atomic Fluorescence Intensity (relative units)
10
10^2
10^3
10^4
10^5
10
1
10
10^2
10^3
10^4
10^5
10^6
Analyte Concentration (ng-ml^{-1})

Figure 14: Analytical Calibration Curves for elements having both strong resonance and nonresonance transitions excited above 355 nm in an air-acetylene flame.

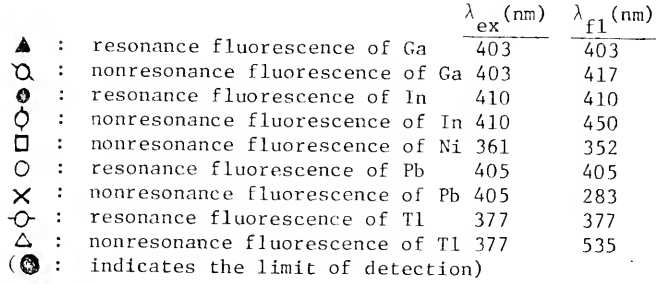

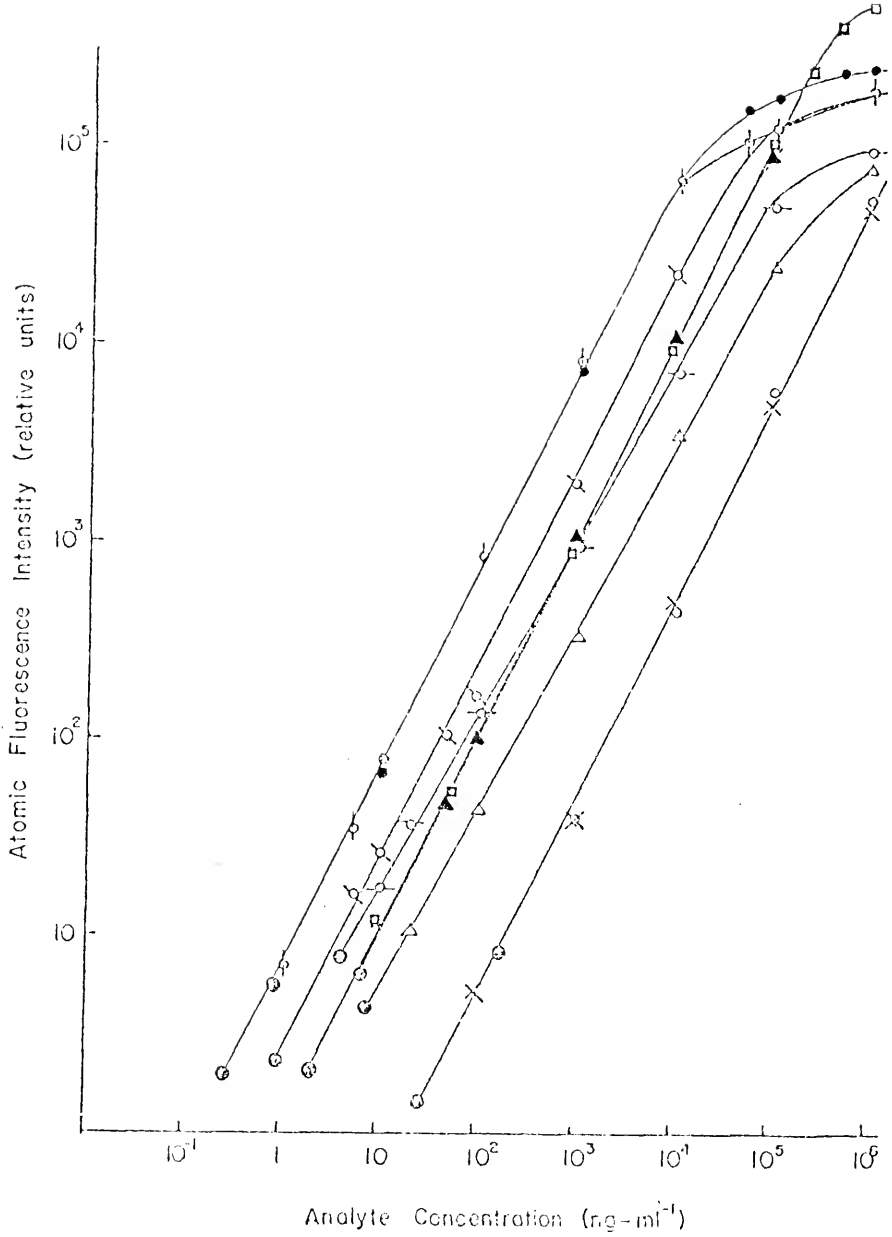
Atomic Fluorescence Intensity (relative units)
10
10^2
10^3
10^4
10^5
10^{-1}
1
10
10^2
10^3
10^4
10^5
10^6
Analyte Concentration (ng-ml^{-1})

Figure 15: Analytical Calibration Curves for elements having transitions excited above 355 nm in a nitrous oxide-acetylene flame

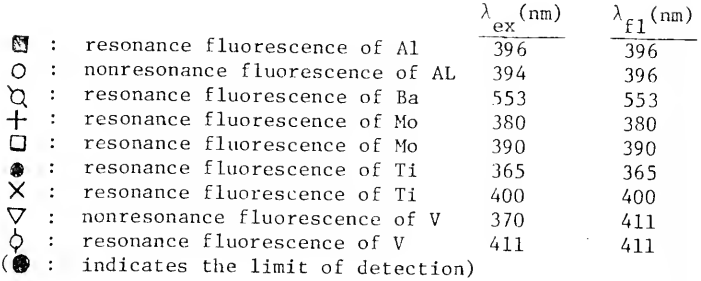

		λ_{ex} (nm)	λ_{fl} (nm)
▨ :	resonance fluorescence of Al	396	396
○ :	nonresonance fluorescence of AL	394	396
⊗ :	resonance fluorescence of Ba	553	553
+ :	resonance fluorescence of Mo	380	380
□ :	resonance fluorescence of Mo	390	390
● :	resonance fluorescence of Ti	365	365
× :	resonance fluorescence of Ti	400	400
▽ :	nonresonance fluorescence of V	370	411
◇ :	resonance fluorescence of V	411	411
(● :	indicates the limit of detection)		

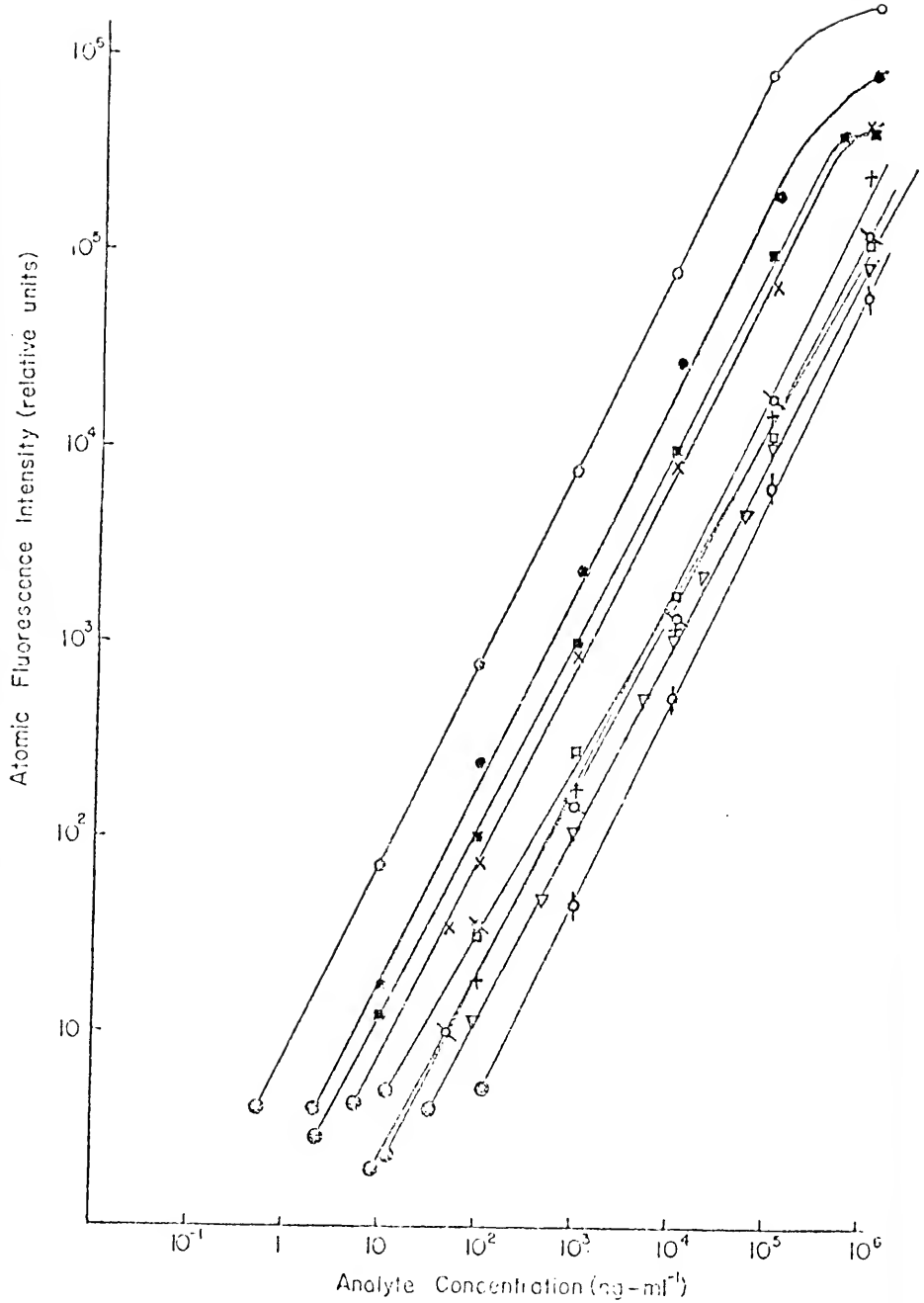
Atomic Fluorescence Intensity (relative units)
10^5
10^4
10^3
10^2
10
10^{-1}
1
10
10^2
10^3
10^4
10^5
10^6
Analyte Concentration (ng-ml^{-1})

Figure 16: Analytical Calibration Curves for elements having transitions excited below 355 nm in an air-acetylene flame

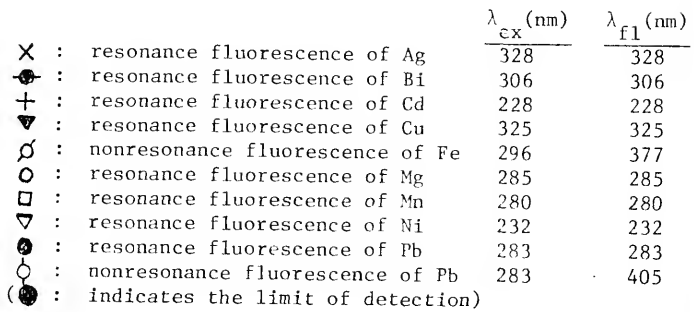

		λ_{ex} (nm)	λ_{fl} (nm)
×	: resonance fluorescence of Ag	328	328
⊕	: resonance fluorescence of Bi	306	306
+	: resonance fluorescence of Cd	228	228
▼	: resonance fluorescence of Cu	325	325
⌀	: nonresonance fluorescence of Fe	296	377
○	: resonance fluorescence of Mg	285	285
□	: resonance fluorescence of Mn	280	280
▽	: resonance fluorescence of Ni	232	232
●	: resonance fluorescence of Pb	283	283
○	: nonresonance fluorescence of Pb	283	405

(● : indicates the limit of detection)

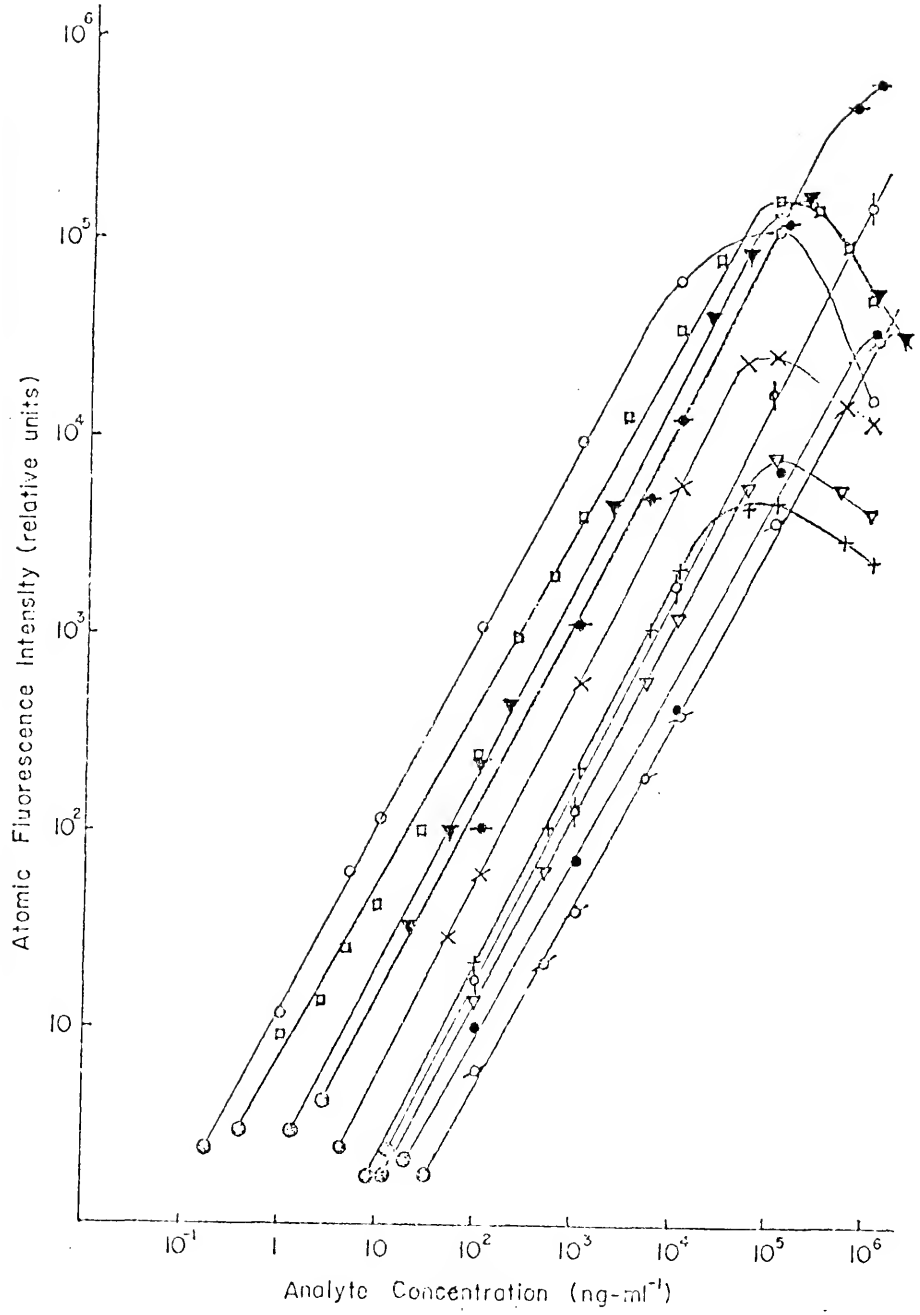
Atomic Fluorescence Intensity (relative units)
10^6
10^5
10^4
10^3
10^2
10
10^-1
1
10
10^2
10^3
10^4
10^5
10^6
Analyte Concentration (ng-ml^-1)

from the analytical curve by that signal level which deviates from linearity by 5%. The upper and lower limits of concentration, as well as the linear dynamic ranges are reported in Table 6. The linear dynamic ranges for almost all elements examined by laser-excited atomic fluorescence flame spectrometry are about 5 to 7 orders of magnitude. The linear dynamic ranges are equivalent to those obtained by the ICP (4 - 7 orders of magnitude), and about one or two orders of magnitude better than by conventional source atomic fluorescence spectrometry, and atomic emission spectrometry. It is also about 2 to 4 orders of magnitude greater than flame atomic absorption and furnace atomic absorption. The high degere of linearity obtained by pulsed laser-excited atomic fluorescence spectrometry is due to the low noise and the high spectral irradiance of the laser resulting in lower limits of detection; at high concentrations, there is negligible self-absorption and also there is a negligible prefilter effect due to the atomic vapor at near saturation conditions (48, 67). The slopes of the analytical curves (sensitivity) shown in Figures 13 - 16 are all close to unity (within 5 %) except for Na, Tl, and Mo resonance fluorescence, which are attributed to a combination of postfilter effect, source irradiances insufficient to produce "saturation" conditions, and ionization of the analyte. All of the analytical calibration curves for resonance lines obtained with doubling of the dye laser output bend over at high analyte concentrations, typical of the analytical growth curves for narrow line source excitation (19). The width of the dye laser bandpass could not be measured but is likely to be ≤ 0.1 Å.

Some analytical calibration curves obtained by using ICP spectrometry become nonlinear at very low concentrations thus affecting the precision of the measurement (110). This has not been shown to occur in laser-excited atomic fluorescence flame spectrometry.

For precise and accurate data over a long time period, which is necessary in any practical analytical work, the atomic fluorescence signal (under beam expansion of the dye laser output) must in most cases be measured relative to the intensity of the laser output (assuming the measurements are being performed on the linear region of the saturation curve). This is due to the fact that the dye laser output decreases with time to varying degrees dependent upon the individual dye degradation. Ratioing is simple to accomplish by reflecting a small amount of the laser output off a quartz plate onto a photodiode and using a dual channel boxcar integrator to ratio the signal.

Spectral Interferences

Spectral interferences often limit or make a particular analysis impossible as is well documented in literature (111). Sometimes, time consuming sample pretreatment separation methods are possible to use, but these methods are not desirable to use in trace analysis because of the possibility of contamination. Due to the narrow spectral bandwidth of the laser output and its pulsed operation, N_2 laser pumped dye laser-excited atomic fluorescnece with gated detection essentially has no or can be adjusted to have no spectral interferences. This is shown in Table 8 and Figure 17 for the case of Mn and Ga at 403.3 nm. Ga has lines at 403.30 nm and 417.21 nm. Mn lines are at 403.08, 403.31 and 403.45 nm. The spectral separation of the

Table 8. Investigation of Spectral Interferences Between Manganese and Gallium

(i) Excited at 403.08 nm/Observed at 403.08 nm
[Observe manganese atomic fluorescence]

Composition	Relative atomic fluorescence intensity
Mn 1 ppm	69
Mn 1 ppm + Ga 5 ppm	70
Mn 1 ppm + Ga 100 ppm	68
Mn 0.5 ppm + Ga 100 ppm	34
Mn 0.1 ppm + Ga 100 ppm	7

(ii) Excited at 403.30 nm/Observed at 403.30 nm
[Observe gallium atomic fluorescence]

Composition	Relative atomic fluorescence intensity
Ga 5 ppm	67
Ga 5 ppm + Mn 1 ppm	108

(iii) Excited at 403.30 nm/Observed at 417.01 nm
[Observe gallium atomic fluorescence]

Composition	Relative atomic fluorescence intensity
Ga 5 ppm	151
Ga 5 ppm + Mn 1 ppm	151

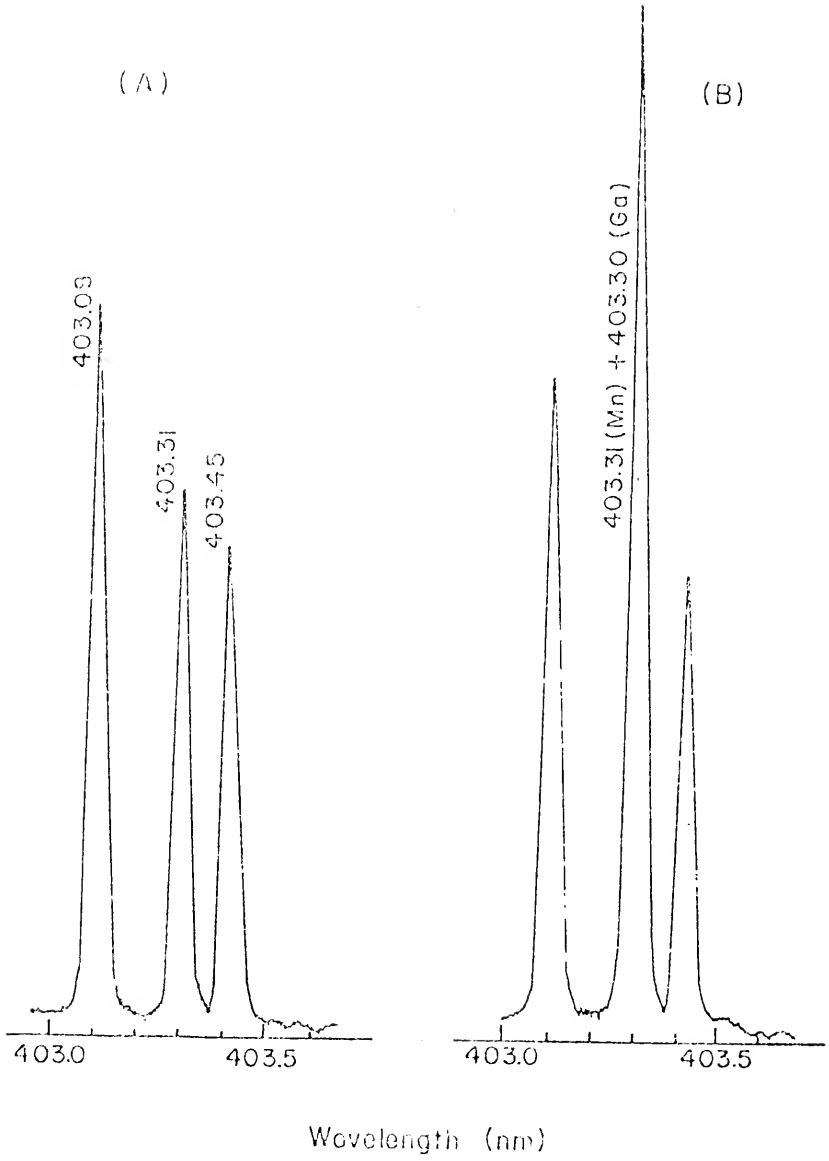

Figure 17: Excitation fluorescence spectrum for (A) a 1 ppm Mn solution; and (B) 1 ppm Mn + 5 ppm Ga solution

two lines for Ga and Mn near 403.3 nm is only 0.01 nm. The specificity factor (the ratio of interferent to analyte concentration which contributes 100% interference using low dispersion) for the analysis of Mn at 403 nm in the presence of Ga is 5 (111). Part (i) of Table 8 shows that by exciting the 403.08 nm transition of Mn and observing the "resonance" fluorescence with a low dispersive spectrometer (1.6 nm bandpass), no interference of Ga on the analysis of Mn is observed even when Ga is present at a concentration 1000 fold greater than that of Mn. This simply demonstrates that due to the narrow spectral bandwidth of the laser, no Ga is being excited and that due to the low duty factor, Ga flame emission is negligible. Part (ii) of Table 8 shows that Mn does interfere with the analysis of Ga approximately in the ratio expected. However, this interference is simply eliminated by using nonresonance fluorescence which detects the Ga fluorescence signal at 417.01 nm, as seen in part (iii) of Table 8. Because of the high irradiance of the laser, negligible beam attenuation in the analyte volume will occur even at high concentrations of the potential interferent.

Spectral interferences in conventional source AF, AA, and in AE due to concomitants and flame background in various flames and furnaces and inert fill gas lines in lamps, are well known. Spectral interferences occur in ICP spectrometry unless sufficiently high resolution detection is employed, because of the high temperatures occurring in the plasma. Nonspectral interferences occurring with the ICP have been found to be relatively small but complex and the setting of the principal experimental parameters of the ICP system are critical as they appreciably affect the magnitude of these interferences (112).

A cw dye laser-excited atomic fluorescence system will also be subject to flame background noise.

The only potential interferences foreseen in pulsed laser-excited atomic flame fluorescence spectrometry with gated detection would arise from molecular fluorescence of species formed in the flame by concomitants and flame gases, and excited by the laser (103). The ground state resonance transition of V at 385.54 nm was not observed due to the difficulty of finding this transition amongst the strong CN molecular fluorescence in this region.

CHAPTER V
PULSED LASER-EXCITED MOLECULAR FLUORESCENCE

Flame Background

As noted in the last chapter, the only spectral interference expected in pulsed laser-excited atomic fluorescence spectroscopy would arise from fluorescence due to molecular species formed in the analytical flame by solution concomitants and flame gases. Although much is known about the flame emission background in air-acetylene flames (104), it was not until recently that the flame fluorescence background was initially investigated (103, 112). Information on the flame emission background in nitrous oxide-acetylene flames, however, is scarce and scattered in the literature, and reports of its flame fluorescence background are even rarer (88). The species expected to be found in these hydrocarbon flames (PH_3 being a contaminant) due to the flame gas components are OH, C_2, CH, PO, CO, NO, CN, CHO, and NH. Figure 18 shows the fluorescence excitation spectrum of CN in the 380 nm region obtained using the N_2 laser pumped tunable dye laser system described in Chapters III and IV. Obviously, knowledge of the complete flame fluorescence background under various flame conditions for these flames would greatly benefit analytical chemists working in atomic fluorescence flame spectrometry.

The high spectral resolution obtained in the CN spectrum (Figure 18) indicated that the pulsed laser fluorescence system could prove to be an invaluable tool for molecular flame fluorescence. Therefore,

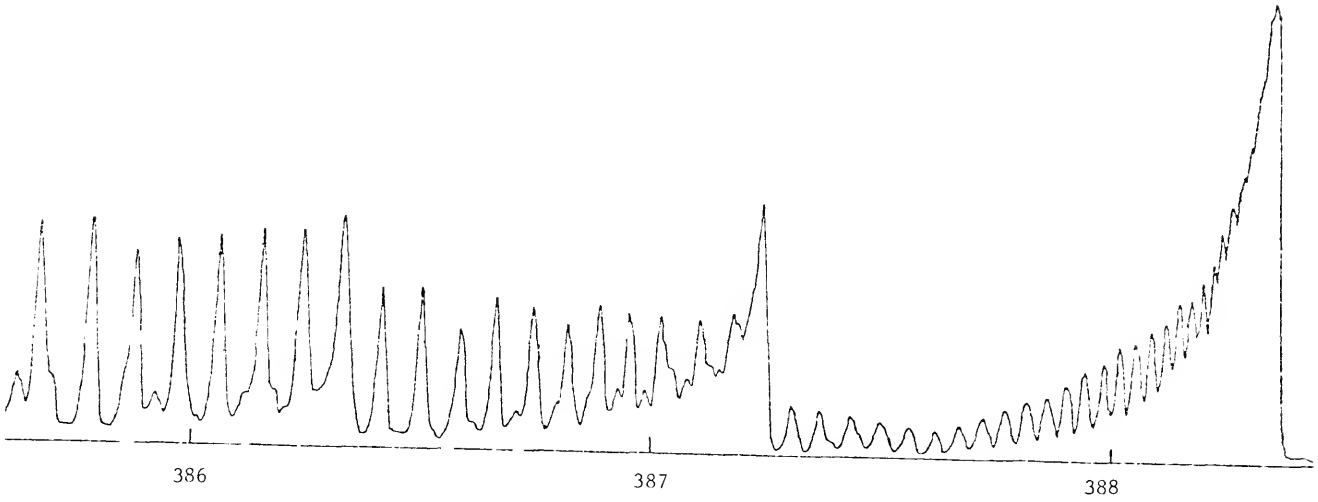

Figure 18: Excitation spectrum of CN in a nitrous oxide-acetylene flame:

λ_{fl} = 385.5 nm, 400 μm slit width, 385 - 389 nm wavelength range, BBQ dye

the possibility of selective excitation of molecular species, which coexist in the flame and have overlapping emission spectra, was investigated. Also, the utility of the laser-excited fluorescence method was evaluated to selectively probe the energy levels of molecular species in flames in order to determine energy levels and band systems.

Selective Excitation of Molecular Species in Flames

The presence of molecular species in flames has been known since the early work of chemists and physicists in flame spectroscopy (104, 113-115). Until recent years, the molecular species in flames have been extensively observed almost exclusively by emission spectroscopy (114). Recently, many works on molecular absorption flame spectroscopy have appeared in the journals (116-124). However, studies of molecular fluorescence flame spectroscopy are still very few (102, 103, 125-130). The molecular species which have been observed by molecular fluorescence flame spectroscopy are CaOH (125, 127-129); CH (126, 128); C_2 (130); and CN (88). In these studies, xenon arc lamps (102, 103, 125, 127) and lasers (88, 126, 128-130) have been used as excitation sources. As mentioned in previous studies (102, 127), conventional xenon arc sources have had limited use as excitation sources due to their instability, scattered light problems, and relatively low spectral irradiances. On the other hand, lasers are promising excitation sources for molecular fluorescence and the technique of laser-excited molecular fluorescence flame spectroscopy should be useful for studies of flame or combustion diagnostics (126, 128-130).

Blackburn, Mermet, and Winefordner used a cw (continuous wave) dye laser, and observed molecular fluorescence of 5 molecular species in argon-oxygen-hydrogen and argon-oxygen-acetylene flames. However, use of cw dye lasers is restricted to wavelengths above ca 520 nm at the present time. Nitrogen laser or flashlamp pumped dye lasers have a considerably wider wavelength range, as well as higher spectral irradiance. The applicability and usefulness of nitrogen laser pumped dye lasers in the wavelength range from 220 nm to 700 nm in laser-excited atomic fluorescence flame spectrometry was shown in Chapter IV.

Molecular fluorescence spectra of BaO, BaOH, and BaCl in an air-acetylene flame were investigated here. The three species coexist in the flame and give molecular emission bands in the same wavelength region. The aim of this work was to show the capabilities of the tunable dye laser in selectively exciting each of the species and observing molecular fluorescence spectra of each distinct species. Because the pulsed dye laser provides a tunable single line source with high spectral irradiance and a narrow spectral bandpass, molecular species in flames can be selectively excited. Also, because the N_2 laser pumped dye laser has such a low duty factor (ratio of source on time to total time), the flame emission background is negligible when a gated detection system is used. This makes pulsed laser-excited molecular fluorescence molecular fluorescence flame spectroscopy a useful diagnostic technique for identification of molecular species and their electronic structures. The study of reaction kinetics (e.g., energy transfer mechanism, chemical equilibria, etc.) in flames is also a promising field of research.

The dye laser and detection system was the same as that described in Chapter III. The nitrogen laser pumped dye laser was operated at 20 Hz repetition rate. The reciprocal linear dispersion of the monochromator was 2 nm mm^{-1}. The photomultiplier used was an R777 from Hamamatsu TV Co. A Model 162/164 boxcar integrator from Princeton Applied Research Co. was used as the signal acquisition and amplification system. The observed time constant of the detection system is ca 2 s. As mentioned in the previous chapters, a beam expander was set between the dye laser and the flame. The beam expander helped to increase the signal levels observed, and minimize the scatter at the emission wavelength, i.e., improvement of the signal-to-noise ratio of the measurement system was achieved by using the beam expander.

All of the molecular fluorescence excitation spectra were observed by scanning the laser wavelength (at fixed monochromator wavelength), and all of the molecular fluorescence emission spectra were observed by scanning the monochromator wavelength (at fixed laser excitation wavelength); all spectra were recorded on a strip chart recorder. A 250-2000 μm monochromator slit width was employed for all excitation spectra. Because the spectral bandwidth (FWHM) of the laser output was less than 0.02 nm in the wavelength region investigated, use of a wide monochromator slit width (low dispersive system) still enabled fluorescence spectra to be obtained with high resolution (<0.02 nm), being determined only by the laser bandwidth. Also, when fluorescence emission spectra were observed, wide (250-1750 μm) monochromator slit widths were employed because of the low intensities of BaO and BaOH molecular fluorescence signals.

An air-acetylene flame was produced on a 10 mm dia. capillary burner which was laboratory-constructed. Phosphine (PH_3)(103) and charcoal traps were used in the acetylene gas line in order to eliminate phosphine and acetone, which are impurity gases in acetylene. A drierite trap was used in the air flow to remove the water vapor. The flow rates of air and acetylene were maintained at 12 l min^{-1} and 2.2 l min^{-1}, respectively.

All chemicals used were reagnet grade. A 0.1 M $BaCO_3$ solution was dissolved in 0.5 M HCl solution, and 5000 $\mu g\text{-}ml^{-1}$ and 10,000 $\mu g\text{-}ml^{-1}$ Ba (as $BaCl_2$) solution were dissolved in deionized water. Deionized water was used as a blank solution in all measurements.

Spectral Characteristics of Barium Compounds

Emission spectra of barium compounds aspirated into an air-acetylene flame was shown in Figure 19 (spectra were observed while aspirating a solution of 0.1 M Ba in ca 0.5 M HCl). Molecular emission bands of BaO (131-133) can be seen over most of the wavelength region of 450-800 nm shown in Figure 19, along with the atomic resonance line (Ba I) at 553.0 nm and the ionic resonance lines at (Ba II) at 455.4 and 493.4 nm. Furthermore, molecular emission bands of BaOH (134, 135) are observed near 487, 512, 732, and 820 nm, and those of BaCl (114, 136) in the 505-535 nm wavelength region.

The emission bands of BaO correspond to the transition $A^1\Sigma\text{-}X^1\Sigma$, where $X^1\Sigma$ is the ground electronic state and $A^1\Sigma$ the excited electronic state. According to previous studies (104, 131, 132), vibrational structures of BaO were assigned, and their sequences are shown in Figure 19. The band heads at 597.6, 622.5, 649.3, 678.3, 709.7, 744.0, and 781.5 nm are due to the (0, 0), (0, 1), (0, 2), (0, 3), (0, 4), (0, 5)

Figure 19: Emission spectrum of barium in the air-acetylene flame (Ba: 0.1 M in 0.1 M HCl solution). The assignments on the top of the spectrum show the band heads due to the molecular vibrations of BaO, where v'' is the quantum number of the vibration in the upper electronic state $A^1\Sigma$. Strontium line (Sr I) at460.7 nm and sodium lines (Na I) at 589.0 nm and 589.6 nm are due to the impurities in the solution. Some other lines could not be identified.

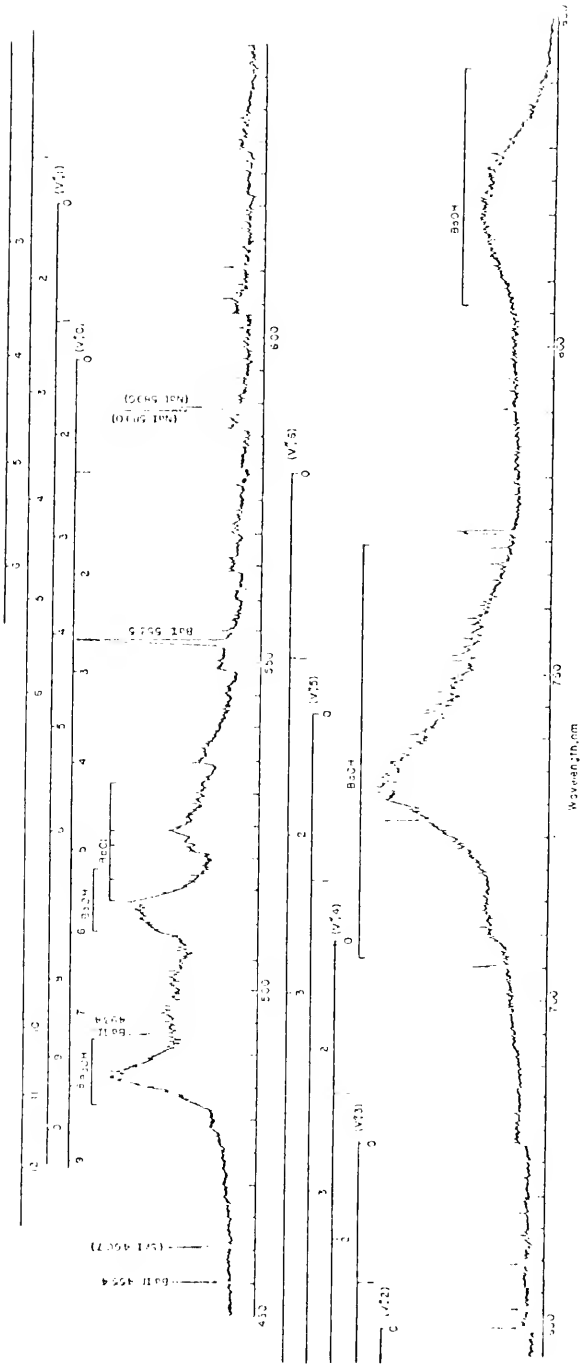
Wavelength,nm

and (0, 6) transitions (v", v'), respectively. The sequences from Δv (= v" - v', where v" and v' are the upper and lower vibrational states in $A^1\Sigma$ and $X^1\Sigma$, respectively) = -6 to Δv = +10 can be seen in the emission spectrum. Some of the molecular band heads overlap with those of BaOH and BaCl and cannot be identified. No effort was made to identify the rotational structures of BaO in the present work. The values of the rotational constants for BaO can be found in the literature (104, 131, 133).

The diffuse bands near 487 and 512 nm were ascribed to BaOH by James and Sudgen (134) and by Charton and Gaydon (135) from studies in flames with different compositions and equal temperatures and from isotope shift measurements, respectively. Other diffuse bands near 732 and 820 nm were also ascribed to BaOH by Lagerquist and Huldt (137) and by Bulewicz (138), although no high resolution spectrometric studies or isotope shifts measurements have been carried out. In the emission spectrum, bands of BaOH near 487 and 512 nm are superimposed with sequences Δv = +8 and +9 of BaO (v", 1) and with Δv = +5 and +7 of BaO (v", 0). The bands of BaOH near 732 nm are also superimposed with sequences Δv = -5 of BaO. Furthermore, the bands of BaOH near 512 nm overlap with those of BaCl.

The molecular bands of BaCl are well known (114, 136). In Figure 20, and in Table 9, the energy levels and transitions for the $C^2\Pi$-$X^2\Sigma$, green system of BaCl are given.

In the emission spectra, the BaCl bands are superimposed upon the molecular emission bands of BaO and BaOH making it difficult to identify the emission bands of BaCl in the flame emission spectra. However, pulsed laser-excited fluorescence spectroscopy allows selective

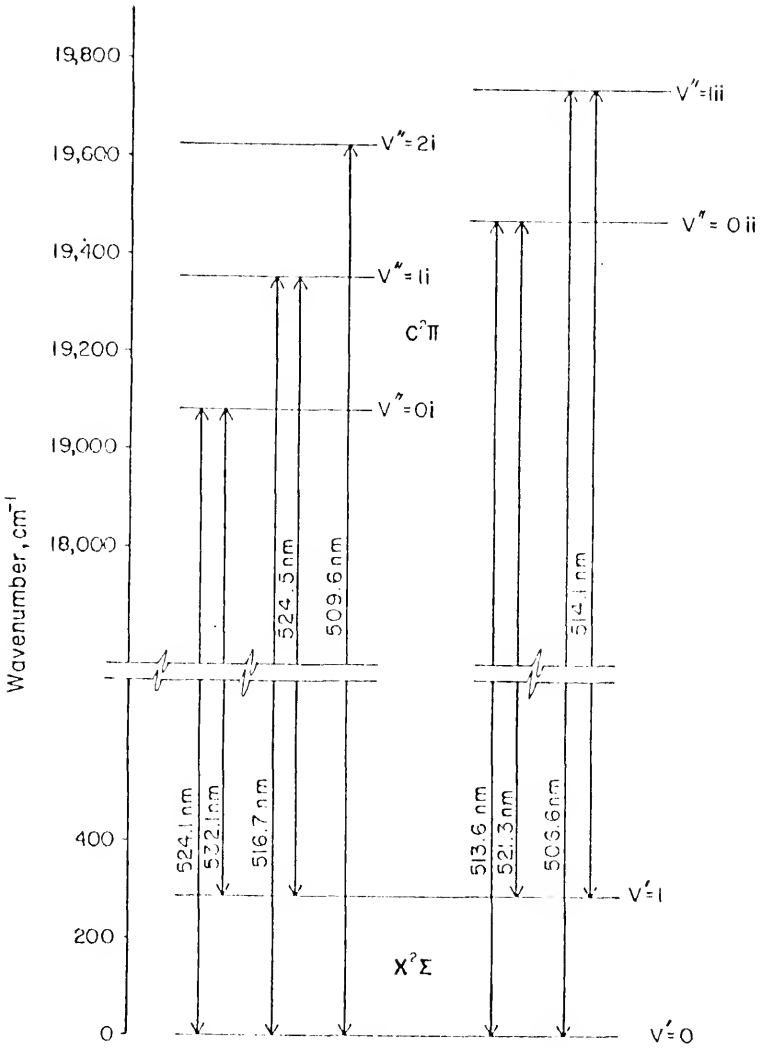

Figure 20: Energy level diagram of BaCl showing observed transitions

Table 9. Spectral Transitions of BaCl
Green System, $C^2\Pi$-$X^2\Sigma$

Wavelength, nm	Transition (v", v')	Energy Levels Upper-Lower, cm^{-1}	Transition Energy, cm^{-1}
System i			
524.05	(0, 0)	19,082-0	19,082
532.1	(0, 1)	19,082-288	19,794
516.7	(1, 0)	19,353-0	19,353
524.52	(1, 1)	19,353-288	19,065
509.6	(2, 0)	19,624-0	19,624
System ii			
513.6	(0, 0)	19,470-0	19,470
521.3	(0, 1)	19,470-288	19,182
506.6	(1, 0)	19,739-0	19,739
514.1	(1, 1)	19,739-288	19,451

excitation and detection of molecular species in flames. In Figure 21, a series of molecular fluorescence excitation spectra, which have as their fluorescence emission wavelengths the main transition of the $C^2\Pi$-$X^2\Sigma$ electronic system, are shown. A fluorescence excitation spectrum over the same spectral region (505-537 nm) using a fluorescence emission wavelength of 487 nm, which corresponds to the most intense BaOH broad band emission, is also shown at two different gain settings in Figure 21. The spectra were taken using 1750 μm monochromator slit widths and are not corrected for detector response, source intensity, or scatter. However, the photomultiplier response and the source intensity are essentially flat over this wavelength region, and the scatter was found to be negligible under the conditions used. The temporal pulse width of the laser is ca 6 ns and a detector gate width of 15 ns was used. Time resolution of the fluorescence signal was not attempted.

Fluorescence of BaCl was clearly and easily observed in a "separated" air-acetylene flame at the wavelengths indicated in Table 9. Even with a low dispersion spectrometric detection system, the band structure was very evident. The relative fluorescence intensities of the transitions at each fluorescence emission wavelength are listed in Table 10. Fluorescence from the (0, 0i) and (0, 0ii) sequences in the $C^2\Pi$-$X^2\Sigma$ system was in all cases the most intense. Thermally-assisted excitation, excitation into the rotational-vibrational levels, radiationless deactivation, spectral bandwidth of the source and detection system, wavelength scan speed, source repetition rate and detection time constant are factors important to the discussion of

Figure 21: Fluorescence excitation spectra of BaCl in an air-acetylene flame (5000 ppm Ba solution as BaCl) at fixed fluorescence emission wavelengths of: λ_{fl} = 532.1, 524.1, 521.3, 516.7, 513.6, and 506.6 nm and of BaOH λ_{fl} = 487 nm.

Experimental conditions:
Monochromator slit width: 1750 μm (spectral bandpass of 3.5 nm):
Scan speed of laser excitation wavelength: 2 nm min^{-1}.
Spectral range of laser excitation wavelength: 505-537 nm.

Note: Xa means the signal level has been reduced by a factor a compared to X1 and to compare spectra on an equal basis those with Xa have signal levels a times larger than those with X1.

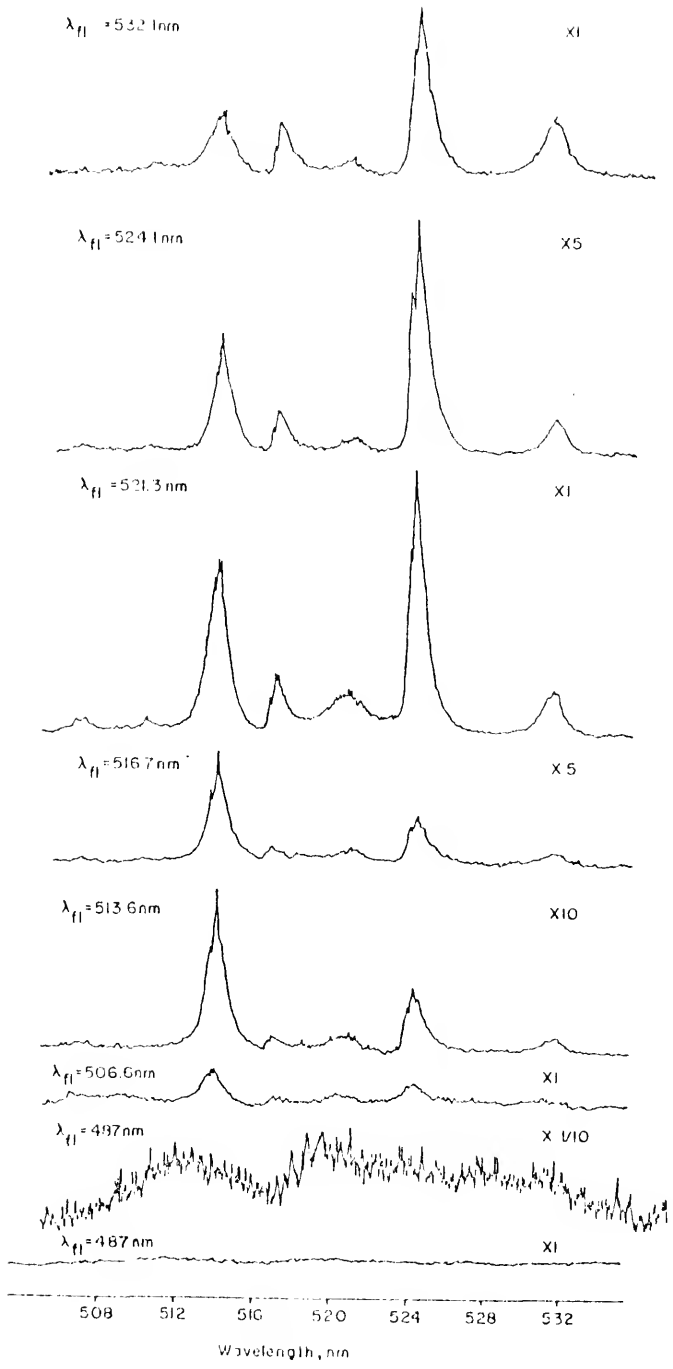
λfl = 532.1nm
X1
λfl = 524.1nm
X5
λfl = 521.3nm
X1
λfl = 516.7nm
X 5
λfl = 513.6nm
X10
λfl = 506.6nm
X1
λfl = 497nm
X 1/10
λfl = 487nm
X1
508
512
516
520
524
528
532
Wavelength, nm

Table 10. Relative Intensity of Peak Fluorescence for BaCl Transitions for the Observed Fluorescence Excitation Spectra

	Fluorescence emission wavelength, nm	Relative fluorescence intensities at BaCl transitions, at the excitation wavelengths						
$C^2\Pi$-$X^2\Sigma$		506.6	509.6	513.6	516.7	521.3	524.1	532.1
System i	524.1	0.03	0.03	0.38	0.14	0.07	0.75	0.13
	532.1	0.01	0.01	0.42	0.03	0.01	0.11	0.04
	516.7	0.02	0.02	0.36	0.06	0.04	0.14	0.04
System ii	513.6	0.04	0.03	1.00	0.10	0.12	0.39	0.09
	521.3	0.01	0.01	0.11	0.04	0.03	0.17	0.03
	506.6	0.01	--	0.03	0.01	0.01	0.02	0.01

the relative molecular fluorescence intensities. More detailed studies on the reaction kinetics should be encouraged.

None of the distinct molecular band structure of BaCl was observable at fluorescence emission wavelengths corresponding to BaOH or BaO transitions, as shown in Figures 21 and 22 for wavelengths corresponding to the maximum broad band emission intensities of BaOH transitions, λ_{fl} = 487 nm and λ_{fl} = 512 nm. No molecular band structure of BaCl was observed at a wavelength of λ_{fl} = 535 nm, or λ_{fl} = 549 nm which corresponds to a BaO transitions outside of the BaOH broad band emission and fluorescence wavelength region. Figure 22 also shows a slower excitation wavelength scan with the fluorescence wavelength set at a wavelength corresponding to the $C^2\Pi$-$X^2\Sigma$ (0, 0ii) transition of BaCl. The fine structure of the BaCl band is clearly observable. Frequency narrowing the dye laser output and scanning slowly over this band would result in even more prominent fine structures. Similar fine structure was observed when this same wavelength region (i.e., λ_{ex} = 510 - 515 nm) was scanned, and the fluorescence wavelength was set to the $C^2\Pi$-$X^2\Sigma$ (0, 0i) transition at λ_{fl} = 524.1 nm. The results shown in Figures 21 and 22 demonstrate the usefulness and potential of pulsed laser-excited molecular fluorescence spectrometry for selective excitation and detection of coexisting species in flames and to investigate the energy levels and reaction kinetics of particular species.

Figures 22a and 23 show near resonance excitation wavelength scans over the most intense BaOH emission wavelength regions at λ_{fl} = 487 nm and λ_{fl} = 512 nm. This is the first time BaOH fluorescence has been reported in flames. It should be noted that fine structure

Figure 22: Fluorescence excitation spectra of BaOH and BaCl in an air-acetylene flame (0.1 M $BaCO_3$ in 0.5 M HCl solution) at fixed fluorescence emission wavelengths of λ_{fl} = 512 nm and λ_{fl} = 513.6 nm, respectively.

Excitation conditions:
Monochromator slit width: 250 μm (0.5 nm spectral bandpass);
Scan speed of laser excitation wavelength: 0.6 nm min^{-1};
Spectral range of laser excitation wavelength: 509-515 nm.

Also see note at end of Figure 21 caption.

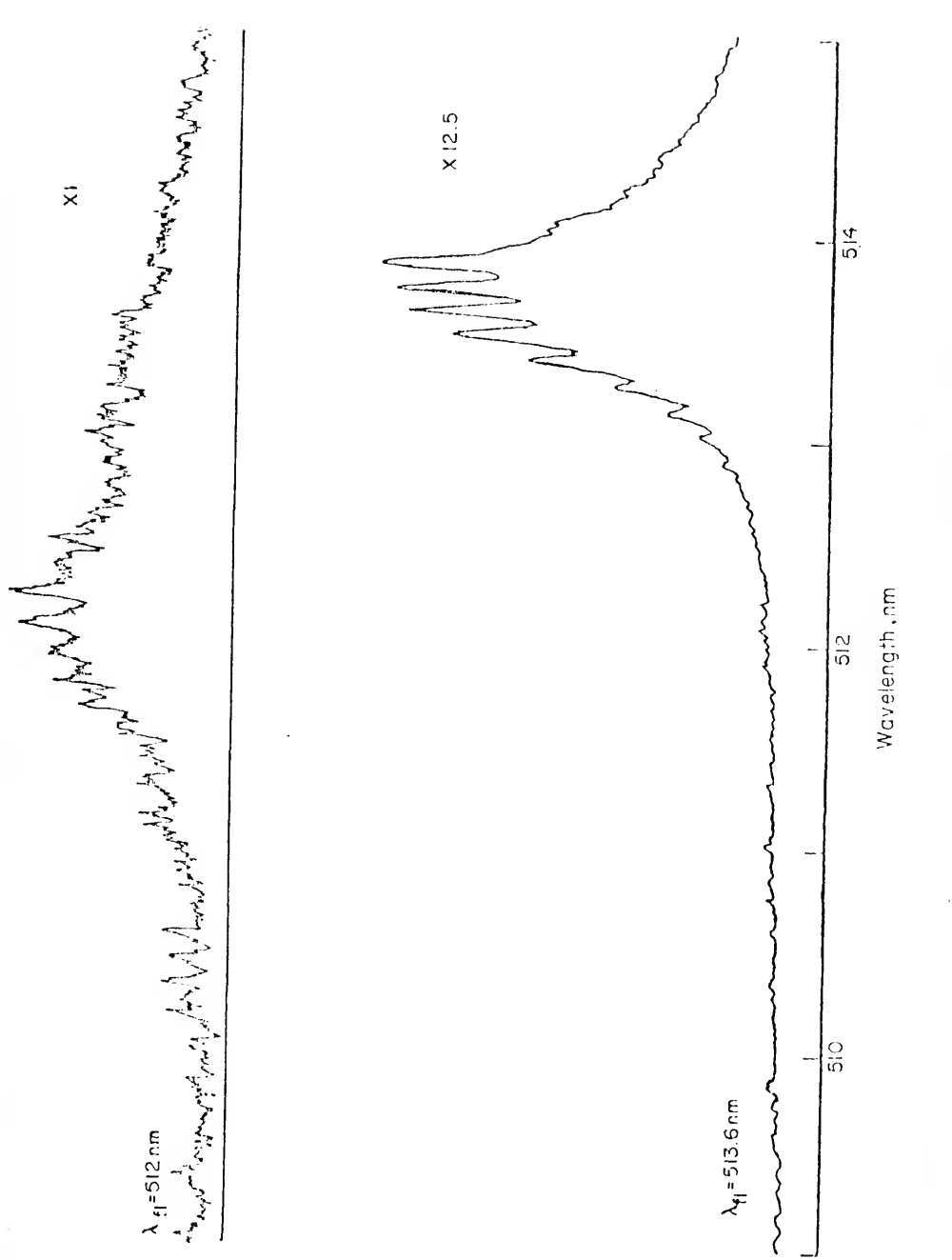
X1
X12.5
λ f1 = 512 nm
λ f1 = 513.6 nm
510
512
514
Wavelength, nm

Figure 23: Fluorescence excitation spectrum of BaOH in an air-acetylene flame (1000 ppm Ba as $BaCl_2$ in deionized water solution) at fixed fluorescence emission wavelength of λ_{fl} = 487 nm.

Excitation conditions:
Monochromator slit width: 1750 μm (3.5 nm spectral bandpass):
Scan speed of laser excitation wavelength: 0.6 nm min^{-1}.
Spectral range of laser excitation wavelength: 483-493 nm.

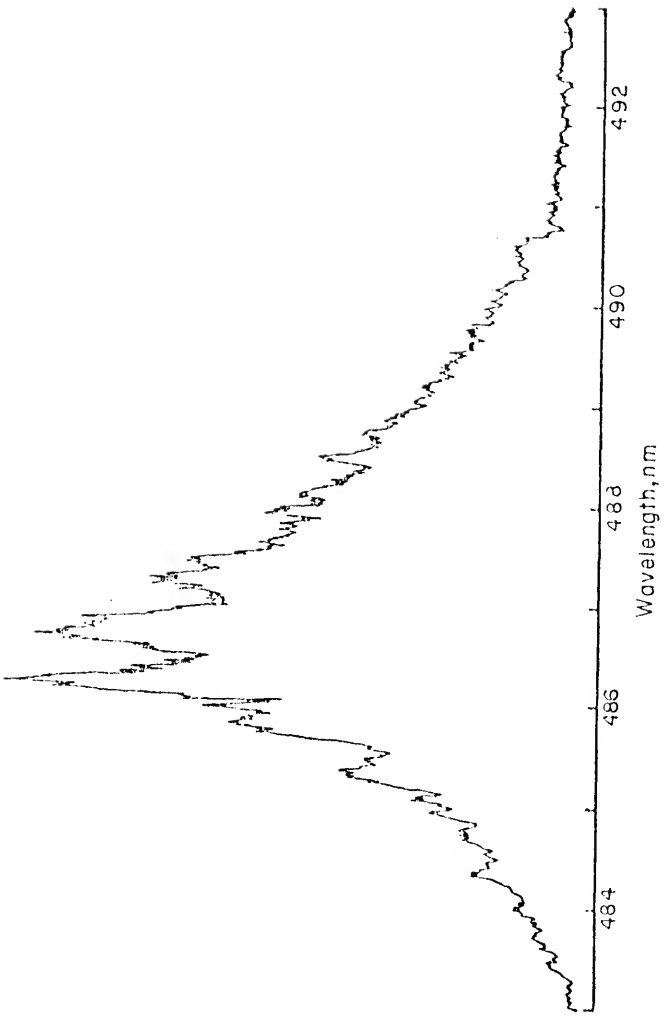
484
486
488
490
492
Wavelength, nm

of BaOH and BaO bands due to rotational levels can be observed in both Figures 22a and 23 even though a low dispersion spectrometric detection system was used because the spectral bandwidth of the laser used in this study is less than 0.02 nm. BaO fluorescence occurs in this wavelength region (Figure 19 describes the BaO bands which overlap with the BaOH bands in this region), but is weaker under the flame conditions used. The fine structure of these bands should be investigated under varying flame conditions. By frequency narrowing the dye laser output and synchronously scanning excitation and detection wavelengths, a true resonance fluorescence spectrum could be obtained which would yield much information about the energy levels of BaOH and BaO. Conventional molecular fluorescence excitation and emission spectra should also be utilized. Fluorescence emission spectra of BaOH are shown in Figure 24 with λ_{ex} = 487 nm. As can be seen, the fluorescence spectra in this wavelength region are very rich and overlap the emission spectra of both BaO and BaCl. BaOH fluorescence was also observed at λ_{fl} = 730 nm with λ_{ex} = 487 nm.

BaO fluorescence in flames was also observed for the first time. Figure 25 shows a near resonance excitation wavelength scan over the $A^1\Sigma$-$X^2\Sigma$ (4, 0) vibrational band at λ_{fl} = 535 nm. The fluorescence envelope of this band is similar to that of the emission envelop (see Figure 19). The fluorescence signal observed here is very weak, and there is much noise on the signal (poor S/N). Flame conditions can be adjusted to increase the BaO fluorescence.

In an attempt to distinguish BaOH from BaO fluorescence in the wavelength region from 480 nm to 540 nm, fluorescence excitation spectra were taken at λ_{fl} = 487 nm, λ_{fl} = 496 nm, λ_{fl} = 512 nm, and λ_{fl} = 535 nm

Figure 24: Fluorescence emission spectra of BaOH in an air-acetylene flame (a. 0.1 M $BaCO_3$ in 0.5 M HCl solution; b. 10,000 ppm Ba as $BaCl_2$ in deionized water solution) at fixed fluorescence excitation wavelength of λ_{ex} = 487 nm.

Excitation Conditions:
Monochromator slit width:
(a) 250 μm (0.5 nm spectral bandpass):
(b) 1750 μm (3.5 nm spectral bandpass):
Scan speed of monochromator wavelength:
0.2 nm s^{-1};
Spectral range of monochromator emission wavelength: (a) 480-513 nm;
(b) 491-550 nm.

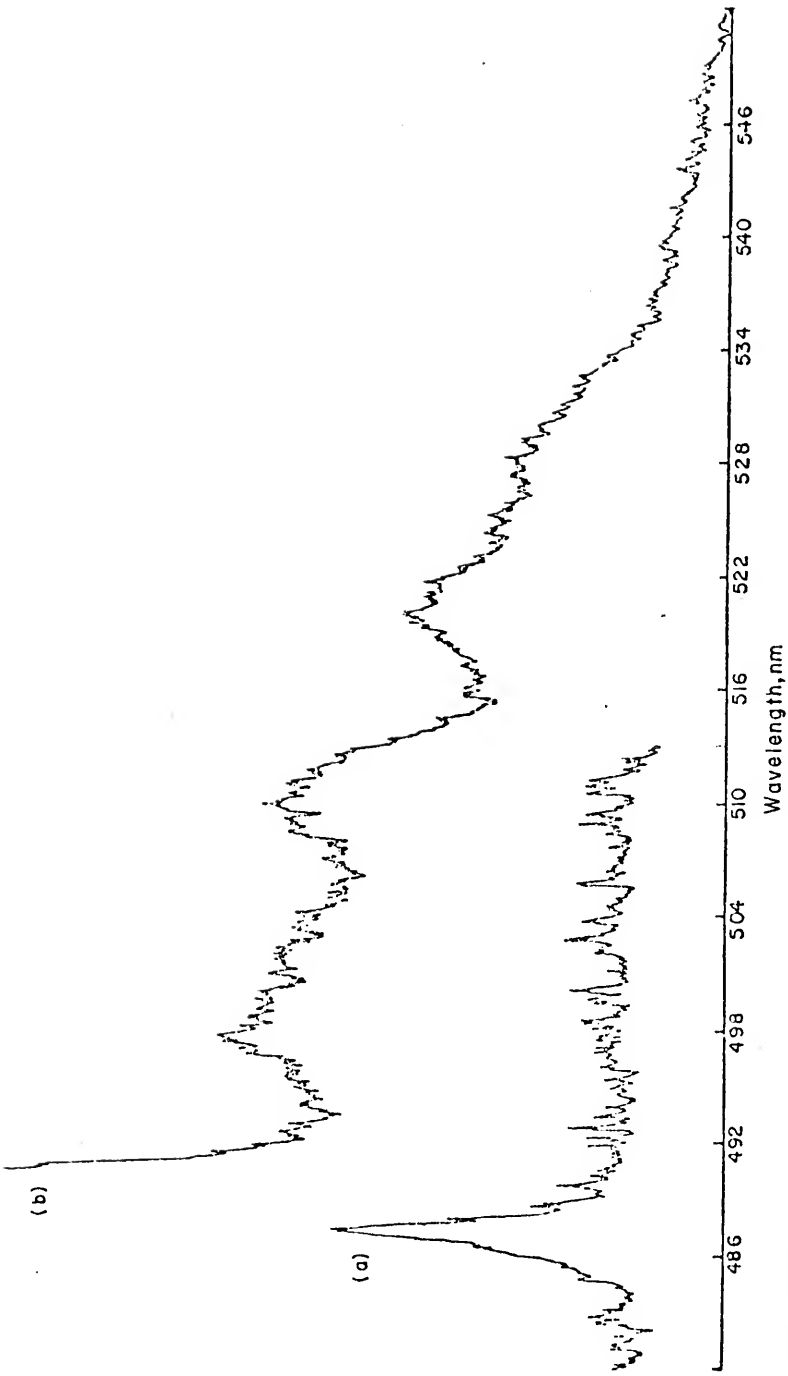
(b)
(a)
486
492
498
504
510
516
522
528
534
540
546
Wavelength, nm

Figure 25: Fluorescence excitation spectrum of BaO in an air-acetylene flame (10,000 ppm Ba as $BaCl_2$ in deionized water solution) at fixed fluorescence emission wavelength of λ_{fl} = 535 nm.

Excitation Conditions:
Monochromator slit width: 1750 µm
(3.5 nm spectral bandpass):
Scan speed of laser excitation wavelength:
0.6 nm min^{-1}.
Spectral range of laser excitation wavelength:
534-538.5 nm.

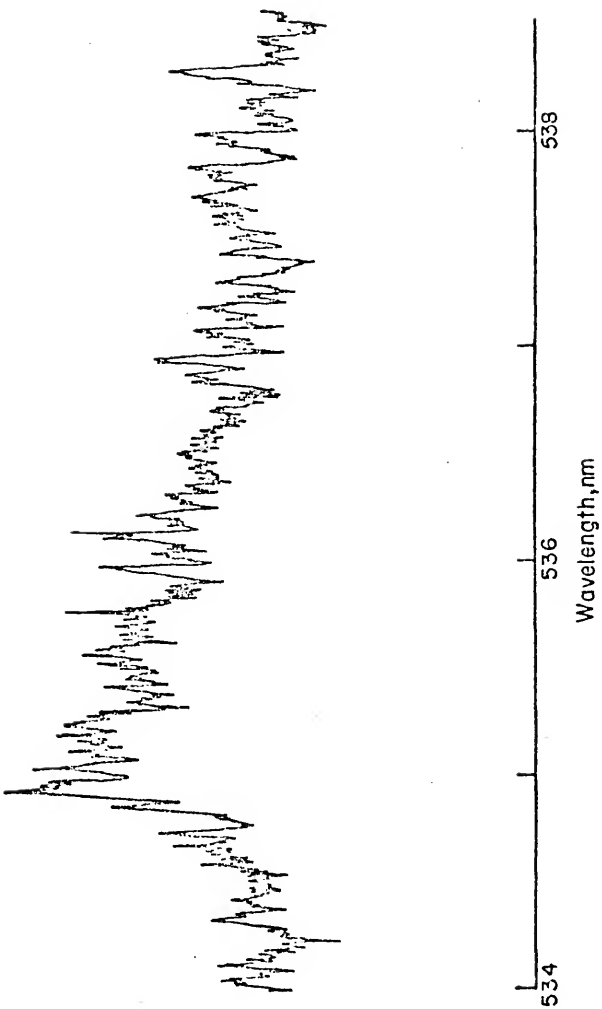
534
536
538
Wavelength,nm

(Figures 26 and 27). The fluorescence spectra at λ_{fl} = 487 nm and λ_{fl} = 512 nm should enhance the BaOH fluorescence, whereas the fluorescence observed at λ_{fl} = 496 nm (corresponding to the $A^1\Sigma$-$X^1\Sigma$ (7, 0) transition of BaO) and λ_{fl} = 535 nm (corresponding to the $A^1\Sigma$-$X^1\Sigma$ (4, 0) transition of BaO) should enhance the BaO fluorescence. Some fine structural differences are observed in the fluorescence spectra taken at λ_{fl} = 496 nm and λ_{fl} = 512 nm. However, a more detailed study is necessary. The broad fluorescence band occurring near 499 nm in the spectrum taken at λ_{fl} = 512 nm which is not observed in the fluorescence spectrum taken at λ_{fl} = 496 nm is attributed to BaOH. The fluorescence of BaOH in this region is stronger than that of BaO under the flame conditions used.

Laser-Excited Molecular Fluorescence of CaOH and SrOH

The orange coloration of flames, when calcium salts are introduced into flames, is known to be due to broad emission bands from 550 nm to 630 nm. Similarly, when strontium salts are introduced into flames, a red coloration is observed due to broad emission bands from 600 nm to 690 nm (114, 139). Initially, the molecular calcium bands found at 554 nm, 602 nm, and 623 nm, and the molecular strontium bands found at 606 nm, 647 nm, 669 nm and 682 nm were ascribed to the monoxides. However, later these bands were attributed to the monohydroxides from spectrometric studies in flames with varied OH content by correlating these emissions to those of the corresponding halides (134), and also by isotope displacement studies (137, 140, 141). Recently, van der Hurk et al. (142) confirmed that these bands were due to the monohydroxides by a method which used the ratio of band to atomic line intensity in two isothermal flames with different known gas composition. In recent

Figure 26: Fluorescence excitation spectra of BaOH and BaO in an air-acetylene flame (5,000 ppm Ba as $BaCl_2$ in deionized water solution) at fixed fluorescence emission wavelengths of λ_{fl} = 487 nm, λ_{fl} - 496 nm, and λ_{fl} = 512 nm.

Excitation Conditions:
Monochromator slit width: 1750 μm (3.5 nm spectral bandpass):
Scan speed of laser excitation wavelength: 2 nm min^{-1};
Spectral range of laser excitation wavelength: 482-505 nm.

Also see note at end of Figure 21 caption.

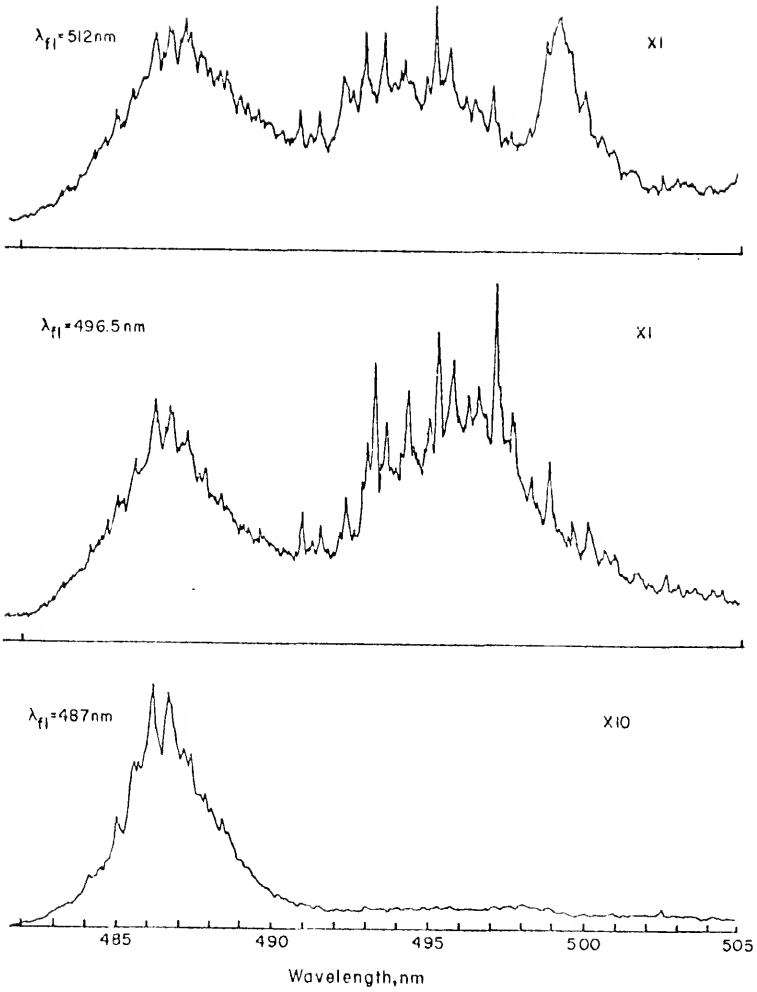
λ_{fl}=512nm
X1
λ_{fl}=496.5nm
X1
λ_{fl}=487nm
X10
485
490
495
500
505
Wavelength,nm

Figure 27: Fluorescence excitation spectra of BaOH and BaO in air-acetylene flame (10,000 ppm Ba as $BaCl_2$ in deionized water solution) at fixed fluorescence emission wavelengths of λ_{fl} = 512 nm and λ_{fl} = 535 nm.

Excitation Conditions:
Monochromator slit width: 1750 μm (3.5 nm spectral bandpass):
Scan speed of laser excitation wavelength: 0.6 nm min^{-1}.
Spectral range of laser excitation wavelength: 484.5-490 nm.

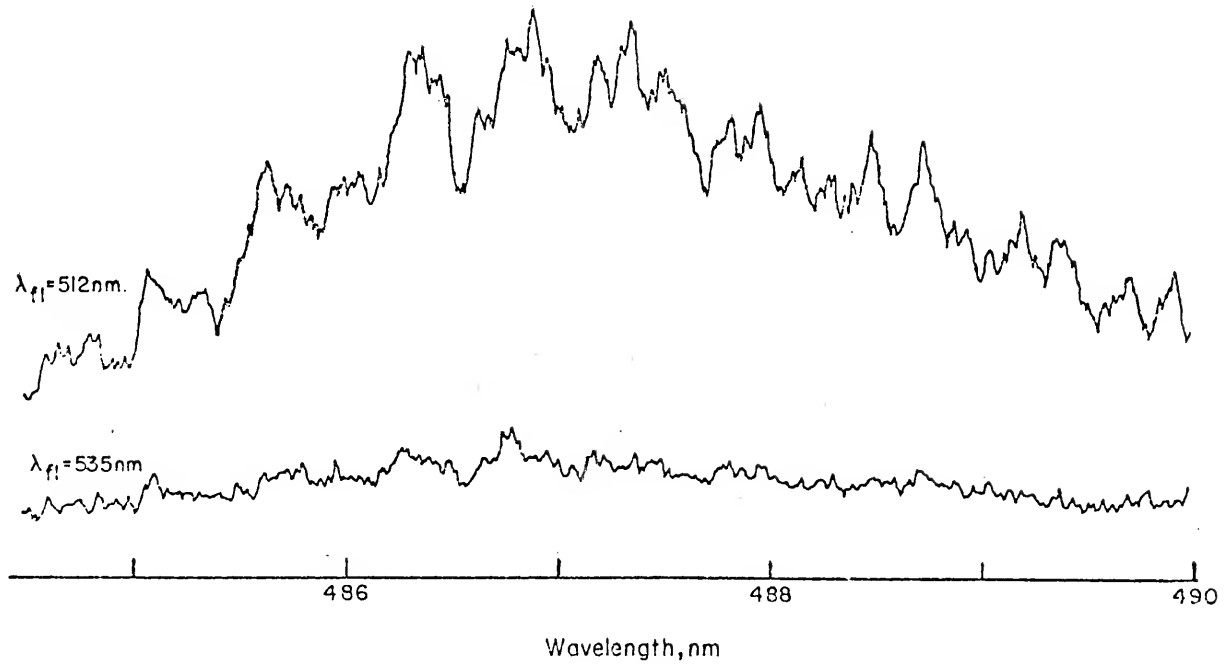
λ_{fl}=512nm.
λ_{fl}=535nm
486
488
490
Wavelength, nm

years, molecular bands of CaOH and SrOH have been observed by absorption (143, 144) and fluorescence (127, 128) methods. Despite these many studies, the energy levels of CaOH have not yet been established except for noting that these molecular bands may originate from two different electronic configurations (127, 134). An energy level diagram for SrOH has been proposed and discussed by van der Hurk et al. (145).

Studies of molecular species in flames have been limited by complex and difficult to control flame conditions, low concentrations of species, low dispersive spectrometric systems, lack of good excitation sources, and so forth. However, laser sources, which have a high spectral irradiance with a narrow spectral bandpass, and a well designed sample introduction and gas flow control system, overcome the limitations mentioned above except for the complex flame chemistry. In fact, CH (126, 128), C_2 (130), and CaOH, SrOH, MnO, and CrO (128) in various flames have been successfully observed by laser-excited molecular fluorescence spectroscopy.

Molecular fluorescence of CaOH and SrOH in an air-acetylene flame were investigated here. Fluorescence excitation and fluorescence emission spectra of CaOH and SrOH were obtained using the pulsed N_2 laser pumped tunable dye laser system described in Chapters III and IV. CaOH fluorescence was investigated from 480 nm to 680 nm in order to examine the electronic and vibrational levels of CaOH.

The output beam of the dye laser was beam expanded to a diameter of ca 5 nm. An air-acetylene flame was burnt on a laboratory-constructed capillary burner fitted with an inert gas sheathing device. Fluorescence signals were detected by a R777 photomultiplier tube

(Hamamatsu TV Co., Middlesex, NJ 08846); processed by a boxcar integrator (Model 162/164, Princeton, NJ 08540); and recorded on a strip-chart recorder.

Stock solutions of 5000 μg ml^{-1} calcium and strontium were prepared by acidic (HCl) dissolution of the carbonates. The salt solutions were aspirated into the air-acetylene flame (air flow rate 12.2 l min^{-1}; acetylene flow rate 2.2 l min^{-1}). Fluorescence excitation spectra, (wavelength of the monochromator was fixed and spectra were observed by scanning the excitation wavelength of the dye laser output), and fluorescence emission spectra, (excitation wavelength of the dye laser output was fixed and spectra were observed by scanning the monochromator), were recorded while aspirating calcium or strontium solutions into the flame. The spectral linewidth of the dye laser (i.e., excitation) output was ca 0.02 nm. The flame temperature at the observation height was ca 2400 K.

No amplitude normalizations were made to correct for dye laser intensity, photomultiplier response, or the slit function of the monochromator.

Spectral Characteristics of CaOH

Emission spectrum of CaOH in an air-acetylene flame is shown in Figure 28. The well-known emission bands near 554 nm, 572 nm, 603 nm, 623 nm, and 645 nm are readily observed. The doublet lines observed near 590 nm are the atomic emission resonance lines of sodium which is a concomitant in the solution. The band near 593 nm can be ascribed to the (0, 0) sequency of the orange system of CaCl. Mavrodineanu and Boiteux (104) identified the following band heads or maximal wavelengths in the emission spectrum of CaOH in an air-acetylene flame: 538.5 nm, 542.5 nm, 555.0 nm, 578.0 nm, and 582.5 nm for the green system; and

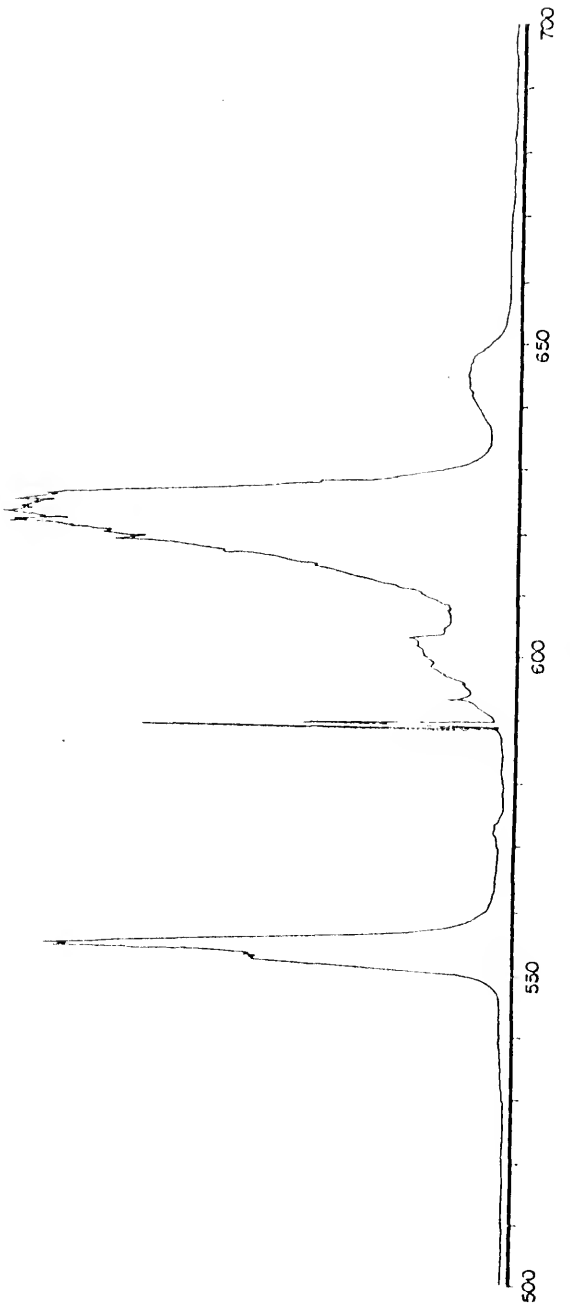

Figure 28: Emission spectrum of CaOH in an air-acetylene flame
Ca: 5000 µg-ml-1, slit width: 10 µm

603.8 nm, 623.0 nm, 645.3 nm, 665.3 nm, 683.9 nm, and 698.0 nm for the orange system.

Fluorescence emission spectra of CaOH in the air-acetylene flame are shown in Figure 29. The spectra were excited at 554 nm and 623 nm. As can be seen from the spectra, strong resonance fluorescence occurs at the same wavelengths as the excitation wavelengths. Although molecular fluorescence intensities of the bands vary with excitation wavelengths, similar band structures as those obtained in emission are observed in the molecular fluorescence emission spectra. It should be noted that the two main bands around 554 nm and 623 nm were also observed when excitation occurred at other wavelengths corresponding to other vibrational levels of the $A^2\Pi$-$X^2\Sigma$ and $B^2\Sigma$-X^2 systems. So far, it has been considered that the two main bands originate from different electronic configurations in the excited states (127, 134). In analogy to alkaline earth halides (because the hydroxyl group behaves in many respects like a halogen atom) and to SrOH (145), the 554 nm and 623 nm main bands may correspond to the (0, 0) bands of the $B^2\Sigma$-$X^2\Sigma$ and $A^2\Pi$-$X^2\Sigma$ systems. Human and Zeegers (127) reported energy exchange between the two electronic levels, using interference filters and a continuum source. Blackburn et al. (128) observed the fluorescence bands near 623 nm and 603 nm, exciting at 554 nm. The presence of these bands were confirmed in the present work, and, in addition, fluorescence from other bands was observed. Because energy exchange between the different electronic levels occurs and because CaO and CaCl have overlapping bands with CaOH in this wavelength region, identification of molecular electronic and vibrational structure of CaOH is difficult. Fluorescence of CaO and CaCl was weaker than that of CaOH, under the

Figure 29: Fluorescence emission spectra of CaOH in an air-acetylene flame

(a) λ_{ex} = 554 nm, Ca: 5000 $\mu g\text{-}ml^{-1}$, slit width: 350 μm;

(b) λ_{ex} = 623 nm, Ca: 5000 $\mu g\text{-}ml^{-1}$, slit width: 350 μm.

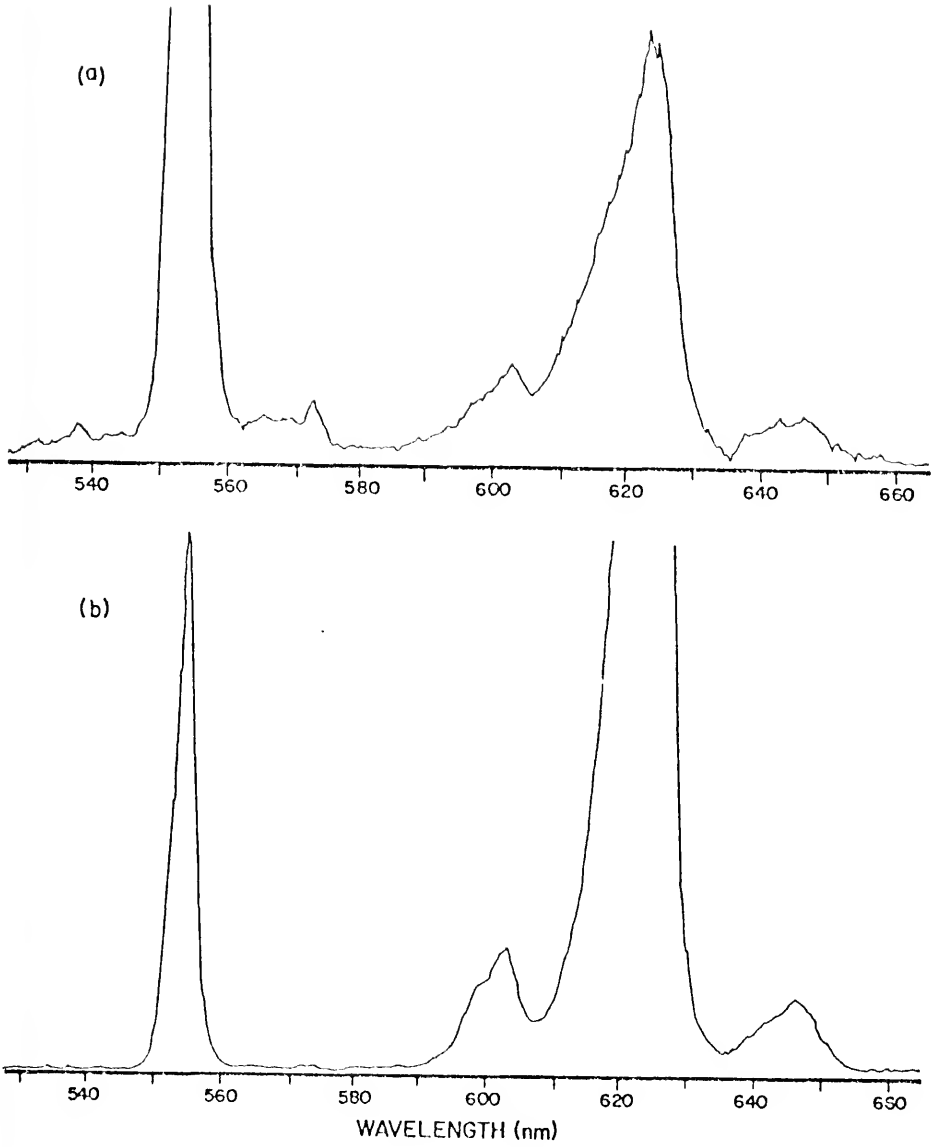
(a)
540
560
580
600
620
640
660
(b)
540
560
580
600
620
640
650
WAVELENGTH (nm)

present flame and experimental conditions. Thermally-assisted activation, as well as radiationless deactivation, is important in the interpretation of the spectra.

In order to further investigate the $A^2\Pi$ and $B^2\Sigma$ systems. fluorescence excitation spectra were observed. Due to the high spectral irradiance and the narrow spectral bandwidth of the laser, fluorescence excitation spectra allow high signal levels with high spectral resolution to be obtained. It should also be noted that high resonance fluorescence signal levels were obtained throughout the entire 480 nm - 680 nm wavelength region investigated; this implies that a system which synchronously scans the laser excitation and monochromator detection (fluorescence emission) wavelength with frequency narrowing of the laser linewidth and ratioing the fluorescence signal to the source intensity would provide a powerful tool for identification of energy levels of molecules.

Fluorescence excitation spectra with fluorescence emission wavelengths at λ_{fl} = 554 nm and λ_{fl} = 623 nm are shown in Figures 30 and 31, respectively. These spectra were obtained with different dyes (laser) (see Figure 8) and with different gain settings. The anomalous peaks observed near 597 nm, for example, are a result of the variation in dye laser source intensity with wavelength (ratioing to the source intensity would eliminate this problem). Peak band intensities are observable near 623 nm, 613 nm, 603 nm, 592 nm, 583 nm, 572 nm, 565 nm, 554 nm, 542 nm, and 538 nm. Near resonance scans over these bands were obtained. Three of these are shown in Figure 32 for the regions near 554 nm, 603 nm, and 623 nm. For the near resonance scan over the 554 nm region, the arrows mark the more

Figure 30. Fluorescence excitation spectra of CaOH in an air-acetylene flame with λ_{fl} = 554 nm and slit width = 1750 μm

(a) Ca: 100 $\mu g\text{-}ml^{-1}$, dye: C495,

(b) Ca: 5000 $\mu g\text{-}ml^{-1}$, dye: R6G,

(c) Ca: 100 $\mu g\text{-}ml^{-1}$, dye: RB.

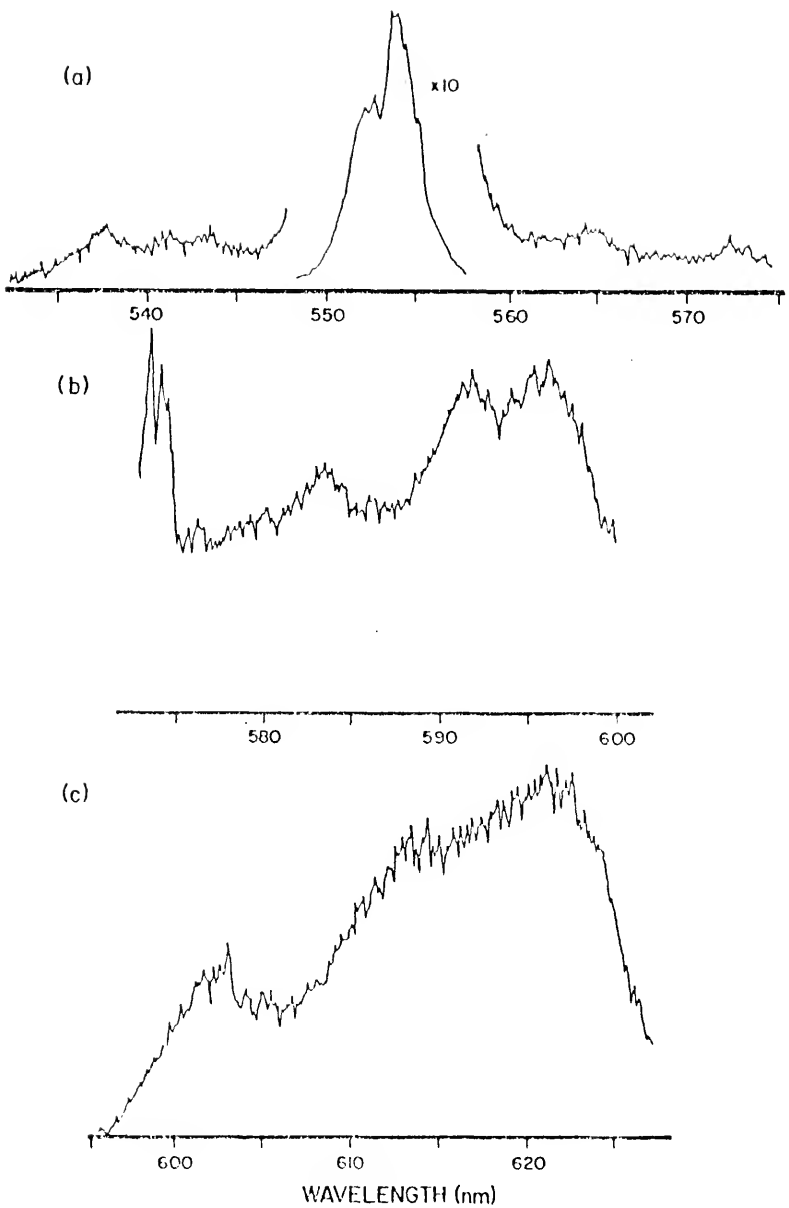
(a)
x10
540
550
560
570
(b)
580
590
600
(c)
600
610
620
WAVELENGTH (nm)

Figure 31: Fluorescence excitation spectra of CaOH in an air-acetylene flame with λ_{fl} = 623 nm and slit width = 1750 μm

(a) Ca: 100 $\mu g\text{-}ml^{-1}$, dye: C495,

(b) Ca: 5000 $\mu g\text{-}ml^{-1}$, dye: R6G,

(c) Ca: 100 $\mu g\text{-}ml^{-1}$, dye: RB.

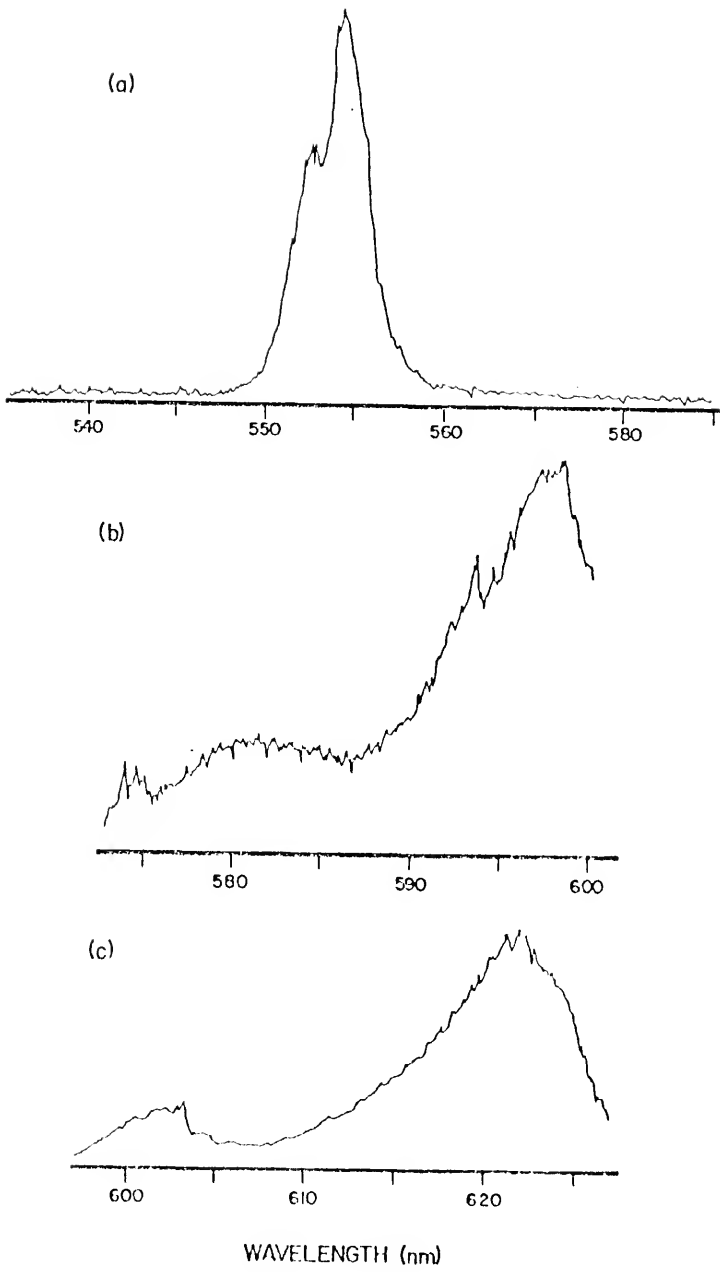
(a)
540
550
560
580
(b)
580
590
600
(c)
600
610
620
WAVELENGTH (nm)

Figure 32: Near-resonance fluorescence excitation spectra of CaOH in an air-acetylene flame

(a) λ_{fl} = 554.3 nm, Ca: 100 $\mu g\text{-}ml^{-1}$, slit width: 2000 μm;

(b) λ_{fl} = 623.5 nm, Ca: 100 $\mu g\text{-}ml^{-1}$, slit width: 2000 μm;

(c) λ_{fl} = 603.0 nm, Ca: 1000 $\mu g\text{-}ml^{-1}$, slit width: 2000 μm.

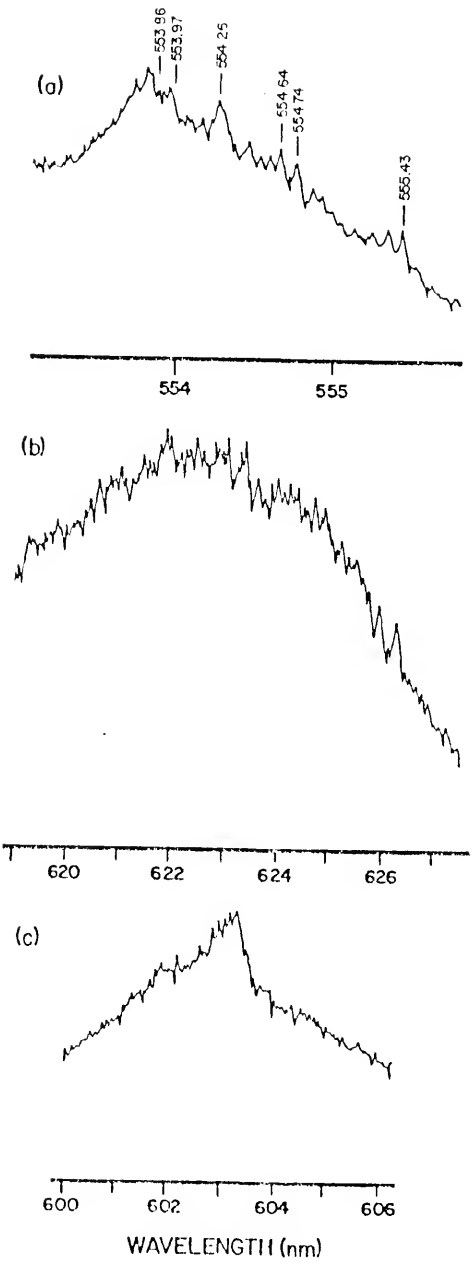
(a)
553.96
553.97
554.25
554.64
554.74
555.43
554
555
(b)
620
622
624
626
(c)
600
602
604
606
WAVELENGTH (nm)

intense peak wavelength observed by flame emission (114, 133). From this data, an approximate preliminary energy diagram is proposed for the $A^2\Pi$ and $B^2\Sigma$ systems, as shown in Figure 33 (also see Table 11).

Because of the diffuseness of the bands and their extensive structure, it is difficult to assign bandheads. Also, as noted earlier, CaO and CaCl have bands which overlap in this region. For more definite assignments of the transitions involved, further studies similar to those of van der Hurk (133) in flames of varying composition and/or temperature are required. Isotope shift studies might also provide useful information.

Spectral Characteristics of SrOH

The studies performed while introducing strontium salts into the flame confirmed the results obtained by Human and Zeegers (127) and Blackburn et al. (128) on the fluorescence structure of strontium compounds observed in flames. The results obtained in this study also compared quite favorably to those obtained by van der Hurk (133) in emission. A fluorescence emission spectra with λ_{ex} = 682 nm is shown in Figure 34. Bands due to SrCl, a coexisting species in the flame, were observed in the present study. Also, a broad band was observed at 591 nm in both fluorescence excitation and fluorescence emission spectra. The energy levels of SrOH have been previously discussed (133, 145). In order to further discuss and assign energy levels, additional studies using the pulsed laser-excited molecular fluorescence technique in flames of varying composition and/or temperature need to be pursued.

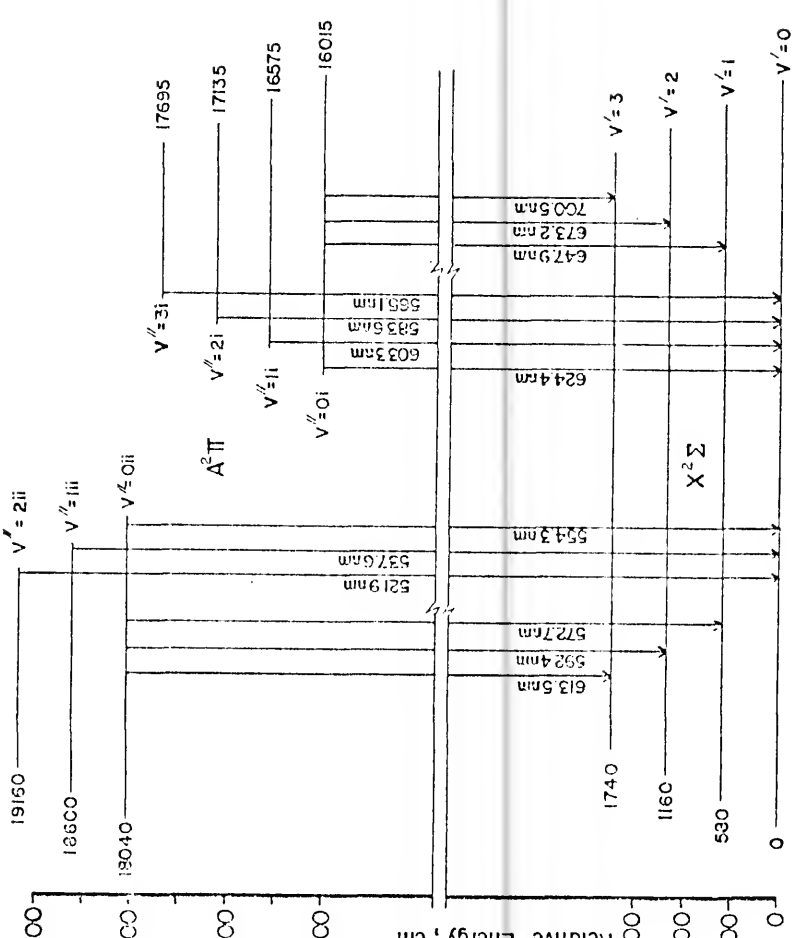

Figure 33: Preliminary energy level diagram for $A^2\Pi - X^2\Sigma$ (i) and $B^2\Sigma - X^2\Sigma$ (ii) systems for CaOH, showing the sequences

Table 11. Approximate Energy Transitions of $A^2\Pi$-$X^2\Sigma$ (i) and $B^2\Sigma$-$X^2\Sigma$ (ii)

Wavelength, nm	Transition (v", v')	Relative energy levels, cm^{-1}	Transition energy, cm^{-1}
521.9	2,0ii	0-19160	19160
537.6	1,0ii	0-18600	18600
538.2	2,1ii	580-19160	18580
554.3	0,0ii	0-18040	18040
554.9	1,1ii	580-18600	18020
555.5	2,2ii	1160-19160	18000
565.1	3,0i	0-17695	17695
572.7	0,1ii	580-18040	17460
573.4	1,2ii	1160-18600	17440
574.0	2,3ii	1740-19160	17420
583.6	2,0i	0-17135	17135
584.3	3,1i	580-17695	17115
592.4	0,2ii	1160-18040	16880
593.1	1,3ii	1740-18600	16860
603.3	1,0i	0-16575	16575
604.0	2,1i	580-17135	16555
604.8	3,2i	1160-17695	16535
613.5	0,3ii	1740-18040	16300
624.4	0,0i	0-16015	16015
625.2	1,1i	580-16575	15995
626.0	2,2i	1160-17135	15975
626.7	3,3i	1740-17695	15955
647.9	0,1i	580-16015	15435
648.7	1,2i	1160-16575	15415
649.5	2,3i	1740-17135	15395
673.2	0,2i	1160-16015	14855
674.1	1,3i	1740-16575	14835
700.5	0,3i	1740-16015	14275

Figure 34: Fluorescence emission spectrum of SrOH in an air-scetylene flame with λ_{ex} = 682 nm

Sr: 5000 $\mu g\text{-}ml^{-1}$, slit width: 250 μm.

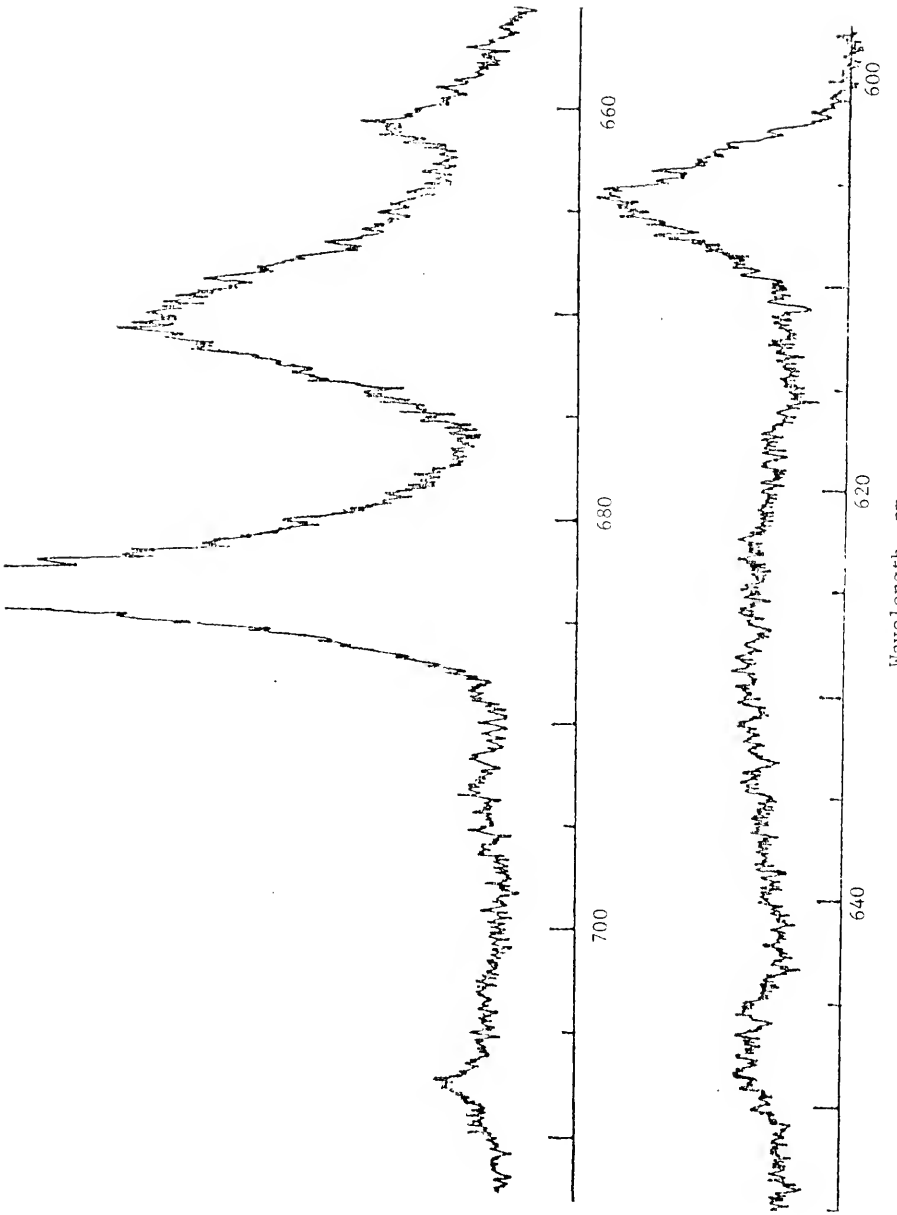
700
680
660
640
620
600
Wavelength, nm

CHAPTER VI
CONCLUSIONS AND DIRECTIONS FOR FURTHER RESEARCH

Pulsed source laser-excited atomic fluorescence with gated detection is superior to all other elemental methods compared here in terms of limits of detection, linear dynamic ranges, and lack of spectral interferences. The ease of operation of the system is solely dependent on the state-of-the-art of tunable dye lasers. The high cost of the system and the requirement of single element detection (slew scanning of the dye laser is possible) will have to be weighed against the need for trace analysis by the analyst. It will also be necessary to investigate other nebulization (e.g., ultrasonic) and atomization sources (e.g., furnaces, ICP, etc.). A pulsed source laser-excited atomic fluorescence system, which optimizes both resonance and nonresonance fluorescence signals via SNR determinations and considers spectral irradiance in terms of approaching saturation, will provide the best method for trace analysis to date. In most cases the detection limits and linear dynamic range could be improved by about 2 to 5 orders of magnitude by (i) optimization of the optical system ($\gtrsim$ 1 order); (ii) optimization of laser beam diameter (i.e., spectral irradiance)($<$ 1 order); (iv) higher output powers (especially in the frequency doubled wavelength region)($\gtrsim$ 1 order); (v) use of ultrasonic (or much improved pneumatic) nebulization ($>$ 1 order); (vi) improvement in flame stability and homogeneity by improved flow system and mixing chamber design ($<$ 1 order); (vii) a more suitable burner configuration ($\lesssim$ 1 order); (viii) optimization

of the electronic detection system (e.g., fast transient response photomultiplier tube and base, pulse stretching, and preamplification) ($\tilde{>}$ 1 order); and (ix) reduction in radio frequency interference noise ($\tilde{<}$ 1 order).

The results described for molecular fluorescence in flames indicate the utility and power of the pulsed laser excited-gated detection fluorescence spectrometric method for the investigation of the energy levels and reaction kinetics of molecular species. High resolution laser spectroscopic techniques, which are experimentally more complex, are available if a particular study requires such resolution. However, the fluorescence system used in this work provides excellent results and dye laser output can be further narrowed to give spectral resolution of less than 0.001 nm, which should be quite adequate for many studies.

With several modifications to the present experimental system, which are listed above (i-ix), the signal-to-noise ratio could be greatly enhanced. These facts plus the results presented here indicate the great potential of pulsed laser-excited molecular fluorescence for not only the identification and determination of energy level transitions of co-existing species in plasmas, but also for the studies of reaction kinetics in plasmas.

Molecular fluorescence of CaOH and SrOH was obtained using pulsed laser excitation. The results obtained for CaOH are presented and an energy level diagram has been proposed based on these results and analogies to SrOH and alkaline earth halides. The molecular fluorescence of BaO, BaOH, and BaCl in an air-acetylene flame have been selectively excited and observed by laser-excited molecular fluorescence spectroscopy. BaO and BaOH fluorescence in flames were

observed for the first time. These results were compared to the emission spectra. Further investigations of these and other molecular and atomic species occurring in flames and plasmas are now possible over the wavelength range from 217 nm to 950 nm. Investigation of well-characterized molecules (e.g., CH, C_2, and OH) will certainly occur soon.

Throughout this work a number of items have been mentioned which would improve the analytical figures of merit of the pulsed N_2 laser pumped tunable dye laser fluorescence system. Also, additional research has been suggested. Because there is an extreme amount of practical and theoretical analytical and diagnostic research yet to be done, priorities must be made.

First, refinement and optimization of the pulsed laser-excited fluorescence system for both analytical and diagnostic work should occur. (A) Nebulizer considerations: Ultrasonic nebulization should be compared with pneumatic nebulization in terms of both efficiency, stability and droplet size, and practicality for routine analytical use. High efficiency, low flow pneumatic nebulizers (28) should also be compared to the conventional pneumatic nebulizers. (B) Burner and gas flow system considerations: Because the theoretical expressions are all based upon having a homogeneous analyte volume, much care should be exercized to ensure this to be true. Use of a rectangular premixed laminar flow flame shielded flame burner with provisions for an inert gas sheath provides the most homogeneous analyte volume and flame conditions. The spacing of holes on the burner top may need to be investigated to ensure greatest analyte distribution homogeneity. Because the length of the monochromator entrance slit is generally 1 cm,

a 1 cm path length of inner flame volume should be provided. The rectangular burner configuration will minimize postfilter effects. The gas flow system should be well regulated for minimum fluctuations of flame gases, should provide traps for any gas impurities, and should allow for variations in the gas flow rates without changing the calibration (146), and provide for good gas mixing of the flame gases. Desolvation may be considered. (C) Atomizer considerations: Although air-acetylene and nitrous oxide-acetylene flames have proven to be very useful atomizers with relatively minimal matrix interference effects and will continue to be used, it would be interesting to investigate furnaces, induction coupled plasmas, and possibly higher temperature flames. The H_2-Ar-entrained air flame may be useful for some elements (e.g., Sn) and in conjunction with sample pre-treatment processes such as hydride generation. (D) Excitation source considerations: The state-of-the-art of N_2 laser pumped dye lasers continues to improve reliability, amplitude stability, beam quality, line width, efficiency, ease of operation, wavelength range, and pulse-to-pulse variations. Higher average power (e.g., use of 50 Hz repetition rate with dye laser system used in this study) must be considered along with rate of dye degradation, but should yield slightly improved results. Spatially filtering the output beam would provide a more homogeneous excitation beam; however, the ease of spatially filtering the beam must be considered for analytical work. The beam size can be reduced from that used in these studies if the detection optics are altered to efficiently use the smaller beam (i.e. flip the monochromator on its side, use a dove prism, or a non-dispersive system). A multipass cell configuration should also be investigated (proper light trapping,

baffling and aperturing of optical train must be used here). These considerations should increase source spectral irradiance, decrease scatter, and improve spatial homogeniety. (E) Detection optics considerations: Because the dye laser is such an intense source, proper care must be taken to ensure that only the analyte volume area of interest is being viewed by the detector. Environmental scatter causes deleterous effects, and the optical train must be properly baffled, light trapped, and apertured. For resonance fluorescence measurements, a two lens detection system properly apertured may prove useful. For nonresonance fluorescence measurements the above requirements are less stringent, and a nondispersive system is seemingly ideal. A nondispersive system consisting of a collimating lens together with a series of interference filters and neutral density filters should yield great enhancement of both signal and linear dynamic range. Again, two or more detection systems could be placed around the flame in order to optimize both resonance and nonresonance detection. (F) Detection electronics considerations: Radio frequency interference (RFI) must be considered as a major source of noise or at least a large factor in the ease of detection. It not only affects this system but also any other system in the laboratory. Presently extensive RFI shielding would be necessary. A photomultiplier base circuit designed according to Harris et al. (96) should improve transient response, linearity, and high current operation. The photomultiplier should be enclosed in a well-shielded housing. All connection cables should remain as short as possible. If RFI is considerably reduced, use of a fast, low noise preamplifier would obviously benefit. Triggering the boxcar integrator from a photodiode signal off the laser pulse itself should

reduce jitter and gate drift; however, a delay line would then be necessary. Ratioing and pulse stretching to improve precision and SNR and reduce drift should be investigated. Use of an analog integrator on the output of the boxcar integrator may also improve precision and SNR.

Upon optimization of the fluorescence system, a complete noise analysis similar to that performed by Bower and Ingle (98) on an atomic absorption system should be performed in order to determine the limiting noise in the system and indicate where further improvements might be made.

Determination of the fluorescence flame background of the flame components and of common major matrix constituents which are likely to form molecular species in flames (e.g., Ca, Mg) is of great importance to both analytical and combustion diagnostic workers.

Determination of flame temperatures by the two-line atomic fluorescence method or via vibrational band intensities is also of great importance to both analytical spectroscopists and combustion diagnostic engineers. Establishment of a standard burner system and flame would greatly aid workers in these fields.

Temperature and concentration profiling of flames using a silicon intensified target (SIT) vidicon tube would yield a great amount of information in a relatively short amount of time and would be of great benefit to combustion engineers.

Multi-element detection using a slew-scan system similar to that employed by Johnson et al. (99) would require computer interfacing of the laser source and the detection system, but would prove to be invaluable to laboratories that need to analyze for a large number of elements on a routine basis.

The independence of quantum efficiency under saturation conditions still needs to be definitely proven experimentally.

The possible applications for the N_2 laser pumped tunable dye laser in molecular fluorescence studies were listed in the introduction (Chapter I) and will not be repeated here.

The primary purpose of this study was to improve the analytical figures of merit for the laser-excited atomic fluorescence spectrometric method and to point out the utility of this fluorescence spectrometric system in molecular fluorescence studies. Although there is much research to be done, this goal was accomplished.

REFERENCES

1. J.D. Winefordner, J. Chem. Ed., submitted.

2. G. Kirchhoff and R. Bunsen, Pogg. Ann., 110, 161 (1860).

3. Ibid., 113, 337 (1861).

4. G. Kirchhoff and R. Bunsen, Phil. Mag., 22, 275 (1861).

5. W.H. Wollaston, Phil. Trans., 92, 365 (1902).

6. J. Fraunhofer, Ann. Phys., 56, 264 (1817).

7. R.W. Wood, Phil. Mag., 10, 513 (1905).

8. E.L. Nichols and H.L. Howes, Phys. Rev., 23, 472 (1924).

9. R.M. Badger, Z. Phys., 55, 56 (1929).

10. A. Walsh, Anal. Chem., 46, 698A (1974).

11. C. Th. J. Alkemade, in "Proceedings of the Xth Colloquim Spectroscopicum Internationale," E.R. Lippincott and M. Margoshes, Eds., Spartan Books, Washington, D.C., 1963.

12. J.D. Winefordner and T.J. Vickers, Anal. Chem., 36, 161 (1964).

13. J.D. Winefordner and R.A. Staab, ibid., p. 165.

14. Ibid., 1367 (1964).

15. R.F. Browner, Analyst, 99, 617 (1974).

16. T.S. West, Analyst, 99, 886 (1974).

17. J.D. Winefordner, Chem. Tech., 5, 123 (1975).

18. J.D. Winefordner, J.J. Fitzgerald, and N. Omenetto, Appl. Spectrosc., 29, 369 (1975).

19. J.D. Winefordner, S.G. Schulman and T.C. O'Haver, "Luminescence Spectrometry in Analytical Chemistry," John Wiley, New York, 1973.

20. G.F. Kirkbright and M. Sargent, "Atomic Absorption and Fluorescence Spectroscopy," Academic Press, New York, 1974.

21. V. Sychra, V. Svoboda and I. Rubeska, "Atomic Fluorescence Spectroscopy," Van Nostrand Reinhold Co., London, 1975.

22. M.L. Parsons, B.W. Smith and G.E. Bentley, "Handbook of Flame Spectroscopy," Plenum Publishing Corp., New York, 1975.

23. J.D. Winefordner, Ed., "Trace Analysis, Spectroscopic Methods for Elements," John Wiley, New York, 1976.

24. J.B. Willis, Spectrochim. Acta, 23A, 811 (1967).

25. H. Massman, Spectrochim. Acta, 23B, 215 (1968).

26. T.R. Copeland, K.W. Olson and R.K. Skogerboe, Anal. Chem., 44, 1471 (1972).

27. N.E. Korte, J.L. Moyers, and M.B. Denton, Anal. Chem., 45, 530 (1973).

28. C.J. Molnar and J.D. Winefordner, Anal. Chem., 46, 1419 (1974).

29. H.J. Issaq and L.P. Morgenthaler, Anal. Chem., 47, 1661 (1975).

30. K.W. Olson, W.J. Haas, Jr., and V.A. Fassel, Anal. Chem., 49, 632 (1977).

31. J. Bradshaw, S. Bayer, S. Weeks, H. Haraguchi, and J.D. Winefordner, to be submitted.

32. R.G. Michel, J. Coleman, and J.D. Winefordner, Spectrochim. Acta, Part B, in press.

33. D.J. Johnson, F.W. Plankey, and J.D. Winefordner, Anal. Chem., 46, 1898 (1974).

34. T.H. Maiman, Brit. Commun. and Electr., 7, 674 (1960).

35. P.P. Sorokin and J.R. Lankard, IBM J. Res. Develop., 10, 162 (1966).

36. F.P. Schäfer, W. Schmidt, and J. Volze, Appl. Phys. Lett., 9, 306 (1966).

37. R.G. Smith, Anal. Chem., 41, 75A (1969).

38. J.P. Webb, Anal. Chem., 44, 30A (1972).

39. F.P. Schäfer, Ed., "Dye Lasers," Springer-Verlag, New York, 1973.

40. R.A. Keller, Chem. Tech., 3, 626 (1973).

41. C.V. Shank, Rev. Mod. Phys., 47, 649 (1975).

42. C.A. Sacchi and O. Svelto, in "Analytical Laser Spectrometry," N. Omenetto, Ed., John Wiley, New York, in press.

43. L.M. Fraser and J.D. Winefordner, Anal. Chem., 43, 1693 (1971).

44. M.B. Denton and H.V. Malmstadt, Appl. Phys. Lett., 18, 485 (1971).

45. L.M. Fraser and J.D. Winefordner, Anal. Chem., 44, 1444 (1972).

46. N. Omenetto, N.N. Hotch, L.M. Fraser, and J.D. Winefordner, Anal. Chem., 45, 195 (1973).

47. N. Omenetto, N.N. Hatch, L.M. Fraser, and J.D. Winefordner, Spectrochim. Acta, 28B, 65 (1973).

48. N. Omenetto, P. Benetti, L.P. Hart, J.D. Winefordner, and C.Th.J. Alkemade, Spectrochim. Acta, 28B, 289 (1973).

49. N. Omenetto, L.P. Hart, P. Benetti and J.D. Winefordner, Spectrochim. Acta, 28B, 301 (1973).

50. E.H. Piepmeier, Spectrochim. Acta, 27B, 431 (1972).

51. Ibid., p 445.

52. J. Kuhl, S. Neumann, and M. Kriese, Z. Naturforsch., 28a, 273 (1973).

53. J. Kuhl and H. Spitschan, Opt. Commun., 7, 256 (1973).

54. D.R. de Olivares, Ph.D. Thesis, Indiana University, 1976.

55. R.B. Green, J.C. Travis, and R.A. Keller, Anal. Chem., 48, 1954 (1976).

56. B.W. Smith, M.B. Blackburn, and J.D. Winefordner, Can. J. Spectrosc., in press.

57. J.A. Gelbwachs, C.F. Klein, and J.E. Wessel, Appl. Phys. Lett., 30, 489 (1977).

58. J.W. Daily and C. Chan, University of California, Berkeley, CA, unpublished work.

59. J. Kuhl and G. Marowsky, Opt. Commun., 4, 125 (1971).

60. W.M. Fairbank, Jr., T.W. Hansch, and A.L. Schawlow, J. Opt. Soc. Am., 65, 199 (1975).

61. H.L. Brod and E.S. Young, Anal. Chem., 48, 344 (1976).

62. B.L. Sharp and A. Goldwasser, Spectrochim. Acta, 31B, 431 (1976).

63. S. Mayo, R.A. Keller, J.C. Travis, and R.B. Green, J. Appl. Phys., 47, 4012 (1976).

64. S. Neumann and M. Kriese, Spectrochim. Acta, 29B, 127 (1974).

65. M.A. Bolshov, A.V. Zybin, L.A. Zybina, V.G. Koloshnikov, and I.A. Majorov. Spectrochim. Acta, 31B. 493 (1976).

66. J.P. Hohimer and P.J. Hargis, Jr., Appl. Phys. Lett., 30. 344 (1977).

67. N. Omenetto and J.D. Winefordner, in "Analytical Laser Spectrometry," N. Omenetto, Ed., John Wiley. New York, in press.

68. B.W. Smith, Ph.D. Thesis, Univerity of Florida, 1977.

69. G.D. Boutilier, M.B. Blackburn, J.M. Mermet, S.J. Weeks, H. Haraguchi, J.D. Winefordner, and N. Omenetto, in press.

70. J.D. Winefordner, J.J. Fitzgerall, and N. Omenetto, Appl. Spectrosc., 29, 369 (1975).

71. N. Omenetto, Anal. Chem., 48, 75A (1976).

72. N. Omenetto, G.D. Boutilier, S.J. Weeks, B.W. Smith, and J.D. Winefordner, Anal. Chem., 49. 1076 (1977).

73. N. Omenetto, L.M. Fraser, and J.D. Winefordner, Appl. Spectrosc. Rev., 7, 147 (1973).

74. G.D. Boutilier, J.D. Bradshaw, S.J. Weeks, and J.D. Winefordner, Appl. Spectrosc., 31, 307 (1977).

75. H. Kaiser, Anal. Chem., 42(2), 24A (1970).

76. Ibid., 42(4), 26A (1970).

77. I.U.P.A.C., Nomenclature, Symbols, Units, and their Usage in Spectrochemical Analysis, Part II, Section 4.1, Revision 1975.

78. N. Omenetto and J.D. Winefordner, Appl. Spectrosc., 26, 555 (1972).

79. A.P. Thorne, "Spectrophysics," Chapman and Hall, Ltd., London, 1974.

80. J.D. Winefordner and R.C. Elser, Anal. Chem., 43, 24A (1971).

81. N. Omenetto. P. Benetti, and G. Rossi, Spectrochim. Acta, 27B, 453 (1972).

82. N. Omenetto. R. Browner, J.D. Winefordner, G. Rossi. and P. Benetti, Anal. Chem., 44, 1683 (1972).

83. H. Haraguchi, B. Smith, S. Weeks, D.J. Johnson, and J.D. Winefordner, Appl. Spectrosc., 31, 156 (1977).

84. H. Haraguchi and J.D. Winefordner, Appl. Spectrosc., 31, 195 (1977).

85. Ibid., p. 330.

86. H. Haraguchi, S. Weeks, and J.D. Winefordner, Can. J. Spectrosc., in press.

87. N. Omenetto and G. Rossi, Spectrochim. Acta, 25B, 297 (1970).

88. L.M. Fraser, Ph.D. Dissertation, University of Florida, 1972.

89. J. Kuhl, G. Marovsky, P. Kunstmann, and W. Schmidt, Z. Naturforsch. 27A, 601 (1972).

90. S.J. Weeks, H. Haraguchi, and J.D. Winefordner, Anal. Chem., in press.

91. D.K. Killinger, C.C. Wang, and I. Hanabusa, Phys. Rev. A, 13, 2145 (1976).

92. D.R.de Olivares and G.M. Hieftje, unpublished work.

93. M.A. Bolshev, A.V. Zybin, V.G. Koloshnikov, and K.N. Koshelev, unpublished work.

94. F.E. Lytle, Anal. Chem., 46, 545A (1974).

95. Ibid., p. 817A.

96. J.M. Harris, F.E. Lytle, and T.C. McCain, Anal. Chem., 48, 2095 (1976).

97. G. Beck, Rev. Sci. Instrum., 47, 537 (1976).

98. N.W. Bower and J.D. Ingle, Jr., Anal. Chem., 48, 686 (1976).

99. D.J. Johnson, F.W. Plankey, and J.D. Winefordner, Anal. Chem., 47, 1739 (1975).

100. T.W. Hänsch, Appl. Opt., 11, 895 (1972).

101. A.A. Pease and W.M. Pearson, Appl. Opt., 16, 57 (1977).

102. H. Haraguchi, W.K. Fowler, D.J. Johnson, and J.D. Winefordner, Spectrochim. Acta, 32A, 1539 (1976).

103. W.K. Fowler and J.D. Winefordner, Anal. Chem., 49, 944 (1977).

104. R. Mavrodineanu and H. Boiteux, "Flame Spectroscopy," John Wiley, New York, 1965.

105. B.W. Smith and M.L. Parsons, J. Chem. Educ., 50, 679 (1973).

106. J.J. Fitzgerald, T.L. Chester, and J.D. Winefordner, Anal. Chem., 47, 2330 (1975).

107. T.L. Chester and J.D. Winefordner, Spectrochim. Acta, 31B, 21 (1976).

108. K.W. Olson, W.J. Haas, Jr., and V.A. Fassel, Anal. Chem., 49, 632 (1977).

109. L.R.P. Butler, International Symposium on Analytical Chemistry in the Exploration, Mining and Processing of Materials, (uncer aegis of I.U.P.A.C.), Abstract 118, Johannesburg, Republic of South Africa, August 23-27, 1976.

110. M.H. Abdallah, R. Diemiaszonek, J. Jarosy, J.M. Mermet, J. Robin, and C. Trassy, Anal. Chim. Acta, 84, 271 (1976).

111. B.E. Buell, in "Flame Emission and Atomic Absorption Spectrometry," J.A. Dean, T.C. Rains, Eds., Marcel Dekker, New York, 1969.

112. W.K. Fowler, Ph.D. Dissertation, University of Florida, 1976.

113. G. Herzberg, "Molecular Spectra and Molecular Structure. I. Spectra of Diatomic Molecules," 2nd ed., Van Nostrand, Princeton, 1950.

114. P.W.B. Pearce and A.G. Gaydon, "The Identification of Molecular Species," 4th ed., Chapman and Hall, London, 1976.

115. P.T. Gilbert, in "Analytical Flame Spectroscopy," R. Mavrodineanu, Ed., MacMillan, London, 1970.

116. S.R. Koirtyohann and E.E. Pickett, Anal. Chem., 37, 601 (1965).

117. Ibid., 38, 585 (1966).

118. H. Haraguchi and K. Fuwa, Spectrochim. Acta, 30B, 535 (1975).

119. H. Haraguchi and K. Fuwa, Anal. Chem., 48, 784 (1976).

120. H. Haraguchi, N. Furuta, E. Yoshimura, and K. Fuwa, Anal. Chem., 48, 2066 (1976).

121. H. Massman, Z. ElGohary, and S. Gücev, Spectrochim. Acta, 31B, 399 (1976).

122. K. Fuwa and B.L. Vallee, Anal. Chem., 41, 188 (1969).

123. E. Yoshimura, N. Furuta, H. Haraguchi, and K. Fuwa, Appl. Spectrosc., in press.

124. N. Furuta, E. Yoshimura, H. Haraguchi, and K. Fuwa, Spectrochim. Acta, in press.

125. D.R. Jenkins, 2nd Int. At. Abs. and Fluorescence Conf., Sheffield (1969).

126. R.H. Barnes, C.E. Moeller, J.F. Kircher, and C.M. Verber, Appl. Opt. 12, 2531 (1973).

127. H.G.C. Human and P.J. Th. Zeegers, Spectrochim. Acta, 30B, 203 (1975).

128. M.B. Blackburn, J.M. Mermet, and J.D. Winefordner, Spectrochim. Acta, Part A, in press.

129. H. Haraguchi, S.J. Weeks, and J.D. Winefordner, J. Quant. Spectrosc. Radiat. Transfer, in press.

130. P. Baronavski and J.R. McDonald, Appl. Opt., 16, 1867 (1977).

131. P.C. Mahauti, Proc. Phys. Soc., 46, 51 (1934).

132. A. Lagerquist, E. Lind, and R.F. Barrow, Proc. Phys. Soc., A63, 1132 (1950).

133. J. van der Hurk, Ph.D. Dissertation. University of Utrecht, 1974.

134. C.G. James and T.M. Sugden, Nature, 175, 333 (1955).

135. M. Charton and A.G. Gaydon, Proc. Phys. Soc., A69, 520 (1956).

136. A.E. Parker, Phys. Rev., 46, 301 (1934).

137. A. Lagerquist and L. Huldt, Naturwissenschaften, 42, 365 (1955).

138. E.M. Bulewicz, Nature, 177, 670 (1956).

139. R. Herrmann and C. Th.J. Alkemade, "Chemical Analysis by Flame Photometry," 2nd Ed., Interscience Publishers, New York, 1963.

140. A.G. Gaydon, Proc. Roy. Soc. (London), A231, 437 (1955).

141. L. Brewer and R.H. Hauge, J. Molec. Spectrosc., 25, 330 (1968).

142. J. van der Hurk, T. Hollander, and C.Th.J. Alkemade, J. Quant. Spectrosc. Radiat. Transfer, 13, 273 (1973).

143. S.R. Koirtyohann and E.E. Pickett, Anal. Chem., 38, 585 (1966).

144. E. Yoshimura, H. Haraguchi, and K. Fuwa, unpublished work.

145. J. van der Hurk, T. Hollander, and C.Th.J. Alkemade, J. Quant. Spectrosc. Radiat. Transfer, 14, 1167 (1974).

146. C. Veillon and J.Y. Park, Anal. Chem., 42, 684 (1970).

BIOGRAPHICAL SKETCH

Stephan John Weeks was born April 13, 1950, in Minneapolis, Minnesota. He attended schools in Minneapolis and Bloomington, Minnesota. In May, 1972, he received the degree of Bachelor of Arts, magna cum laude, from St. Olaf College, Northfield, Minnesota.

He is a member of the American Chemical Society and the Optical Society of America.

I certify that I have read this study and that in my opinion it conforms to acceptable standards of scholarly presentation and is fully adequate, in scope and quality, as a dissertation for the degree of Doctor of Philosophy.

James D. Winefordner, Chairman
Graduate Research Professor of Chemistry

I certify that I have read this study and that in my opinion it conforms to acceptable standards of scholarly presentation and is fully adequate, in scope and quality, as a dissertation for the degree of Doctor of Philosophy.

Patrick L. Brezonik
Professor of Environmental Engineering Sciences

I certify that I have read this study and that in my opinion it conforms to acceptable standards of scholarly presentation and is fully adequate in scope and quality, as a dissertation for the degree of Doctor of Philosophy.

Kuang Pang Li
Assistant Professor of Chemistry

I certify that I have read this study and that in my opinion it conforms to acceptable standards of scholarly presentation and is fully adequate in scope and quality, as a dissertation for the degree of Doctor of Philosophy.

Roger G. Bates
Professor of Chemistry

I certify that I have read this study and that in my opinion it conforms to acceptable standards of scholarly presentation and is fully adequate in scope and quality, as a dissertation for the degree of Doctor of Philosophy.

Gerhard M. Schmid
Associate Professor of Chemistry

This dissertation was submitted to the Graduate Faculty of the Department of Chemistry in the College of Arts and Sciences and to the Graduate Council, and was accepted as partial fulfillment of the requirements for the degree of Doctor of Philosophy.

December, 1977

Dean, Graduate School